ReB_2 and Re_7B_3: Synthesis, Characterization and Theoretical Calculations

by

Zeynep Gizem Narin

A Thesis Submitted to the

Graduate School of Sciences and Engineering

in Partial Fulfillment of the Requirements for

the Degree of

Master of Science

in

Material Science and Engineering

Koç University

September 2014

Koç University

Graduate School of Sciences and Engineering

This is to certify that I have examined this copy of a master's thesis by

Zeynep Gizem Narin

and have found that it is complete and satisfactory in all respects,

and that any and all revisions required by the final

examining committee have been made.

Committee Members:

_____

Mehmet Suat Somer, Ph. D. (Advisor)

_____

Uğur Ünal, Ph. D.

_____

Kaan Güven, Ph. D.

Date: _____

To my lovely family & Oral Ekdal

ABSTRACT

The investigation of superhard materials has attracted much interest due to their applications in industry. Diamond is the hardest and most incompressible single-phase material known up to now. Several researchers have devoted themselves to produce new superhard materials, as hard as or even harder than diamond. One of those promising material is rhenium diboride (ReB_2). In addition to ReB_2, Re_7B_3 is also considered from quantum chemical calculations as another possible superhard compound. The present thesis consists of two parts: mechanical characterization of arc melted ReB_2 and synthesis and comprehensive characterization of Re_7B_3.

The controversial Vickers hardness range of ReB_2 has not been cleared out by experimentalists and theoreticians. This large range, reported as 20 GPa to 48 GPa, causes an argument on whether ReB_2 is a superhard material or not. In order to clarify this point and to understand the actual hardness, we have examined how hardness of ReB_2 changed in correlation with the excess boron amount in the compound. Arc melting synthesis of ReB_2 is only possible when surplus of boron is employed. Until now, there is no clear information how much excess should be applied. To investigate the effect of excess boron in the final product, a set of ReB_2 compound was synthesized with two different boron contents, Re:B=1:4 and 1:7. By the Vickers micro-indentation hardness test, average hardness of ReB_2 was measured 24 GPa. As the free boron content increased from $ReB_{3.5}$ to $ReB_{5.5}$, the average hardness decreased from 24.89 ±0.66 GPa to 23.88 ±0.34 GPa. It is the first result ever that compares the hardness values of ReB_2 depending on the boron excess in the ReB_2 structure. Hence, the inverse relationship between excess boron amount and the hardness of ReB_2 was successfully proved for the first time ever. The obtained micro-hardness values are lower than the corresponding average values of 35 GPa reported by Chung *et. al.* [1] This may be due to the fact that the limitation effect of excess amorphous boron in the structure. Different experiments have been conduct to reduce/remove the rest (unreacted) boron from ReB_2. Hereby, HNO_3 treatment and cracking and re-melting methods were most successful ones. As reported by ICP-OES results, $ReB_{3.5}$ decreased to $ReB_{3.3}$ by nitric acid treatment, while $ReB_{3.6}$ decreased to $ReB_{2.9}$ by cracking and re-melting method. In

addition, crystalline boron was used as a reactant instead of the amorphous powder to investigate the effect of allotropic forms and purity of boron on the ReB_2 synthesis. There is no need to employ surplus of boron for the synthesis from the crystal boron.

Among the Re-B system, Re_7B_3 has not been studied as extensively as ReB_2. Recently the superconductivity of Re_7B_3 was discovered with the transition temperature of 3.3 K for the first time.[2] Besides the superconductivity of Re_7B_3, there is an interest in checking the hardness properties of the Re-B compounds. Örmeci *et. al.* also investigated the hardness of Re_7B_3 by using the crystal structure and the tabulated atomic radii by the FPLO package.[3] There was a basic conflict either to use B-B interaction as a bond in the calculations -14 GPa- or to not use it -20 GPa- . For deeper understanding of this phenomenon -in other words- the hardness of Re_7B_3, we have decided to synthesize Re_7B_3 as a pure powder and characterize its chemical, physical and mechanical properties. Experimental results proved that the hardness of Re_7B_3 is 19 GPa. So, the B-B interaction should be considered in the hardness calculations. The compound Re_7B_3 has not been synthesized as a pure phase so far. Usually, Re_3B or ReB_2 are the byproduct as a minor phase. Therefore, it is a big challenge to synthesize a single phase of Re_7B_3 not only because of the narrow phase region of Re_7B_3, but also due to the incalculable boron loss during the synthesis. In this thesis, we investigated the synthesis of Re_7B_3 with three different methods; synthesis by the direct reaction of elemental component at high temperature, synthesis in a metal flux, and arc melting synthesis. The preparation of Re_7B_3 was accomplished by the lead flux method for the first time ever. By applying arc melting method and by tuning the starting composition, we obtained Re_7B_3 as the main product (ca. 95 wt. %). In the second part of the thesis, the detailed synthesis method was reported with the chemical, physical and mechanical characterization results done by XRD, ICP-OES, EDXS, SEM, Vickers micro-indentation, wear test, magnetic susceptibility, and specific heat capacity measurements.

ÖZET

Endüstriyel uygulama alanları nedeniyle son yıllarda sertliği yüksek olan (aşırı sert) malzemelerle ilgili çalışmalar büyük ilgi toplamıştır. Şimdiye kadar bilinen en sert ve sıkıştırılmaya karşı en dayanıklı malzeme elmastır. Birçok bilim adamı en az elmas kadar sert malzeme bulmak için birçok çalışma yapmıştır. Bu çalışmalar sonucunda, renyum diborür (ReB_2) en umut vaat eden bileşik olarak belirlenmiştir. ReB_2'e ek olarak da kuantum kimyasal hesaplamaları sonucunda, Re_7B_3 olası sert bir bileşik olarak değerlendirilmiştir. Bu tez çalışması iki projeden oluşmaktadır. Birincisi, ark eritme yöntemi ile sentezlenen ReB_2'ün mekanik özelliklerinin içerisindeki bor miktarına göre incelenmesi; ikincisi ise, Re_7B_3 için yeni üretim metotlarının geliştirilmesi ve kapsamlı karakterizasyon çalışmasıdır.

ReB_2'ün Vickers sertlik aralığı, teorisyenler ve deneysel çalışanlar tarafından net bir biçimde belirlenememiştir. Tam belirlenemeyen ve 20 ile 48 GPa arası çeşitlilik gösteren sertlik aralığı yüzünden, ReB_2'ün aşırı sert olup olmadığı tartışmaya açık hale gelmiştir. Bu belirsizliği gidermek ve gerçek sertlik değerini saptamak için, ReB_2'ün mekanik özelliği üzerine çalışıldı ve bunu sentez sonrasında yapı içerisinde kalan fazla borun mekanik özelliği nasıl etkilediği incelendi. Ark eritme metodu ile ReB_2'ü sentezlemek ancak reaksiyona fazla bor ile başlayarak mümkün olmaktadır. Ancak sentez için ne kadar fazla bor kullanmak gerektiği şimdiye kadar net bir biçimde belirtilmemiştir. Son ürünün yapısında kalan bor fazlalığının ReB_2'ün mekanik özelliklere etkisini araştırmak için iki farklı kimyasal mol oranı kullanılmıştır, Re:B=1:4 ve 1:7. İstanbul Teknik Üniversitesi'nde yapılan Vickers mikro indentasyon test tekniği ile, ilk defa ReB_2 yapısındaki bor fazlalığının ReB_2'ün sertlik değerlerini düşürdüğü saptanmıştır. Bu saptamanın üzerine, çeşitli deney metotları ile yapıdaki bor fazlalığı uzaklaştırılmaya çalışılmıştır. Nitrik asit uygulaması ve kırıp yeniden sentezleme metodu başarılı sonuçlar vermiştir. Bunlara ek olarak, amorf bor ile senteze başlamak yerine daha stabil kristal bor ile reaksiyon tekrarlanmış ve aradaki farklılık gözlemlenmiştir. ReB_2 projesinde, kimyasal, fiziksel ve mekanik özellik incelemeleri XRD, ICP-OES, EDXS, SEM, Vickers sertlik cihazı ve aşınma cihazları ile yapılmıştır.

Re-B sistemleri arasında; Re_7B_3, ReB_2 kadar kapsamlı bir biçimde çalışılmadı. 2003 senesinde, sürpriz bir biçimde Re_7B_3'ün süper iletkenliği kesfedildi.[2] Bunun dışında, Örmeci tarafından yapılan teorik FPLO paket hesaplama çalışmalarında Re_7B_3 için iki ayrı sertlik değeri hesaplandı. Bu iki ayrı sonucun sebebi Re_7B_3 yapısındaki B-B etkileşiminin bağ olarak değerlendirilip değerlendirilmeme durumundan kaynaklanmaktadır.[3] Re_7B_3'ün sertliğini net bir biçimde anlayabilmek ve saf bir biçimde sentezlenip fiziksel, kimyasal ve mekanik özelliklerini kapsamlı olarak raporlamak bu projenin başlıca amacıdır. Re_7B_3 şimdiye kadar saf bir biçimde tek faz olarak sentezlenemedi. Genellikle, ReB_2 ve Re_3B impüriteleri ile gözlemlendi. Re-B faz diyagramında Re_7B_3'ün dar bir alanda yer alıyor olmasının yanı sıra üretim esnasında kullanılacak bor fazlalığının hesaplanamaması Re_7B_3'ün tek bir fazda üretilmesini zorlaştıran başlıca sebeplerdir. Biz bu projesinde, üç farklı üretim şekli ile Re_7B_3'ün saf bir biçimde sentezlenmesi üzerine çalıştık. Birincisi yüksek sıcaklık altında elementlerin karışım metodu, ikincisi metal eriğiyi ile sentezleme metodu, üçüncüsü ise ark eritme tekniğidir. Yapılan çalışmalarda, Re_3B impürite olarak görülmesine rağmen, Re_7B_3 ilk defa kurşun eriğiyi içinde sentezlenmiştir. Ark eritme tekniği ile ise daha başarılı sonuçlar elde edilmiştir. % 95 saflık değerinde Re_7B_3 başarı ile sentezlenmiştir. Takibinde ise, kimyasal, fiziksel ve mekanik özellikler XRD, ICP-OES, EDXS, SEM, Vickers sertlik testi, aşınma testi, manyetik duyarlılık ölçümü ve özgül ısı kapasitesi ölçümleri ile raporlanmıştır.

ACKNOWLEDGEMENTS

First and foremost, I would like to thank to Professor Mehmet Suat Somer for his invaluable supervision and constant support throughout my undergraduate and M.S. studies. He believed in me and provided infinite freedom to conduct my projects on my own. Towards the end, he taught me both the principles of human traits and professional scientific approaches. I also want to thank Dr. Alim Örmeci, who is the motivation of the Re_7B_3 project that has extended into my master thesis, with his theoretical calculations.

My sincere thanks to my thesis angel: Dr. Pınar Tatar Güner. I've had the pleasure to have known her for many years. She was always there to encourage me when I lost my motivation throughout my undergraduate and M.S. years. She was an excellent role model for me on how a Turkish woman should be in a social and professional life. I don't know how I could've finished my thesis without her superior guidance, "harsh" criticisms, and deepest help. She provided a great contribution to my thesis.

I should also thank Dr. Peter Hoehn. I am so glad to have had the opportunity to work with him at Max Planck Institute in Germany. He supported me, educated me, and most importantly taught me that the ideals of German discipline do not depend on hard work, but effective work. He gave me the infinite freedom to make mistakes while I was working in the laboratory for pure "knowledge" without any application concerns.

I would also like to thank every professor who helped me to improve upon myself. First I would like to thank Professor Levent Demirel. He gave me the opportunity to work in his physical chemistry laboratory in my first year at Koç without any prior experience in the Chemistry lab. I would like to thank Dr. Uğur Ünal as he was my advisor during my undergraduate years. I've never hesitated to knock on his door to discuss my projects or talk about anything else. I am also thankful for Professor Ersin Yurtsever, Dr. Özgür Birer, and Dr. Funda Acar Yağcı. They asked me tough questions during my independent presentations that made me think twice on my study, which resulted in me working even harder. I would like to thank Professor Yılgör and Emel Yılgör for teaching me how things work in the industry. I appreciate taking laboratory

courses from Dr. Annamaria Miko and Dr. Duratha Haciu. They were so kind and friendly while they were educating me and improving my laboratory skills.

I would like to thank my thesis jury members Dr. Uğur Ünal and Dr. Kaan Güven for having accepted the evaluation of this work. In characterization parts, I have benefited from the resources of Max Planck Institute for X-ray crystal analyses, magnetic susceptibility, and specific heat capacity measurements with the help of Dr. Umut Aydemir and Walter Schnelle. I performed all of my mechanical tests within the laboratories of Professor Hüseyin Çimenoğlu of Istanbul Technical University. I would like to thank the great efforts of Faiz Muhaffel and Meltem İpekçi for the Vickers hardness and wear tests. I am grateful to Dr. İbrahim Hocaoğlu for ICP-OES measurements and would also like to thank him for taking time out to help with my research. Moreover, I am thankful to KUYTAM. Dr. Barış Yağcı and Cansu Yıldırım helped me a lot throughout the operation of several devices. One time they saved my stuck sample from the black hole of a polishing device with excellent team work. Finally, I would like to thank Muharrem *abi* for his amazing glassworks and chemical provisions.

Thanks to all the members of the inorganic laboratory team: Meltem İpekçi, Ali Bateni, Umut Aydemir, Kamil Kiraz, Selçuk Acar, Ali Baş, Ahmet Topçu, Gökçe Güven, Christian Benda, Ceren Zor, Monika Kazancıoğlu, Gerçek Armağan, Müjde Yahyaoğlu and my sweet “slave” Tuğçe Üstün for making those long years as enjoyable as they were. I would like to especially thank Burcu Uslu. She made me who I am in laboratory.

Thanks to all of my fellow colleagues in Material Science and the Engineer faculty: Pınar Dağtepe, Erhan Acar, Fatma Demir, İbrahim Hocaoğlu, Özlem Ünal, Emek Durmuşoğlu, and Ceren Yılmaz. They taught me a lot about life and were nearby whenever I need their support. I would like to give special thanks to my sweetie Gizem Yeşilyaprak. She has always motivated me to write my first sentence of my thesis and helped me to overcome the external challenges I face in my private life. I deeply appreciate all of my friends for having such unique personalities.

Finally and most importantly, I would like to thank my parents: my biggest support in my life Muradiye Narin and my life coach and best friend Çetin Narin. Moreover, I give deep thanks to my little brother Yankı for his sensibility and endless love. They trusted me in every single step I have taken thus far. I am so lucky to be a part of such a lovely family. Last but not least I give my thanks to Oral Ekdal and his beautiful family for holding my hands throughout my Koç years. This thesis is dedicated to those wonderful people…

TABLE OF CONTENTS

LIST OF TABLES

LIST OF FIGURES

Chapter 1

Introduction of Re-B system

1.1. Introduction of ReB_2

For the past several decades, hard and superhard materials have been a subject of great interest due to both technological applications and fundamental science. So, the modern superhard materials would take the place of diamond and the curiosity to know their structure and bonding would be explained which determine superior properties of these materials. Most of the scientists agree on the definition of "superhard" material as a material has Vickers hardness (H_V) higher than 40 GPa, such as diamond, cubic boron nitride (c-BN), B_6N, and BC_2N. To search for novel superhard materials, researchers have followed two different approaches. First, they have inspired from diamond, the hardest material known with Vickers hardness of 70-100 GPa, and the related materials. In the earlier 2000s, diamond-like BC_2N has been synthesized with the Vickers hardness of 76 GPa.[4] Afterwards, cubic BC_5 was synthesized with the Vickers hardness of 71 GPa by ultimate metastable solubility of boron in diamond.[5] The theory behind of diamond related materials is that they all consist of light element compounds in the B-C-N-O system with strong covalent and short bonds. Nevertheless, they are expensive materials because they should be produced under extremely high temperature and high pressure. In addition, they are not applicable to cut steel and other ferrous metals because of undesired iron carbide formation during high-speed machining. In the second approach, two design parameters have been optimized to create ultra in-compressible superhard materials: high-valance electron density and bond covalency.[1] Thereby, light elements combined with the transition metals., which have high valence electron density (electrons/unit volume), and formed compounds with strong covalent bonds, such as ReB_2, OsB_2, IrN_2, OsN_2, PtN_2, Ru_2C and PtC and so on.[6–12] Fortunately, these transition

metal binaries possess high bulk moduli (B_0) which has little direct connection with hardness, i.e. B_0=360 GPa for ReB_2 while B_0=442 GPa for diamond.[1,13] Beside high bulk moduli, they can be produced under atmospheric pressure which allows less expensive production.

According to the second approach, ReB_2 is an excellent candidate to be a superhard material by the optimization of high valence electron density and bond covalency. Re has the second highest valence electron density among the all other transition metals. The strongest covalent bonds can be formed easily by B, C, and N.[14] Rhenium diboride (ReB_2) has been synthesized for the first time ever in 1962 by LaPlaca and Post without any concern about hardness.[15] And then, many scientists have produced ReB_2 with different techniques.[1,6,15–28] After years, Chung *et. al.*[1] reported that ReB_2 is an ultra-incompressible and superhard material with average Vickers hardness of 48 GPa and scratches a diamond surface in Figure 1.1.1.

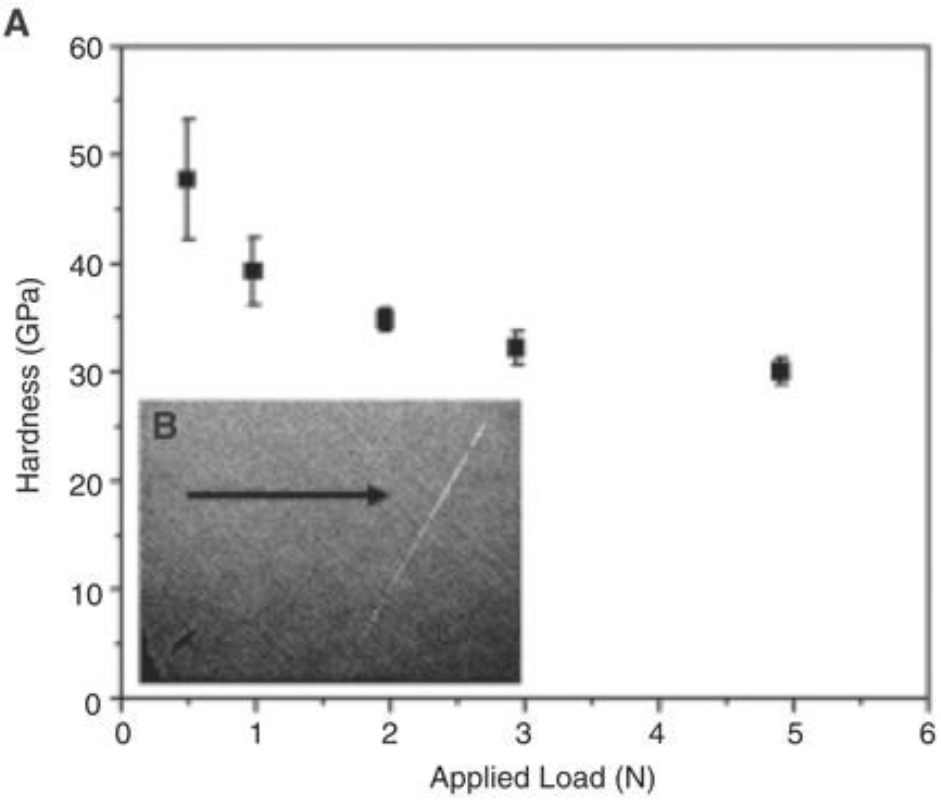

Figure 1.1.1 a) Vickers hardness of ReB_2 plotted as a function of applied load **b)** a scratch mark on the surface of a natural diamond by an ingot of ReB_2 [1]

However, Dubrovinskaia et al.[29] questioned the validity of this claim and interpreted the same graph with the average hardness of ReB_2 as 30.1 (±1.3) GPa. So, according to Dubrovinskaia, ReB_2 may not be a superhard material.

As a respond of the comment of Dubrovinskaia *et. al.*, Chung *et. al.* has presented AFM (Atomic Force Microscopy) image of a scratch mark made by ReB_2 on diamond surface which proves the superhard nature of ReB_2.[30]

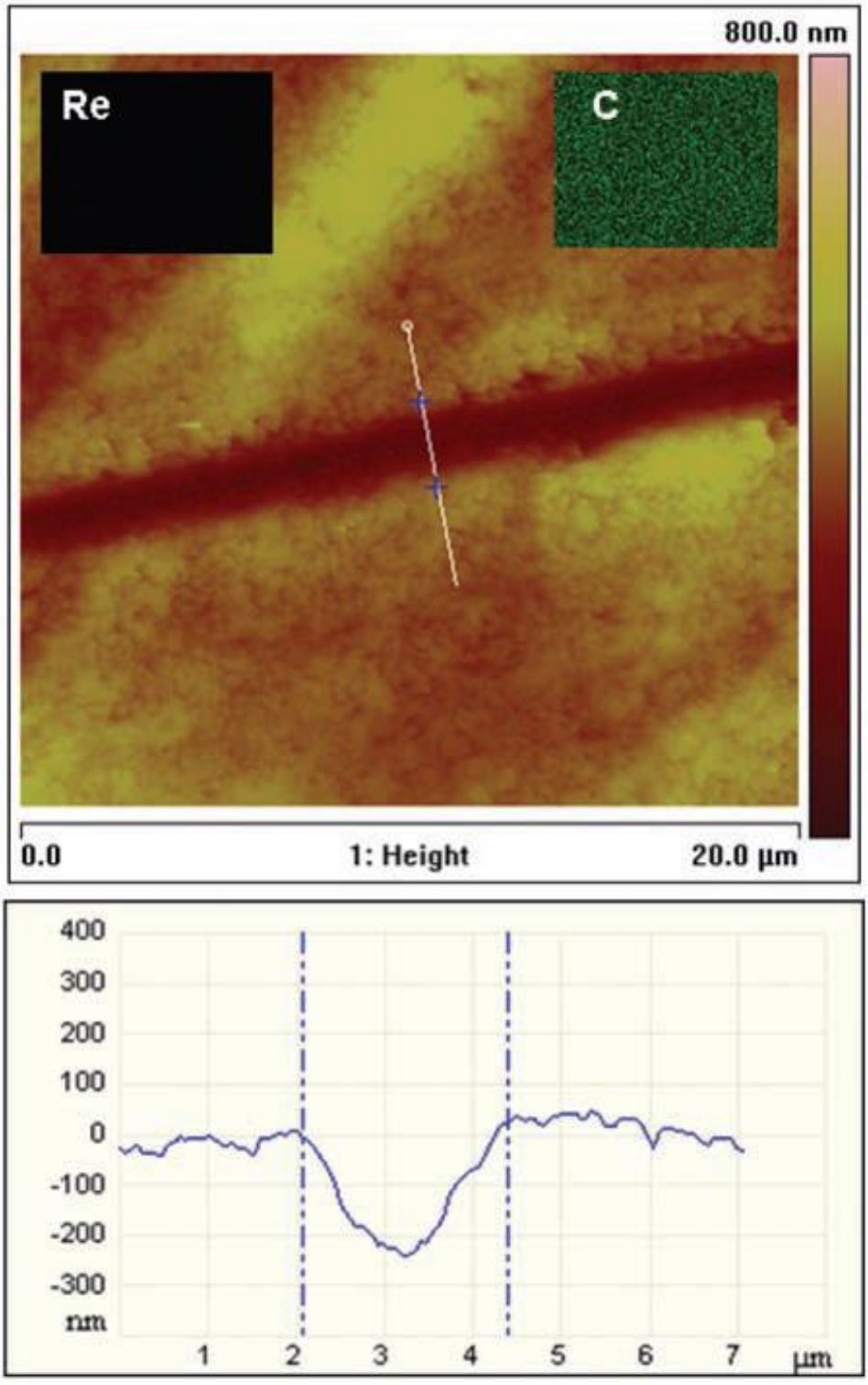

Figure 1.1.2 An AFM image with the corresponding depth profile of a scratch mark made by ReB_2 on the diamond surface [30]

According to the AFM image, approximate depth has been reported as 230 nm within 2 μm. Elemental mapping has been showed that there is no rhenium deposit left on the diamond surface which proves its superhard nature.

This hot discussion between Chung *et. al.* and Dubrovinskaia *et. al.* has forced to many scientists to check the hardness of ReB_2. Recently, the Vickers hardness of ReB_2 was reported about 39.3 GPa under applied load of 0.49 N, but load-variant hardness was only 26.2 GPa.[11] The hardness of the reactive spark plasma sintered ReB_2 was obtained in the interval 20.7–31.1 GPa depending on the applied load.[22] Nevertheless, the scratching diamond surface by ReB_2 was not reproduced by these researchers as reported by Chung *et.al.* [30]

Since the experimental results have not ended the discussion, theoreticians have studied on hardness of ReB_2, too. The average hardness of ReB_2 was calculated as 46 GPa by Zhou *et. al.*[31] According to the atomic properties and bond strengths, Simunek *et.al.* has calculated the hardness of ReB_2 as 35.8 GPa.[3] However, in the calculation of Simunek *et. al.*, metallic bonds on the hardness were not taken into consideration. More recently, Zhong *et. al.* has reported the hardness of ReB_2–ReB_2 as 39.1 GPa with the addition of Re-Re metallic interaction effect. Neither experimentalists nor theoreticians have disagreed on the actual hardness of ReB_2 yet.

In order to clear this conflict, we should understand what makes ReB_2 special and what factors varies/degrades its hardness. First, the crystal structure should be examined well. It has the highest B:Re ratio among the other rhenium boride phases – Re_3B, Re_7B_3 and ReB_2 – and so it exhibits strong and highly covalent bonding.[1,16] Covalent Re–B bonding possess some degree of ionic bonding due to the strong hybridization between Re *5d* and B *2p* states.[31] B–B bonds are stronger than Re–B and these difference creates anisotropic compressibility and rigidity of the structure.[32] For deeper understanding, the crystal structure of ReB_2 is given in Figure 1.1.3.

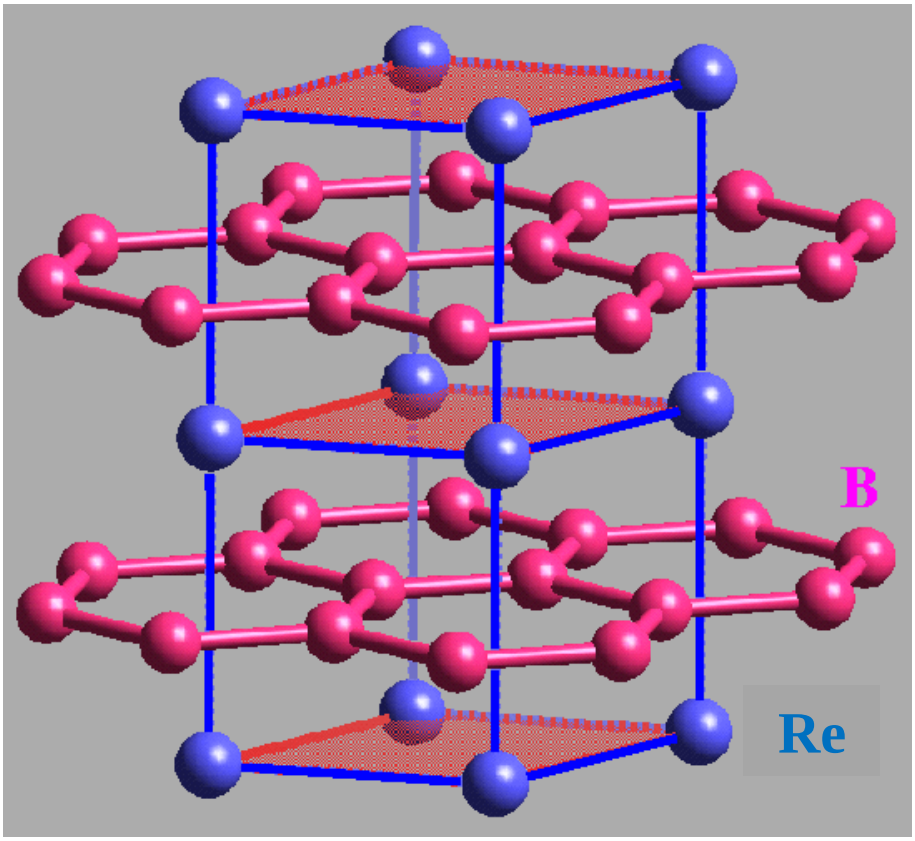

Figure 1.1.3 Crystal structure of ReB_2 which illustrated with multiple unit cells[1]

The pink spheres show B atoms, while blue ones show Re atoms. ReB_2 has a hexagonal structure ($P6_3/mmc$, a=2.900 Å and c=7.478 Å).[1] It consists of alternating layers of hexagonally packed Re and puckered hexagonal networks of B. The anisotropic nature of the compound, layered perpendicular to the c-axis along the (00l) plane, increases mechanical properties by the covalent bonding of Re and B atoms between layers.[20,33]

As we mentioned above, synthesis techniques of ReB_2 affect the purity of the product as well as its mechanical properties. To date, ReB_2 crystals have been produced by several techniques, such as, flux-grown method, zone-melting and arc melting.[1,34,35] Their Vickers hardness reported as 37.2 GPa for zone melted ReB_2, 36.4 GPa for arc melted ReB_2, and 36.2 GPa for flux grown ReB_2. The morphology and the composition of Re–B are other factors affecting the hardness and purity of ReB_2. This has not been discussed much. The excess amorphous boron, located along the grain boundaries of

polycrystalline ReB_2 would reduce the mechanical properties of ReB_2. Thus, hardness of ReB_2 ranges.

To understand the actual Vickers hardness of ReB_2 and to prove the effect of excess amorphous boron on the hardness, in this thesis, we decided to synthesize ReB_2 by arc melting method and evaluate its Vickers hardness depending on the excess boron in the crystal structure.

1.2. Introduction of Re_7B_3

Rhenium borides have been the focus of attention for the scientists for decades because of their superior mechanical and electrical properties.[10,36–38] The mechanical properties make them especially practical in numerous technological applications; for example, in cutting and grinding tools, abrasive resistance (or superhard) coating in the aerospace and defense industries.[39–42] Among the Re-B system, the crystal structure, mechanical and electrical properties of ReB_2 have been studied extensively from experimental and theoretical sides.[1,9,17,20,22,24,36,37,43–45] However, Re_7B_3 has not been studied widely because it is not thermodynamically stable as much as ReB_2 and Re_3B.[46]

After the discovery of superconductivity in magnesium diboride, MgB_2, there has been a renewed interest on boride compounds. MgB_2 has been reported to be superconducting at 39 K which is the highest superconducting transition temperature, T_c, determined for a non-copper-oxide superconductor.[47] The explanation for the superconductivity of MgB_2 focuses on the metallic nature of a two dimensional layer formed by boron atoms. The high vibrational frequencies of boron atoms create strong electron-phonon interactions. Thus, those interactions ensure a high superconducting transition temperature. Researchers studied the relationship between the superconducting properties and the B-B bonds in these Re-B compounds to understand the superconductivity in boride compounds in depth.[2] The networks of boron atoms in the borides are shown in Table 1.2.1.

Table 1.2.1 The geometric arrangements of boron atoms in the borides. [2]

Formula	Examples	B-B bonds	
M_4B	Mn_4B	Isolated atoms	
M_3B M_2B	Ni_3B Be_2B		
M_3B_2	V_3B_2	Pairs	
MB	NiB FeB	Zig-zag chains	
$M_{11}B_8$	$Ru_{11}B_8$	Branched chains	
M_3B_4	Ta_3B_4 Cr_3B_4	Double chains	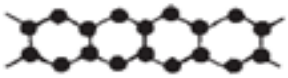
MB_2	MgB_2 TiB_2 CrB_2 ZrB_2	Two dimensional network	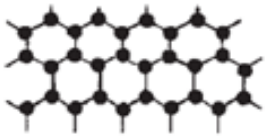

As shown in Table 1.2.1, boron atoms are bonded as two dimensional honeycomb networks in the boron rich compounds, MB_2 (M: metal element). In the metal rich compounds, M_3B, M_2B, and M_3B_2, the boron atoms are either isolated or paired. Although boron atoms are isolated, there are B-B interactions as a triangle form in the crystal structure of Re_7B_3 shown in Figure 1.2.1. Consequently, the superconducting transition temperature of ReB_2 and Re_3B have been reported as in the range from 4.5 K to 6.3 K, depending on the boron concentrations (Re:B= 1:1.8 to 1:2) and 4.8 K, respectively.[48] Although the superconductivity properties of the Re-B compounds with the crystal structure have not been correlated, the superconductivity of Re_7B_3 were discovered with the transition temperature of 3.3 K for the first time.[2]

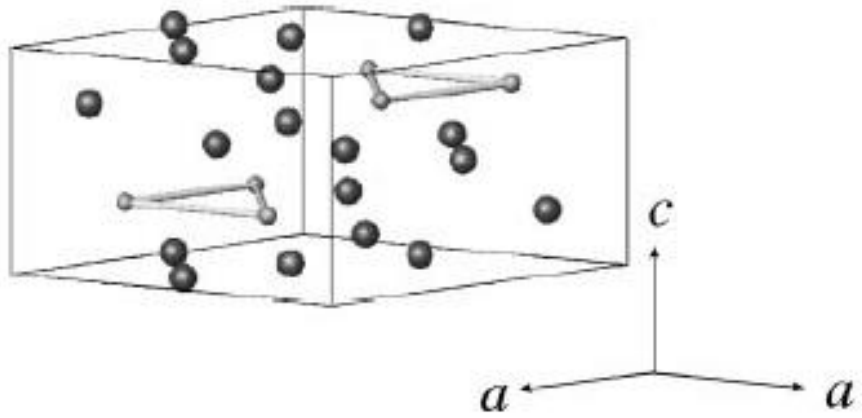

Figure 1.2.1 The crystal structure of Re_7B_3 ($P6_3/mc$). The dark gray circles show Re atoms and the light gray circles show B atoms. The black lines in this figure show unit cell.[2]

Besides the superconductivity of Re_7B_3, there is an interest in checking the hardness properties of the Re-B compounds. Antonin Simunek *et. al.* has defined a formula to estimate hardness of crystals by using the crystal structure and the tabulated atomic radii.[3] Since hardness measurements show a certain range of values but not an exact result, the theoretical hardness values obtained from the formula of Simunek *et. al.* are reliable. Örmeci *et. al.* has calculated the hardness of ReB_2 by using the same formula. Although this formula is used only for covalently bonded materials, it also gives appropriate results for intermetallic systems, i.e diborides. Then, the results obtained by using the formula of Simunek *et. al.* have been compared with the results obtained from quantum chemical calculation results. Since they support each other, Örmeci *et. al.* also investigated the hardness of Re_7B_3 to check the reliability range of the formula.

Basically, Re_7B_3 is different from ReB_2 because of the B-B distance in the crystal structure. In Figure 1.2.2, the average B-B bond length in ReB_2 is 1.82 angstrom.[34] In the boride system, hardness mainly depends on B-B bonds, rather than Re-B and Re-Re bonds.[19] The shortest B-B distance in Re_7B_3 is 3.24 angstrom.[49] This length is too long to be a B-B bond. When the B-B interactions are neglected and Re-B metallic bonds only are used in the formula, the hardness of Re_7B_3 is obtained as 15.3 GPa. When the B-B interaction is also used, the hardness value increases to 20 GPa. This conflict is

enough to debate the validity of the formula. Thereby, there increase another motivation to investigate Re_7B_3, experimentally.

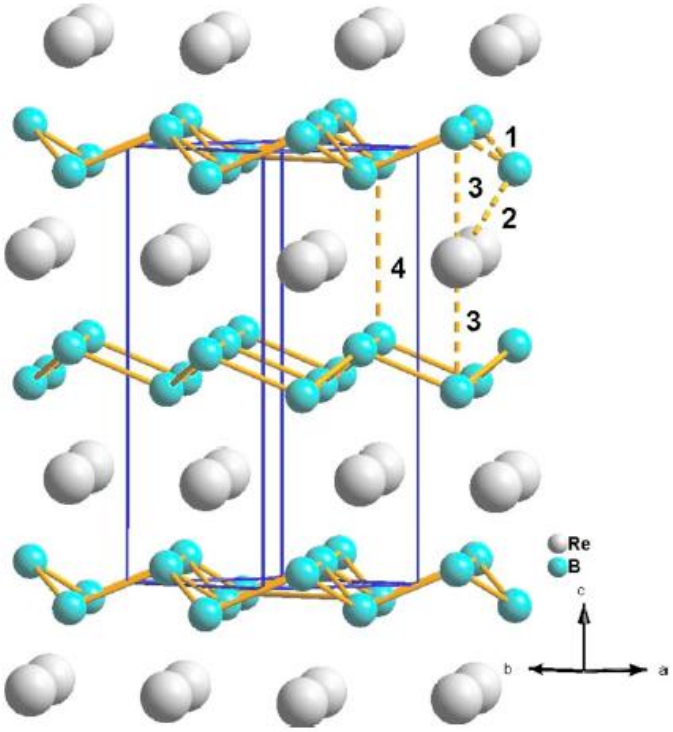

Figure 1.2.2 The crystal structure of ReB_2 ($P6_3/mmc$). The different bonds are designated by numbers (1: B-B bond, 1.815 Å, 2: Re-B bond, 2.258 Å, 3: Re-B bond, 2.220 Å, 4: B-bond, 3.033 Å) [34]

Re_7B_3 is also examined from quantum chemical calculations as another possible superhard material. The bulk modulus of Re_7B_3 is 400 GPa, meaning that based on this data only, Re_7B_3 is expected not to be as hard as diamond but harder than ReB_2. Calculations for Re_7B_3 are tabulated in Table 1.21.2.2.

Table 1.21.2.2 Calculated equilibrium lattice parameters a_o and c_o, bulk modulus B_o for Re_7B_3 compared with data available for diamond and ReB_2.

	a_o (Å)	**c_o (Å)**	**B_o (GPa)**
Diamond	3.500	_	459
Re_7B_3	7.459	4.854	400
ReB_2	2.872	7.405	360

For deeper understanding of this phenomenon -in other words- the hardness of Re_7B_3, we have decided to synthesize Re_7B_3 as a pure powder and characterize its chemical, physical and mechanical properties.

Before synthesizing Re_7B_3, the phase diagram of the system Re-B should be understood well. The phase diagram is given in Figure1.2.3. The Re-B system shows the existence of three known borides ReB_2, Re_3B and Re_7B_3. Regions of the homogeneity of Re_3B and Re_7B_3 are very narrow when the rhenium content of the alloys is varied from 70 to 80 atomic, at. %.

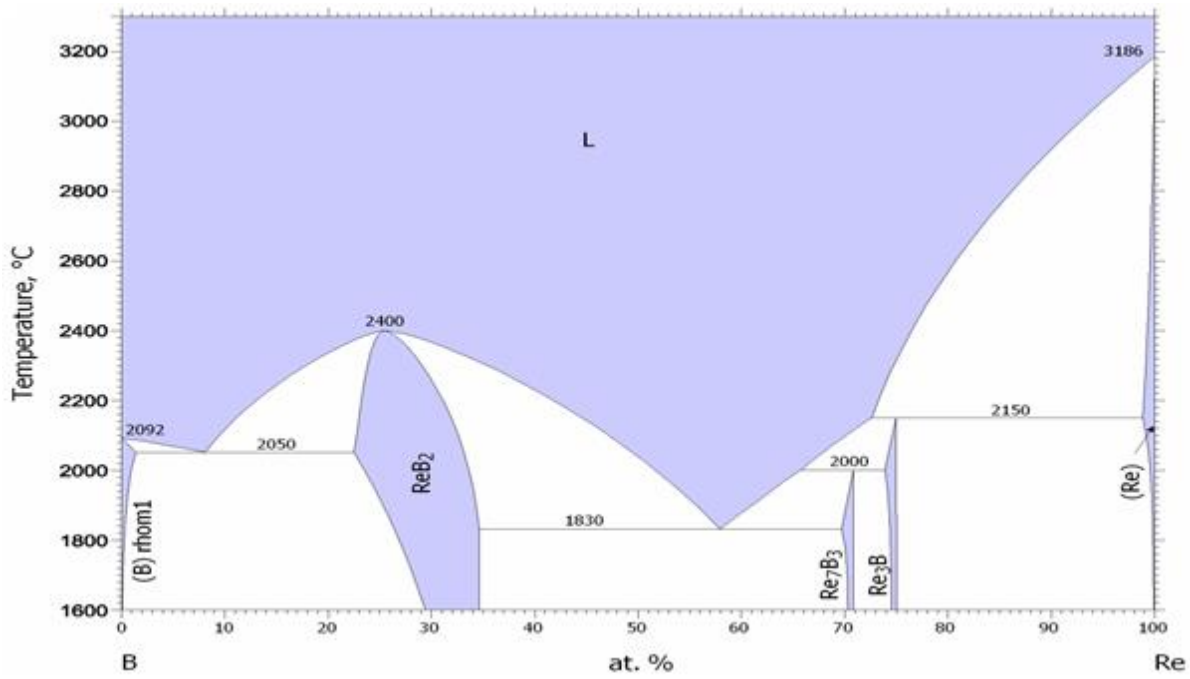

Figure1.2.3 Phase diagram of the system rhenium-boron

The details of the initial and final melting temperatures of the alloys, phase composition study, metallographic examination and micro-hardness determinations are presented in

Table 1.2.3. The Alloys #7 and # 8 show that the compound Re_7B_3 is never synthesized as pure phase. Usually, Re_3B or ReB_2 are seen in the product as a minor phase. Therefore, it is a big challenge to synthesize a single phase of Re_7B_3 because not only of the narrow region of Re_7B_3, but also the boron lost during the synthesis.

Table 1.2.3 X-Ray Structural, and Metallographic Analyses of Rhenium-Boron Alloys [49]

Alloy no.	B at. %	B wt.%	$t_{i.m.}$, °C	$t_{f.m.}$, °C	Phase composition	Microstructure and microhardness, daN/mm^2
1	15	1.0	2130	2250	Re_3B, Re	Noneq. condition, incompl. melted, spherical Re grains
2	20	1.4	2120	2150	Re_3B	Incompl. melted, Re_3B, spherical Re grains (H_μ =410 ± 50)
3	25	1.9	2150	2310	Re_3B	Large Re_3B grains (H_μ = 1690 ± 150)
4	27	2.1	2170	?	The same	The same
5	28	2.1	2000	2170	Re_3B (Re_7B_3)	The same
6	30	2.4	2020	2160	Re_7B_3, Re_3B	Segregation, peritectic crystallization
7	33	2.5	2000	2070	Re_7B_3 (Re_3B)	Essentially one phase (H_μ = 1690 ± 150)
8	40	3.8	1820	1840	Re_7B_3 (ReB_2)	Eutectic + excess Re_7B_3 precipitates
9	45*	4.6	1850	1900	The same	-
10	50	5.5	1800	1900	Re_7B_3, ReB_2	Eutectic + excess ReB_2 precipitates
11	55*	6.6	1860	2000	-	-
12	60	8.0	1820	2210	ReB_2 (Re_7B_3)	Primary ReB_2 precipitates + eutectic
13	63	9.0	1900	2270	-	-
14	67	10.4	1880	2280	ReB_2	ReB_2 phase, very little eutectic
15	70	11.2	1900	2280	The same	Essentially one phase
16	72	14.4	2200	2340	The same	The same
17	75	14.8	2340	2400	The same	Large "ReB_3" grains (H_μ = 3100 ± 200)
18	75*	14.8	2150	2400	The same	-
19	78	16.8	2140	2340	ReB_2	Essentially "ReB_3" decomposes in solid state
20	80*	18.0	2050	2250	The same	The same
21	86	25.8	2150	_	The same	Excess "ReB_3" precipitates + eutectic
22	90	34.5	2060	2130	ReB_2 (B)	Eutectic + excess "ReB_3" precipitates
23	92	41.0	2050	?	The same	Eutectics, few excess precipitates
24	97	63.5	2050	2200	The same	Excess boron precipitates (H μ 3400 ± 200) +eutectic

*Boron of 99.8 % purity was used for these alloys.

In this thesis, we investigated the synthesis of Re_7B_3 with three different methods, synthesis by the direct reaction of elemental component at high temperature, synthesis in a metal flux, and arc melting synthesis. The lead flux method was applied for the first time ever for the synthesis of Re_7B_3. The compound Re_7B_3 has never been synthesized as a pure phase so far. By applying arc melting method and by tuning the starting composition, we obtained Re_7B_3 as the main phase (ca. 95 wt. %). Experimental methods and optimizations of starting composition were presented in Chapter 4.

Chapter 2

Experimental Methods and Theoretical Concepts

2.1. Materials, Chemicals Used, Sources and Quality

All educts, except boron, were highly pure chemicals and commercially purchased. There are only a few companies who produce boron with high purity such as H.C. Starck. Most of boron production is accompanied with magnesium impurity because of the preparation of amorphous boron. For this study, 95-97 wt% pure amorphous boron was purchased from Pavezyum Company, Turkey.

Table 2.1.1 Elements used, their sources and certified purities

Elements	Atomic Weight (g/mol)	Melting Point (^{o}C)	Physical State	Company	Purity %
Tantalum (Ta)	180.9478	2996	Ampoule	ChemPur	99.9
Nickel (Ni)	58.693	1453	Powder	Alfa Aesar	99.9
Rhenium (Re)	186.207	3186	Powder	ChemPur	99.9
Niobium (Nb)	92.9064	2477	Ampoule	ChemPur	99.9
Boron (B)	10.8110	2076	Powder	Pavezyum	95-97

2.2. Experimental Methods

2.2.1. Arc Melting

Arc melting furnace was used for the syntheses of rhenium borides and ternary borides in our work. Additionally, it was applied for sealing of Ta ampoules that were used as a container for the reacting materials. Even though starting materials is pressed into pellets at various pressures to increase possibility of reaction, many of the syntheses still need high temperature to be completed. For that purpose, arc melting system enables greater operation temperatures than 3000 ºK while many commercial furnaces cannot. Besides that, it has several advantages such as ease of operation, compact and portable, instant high temperature, and extremely pure melts.

Centorr arc furnace 5SA/38042-A consists of the single arc furnace, a D.C. power supply, a vacuum pump and a water cooling system. In Figure 2.2.1, our arc melting system is illustrated. The arc furnace is covered with two silica windows, which allow observing the melting/sealing procedure. In the gun, a tungsten electrode is used because it can withstand high temperatures with minimal melting and erosion. An arc starter and water cooled copper hearth are also equipped in the arc furnace system. Arc melting operation temperature is arranged by the D.C power supply as ampere. It is corresponding to temperature in the range from 3000 ºC to 7000 ºC.

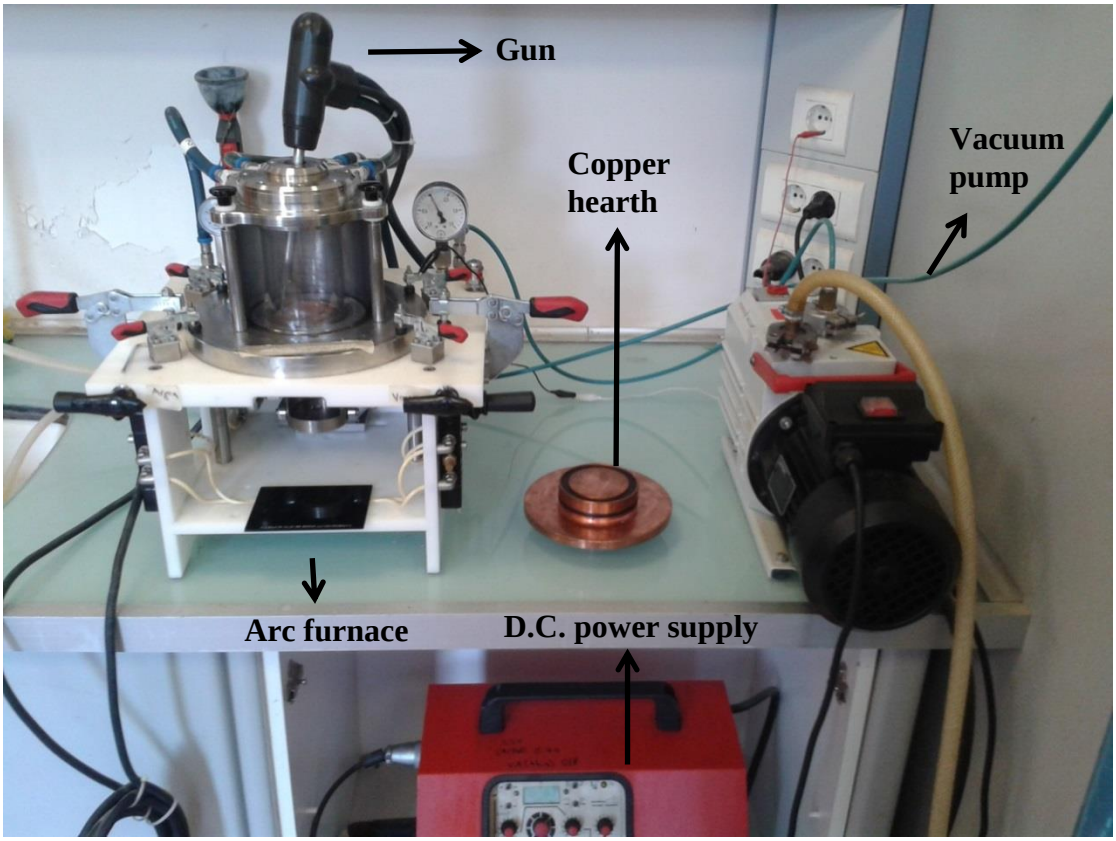

Figure 2.2.1 Arc melting system

To use the arc furnace system, the suitable copper heart is chosen. In Figure 2.2.2, they all are presented. First one for sealing of tubes, second one for bigger amount of production, the third one for small amount of synthesis are preferred. And then, suitable hearth is put into the stage. The stage is elevated to the final position in the chamber. Then, the chamber is locked. The furnace is purged by a vacuum pump to 10^{-1} mbar and backfilled with argon. Once the system evacuated and refilled, the desired power ampere level on the power supply is set. The tungsten electrode is brought to a position near the edge of pellet to be melted or touched the arc starter. Then arc is struck. With the angular movement of gun, the pellet is melted completely. The specimen is often turned over and re-melted to obtain uniform and homogeneous melt. During the arc process, copper hearth was cooled to prevent any damage on the copper hearth and the whole system.

Figure 2.2.2 Different types of copper hearts depending on the usage

2.2.2. The Flux Method in Solid State Chemistry

For the production of Re-B compounds, synthesis techniques generally involve very high temperature, such as, arc melting and radio frequency induction heating. These methods are necessary because the starting materials need very high temperatures to reach sufficient diffusion for reaction to take place. Flux method is an alternative route for performing high temperature reactions at more moderate temperatures. This method enhances the diffusion process in solid-state synthesis, by using molten salts or metals as solvent. Several key characteristics must be provided for a metal to be a viable flux for reaction chemistry:

i. The metal should form a flux at reasonably low temperatures so that normal heating equipment and containers can be used.
ii. The metal should have a broad liquid range between its melting point and boiling point temperatures.
iii. The flux metal should be easily separated from the products, by chemical dissolution, filtration during its liquid state, or if necessary mechanical removal.
iv. The metal flux should not form highly stable binary compounds with any of the reactants and should not react with the reaction container.

There are several types of metal fluxes; the most commonly employed ones tin, lead, zinc, aluminum, gallium, and indium. In this study, lead was used for the first time ever for the synthesis of Re_7B_3.

2.2.3. Schlenk Line

In our study, the Schlenk line was used for evacuating and sealing of the reaction vessel in the synthesis of Re_7B_3. Schlenk line provides an intelligence way to evacuate and also replace atmospheric gas with inert gas in the reaction tube. It is a glassware apparatus. It consists of a dual line with several ports in Figure 2.2.3. One line is connected to high-vacuum pump while the other one is connected to the inert gas supply, which is argon in our laboratory. The system has also a cold trap which is cooled down with liquid nitrogen to protect the pump from aggressive and corrosive gases and liquids. The high-vacuum pump decreases pressure down to about 10^{-3} mbar. The line with the argon flow is equipped with a mercury bubbler for gas release. This bubbler, also, monitors the general flow of gas.

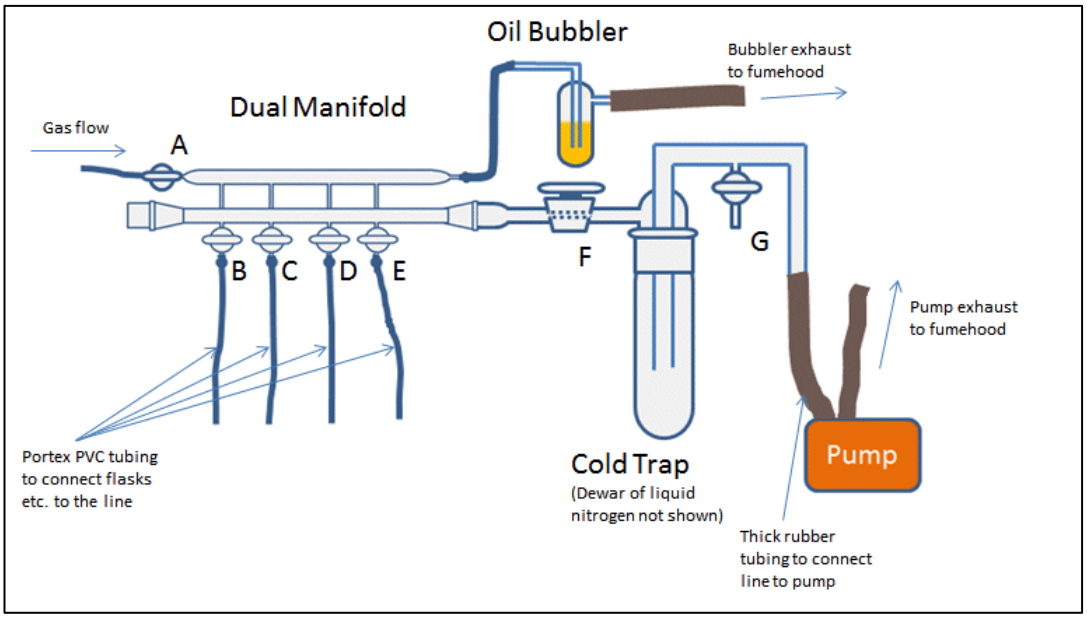

Figure 2.2.3 Complete Schlenk line set-up

2.2.4. Furnaces Used

i. Tube Furnace

Through application of Kanthal wire and silicon carbide heating elements the temperature range extends to 1600°C as operation temperature. The furnace can be arranged to operate at vertical, horizontal and at a degree. Heat shields are provided to minimize heat loss at high temperatures.

Figure 2.2.4 Universal tube furnace (Protherm ®)

ii. Vacuum Furnace

In Re_7B_3 flux synthesis study, the sealed reaction vessel was placed into the vacuum furnace (Nabertherm ®), which can be programmed within the temperature range 20 – 1100 ºC. The furnace was heated to 800 ºC. After annealing four hours at the specific temperature, the reaction vessel was taken out for cooling.

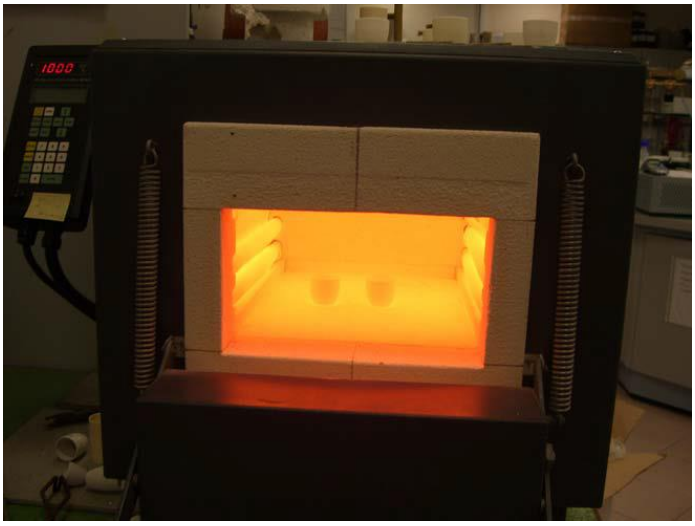

Figure 2.2.5 The vacuum furnace (Nabertherm ®)

2.3. Materials Characterization Techniques

2.3.1. X-Ray Powder Diffraction Techniques

i. Theory

The discovery of diffraction of x-rays by crystal allows the experimental determination of crystal structure. X-ray diffraction is a scientific technique for structural characterization of single and polycrystalline specimen. There are two types of x-ray diffraction techniques: single and powder. For a good crystal structure determination, well-formed single crystal should be used. Powder diffraction is not suitable enough for structure determination because it gives limited amount of reflection. Nonetheless, x-ray powder diffraction can be used to determine crystal structure if it is not too complex. It can also be used to identify unknown samples, analyze quantitatively powder mixtures, and measure lattice parameters precisely. [50]

A crystal is a solid object with a basic pattern of atoms. Those atoms repeat the pattern in three dimensions. There are three vectors describing those translations in space. Their total operation forms the lattice. Then, smallest repeating volume of the lattice forms the unit cell and symmetry operations on the lattice for the crystal systems. Possible considerations create seven crystal systems which are listed in the Table 2.3.1.

Table 2.3.1 Crystal systems with their restrictions

Restriction in	Cell edges	Cell angles
Triclinic	None	None
Monoclinic	None	$\alpha=\gamma=90^o$
Orthorhombic	None	$\alpha=\beta=\gamma=90^o$
Tetragonal	a=b	$\alpha=\beta=\gamma=90^o$
Trigonal, hexagonal	a=b	$\alpha=\beta=90^o$, $\gamma=120^o$
Cubic	a=b=c	$\alpha=\beta=\gamma=90^o$

Common method of generating x-rays in laboratories is the x-ray tube (Figure 2.3.1), in which rapidly moving electrons strike a solid target and their kinetic energy is converted into radiation. Although it is a simple and relatively cheaper device, the overall efficiency of an x-ray tube is lower than 1%. Most of the energy supplied to the tube is converted into heat; therefore, the device must be continuously cooled to avoid target (anode) meltdown. [51]

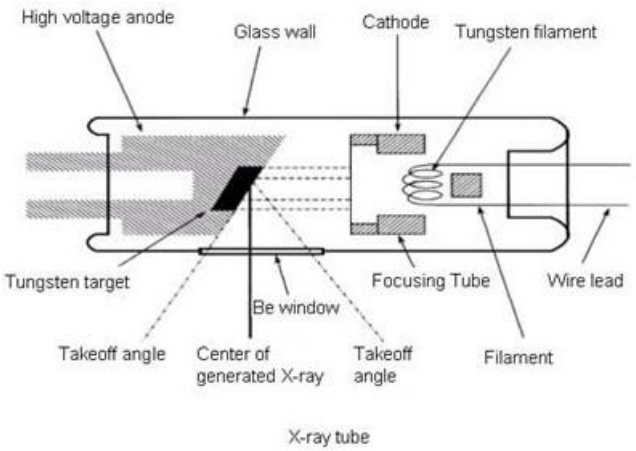

Figure 2.3.1 X-ray tube and formation of x-rays

In the X-ray tube, electrons are emitted from cathode, usually electrically heated tungsten filament, and accelerated towards anode by a high electrostatic potential (30 to 60 kV). The typical current in an x-ray tube is between 10 and 50 mA. As stated above, during transportation, electrons hit the target material and their kinetic energy turns into a characteristic radiation. By changing the anode material, emitted x-ray can be changed. For x-ray diffraction, K_α radiation is normally employed and in order to eliminate the radiations from lower wavelengths such as K_β suitable filter is used.[52] The following table shows the five common anode materials and the suitable filters.[53]

Table 2.3.2 Common anode sources with suitable filters

Metal	**Wavelength (Å)**			**β Filter**
	$K_{\alpha 1}$	$K_{\alpha 2}$	K_β	
Cr	2.28975	2.293652	2.08491	V
Fe	1.93608	1.94002	1.75664	Mn
Co	1.78900	1.79289	1.62082	Fe
Cu	1.54059	1.54441	1.39225	Ni
Mo	0.70931	0.71361	0.63230	Nb, Zr

Another important consideration in selecting x-ray wavelengths for a powder diffraction experiment is whether or not the studied material contains chemical elements with their K-absorption edges located just above the used characteristic wavelength. For example, K-absorption edge of Co is ~1.61 Å. The strongest $K\alpha_1/K\alpha_2$ spectral lines of copper have wavelengths ~1.54 Å. Hence, nearly all characteristic Cu radiation will be absorbed by Co, and this type of x-ray tube is not suitable for Co-based materials.

X-ray diffraction geometry is based on Bragg equation given as:

$$2d_{hkl}\sin\theta_{hkl} = n\lambda \qquad \text{(Eq.2.1)}$$

where d refers to interplanar spacing , hkl are called as Miller indices specifying plane orientation with respect to the unit cell edges, θ is the incident / scattering angle or called as

Bragg angle, n is the order of diffraction and the λ is the wavelength of X-ray beam (Figure 2.3.2).

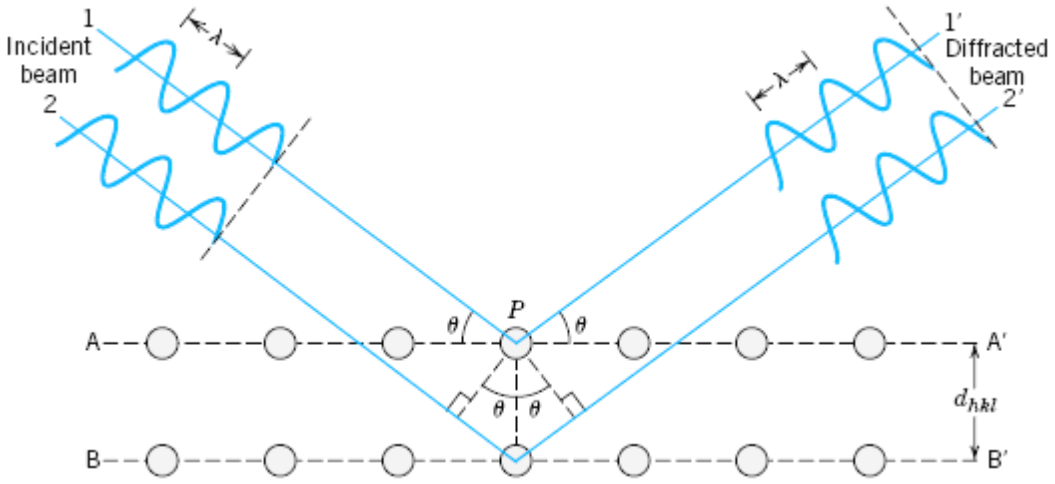

Figure 2.3.2 The Bragg construction for diffraction of X-rays on lattice planes

According to Bragg's law, an individual crystal gives a diffraction pattern with discrete diffraction beams. However, a stationary single crystal gives very few reflections. Therefore, the crystal must be rotated to obtain a full diffraction pattern. If many crystals of the same sample are exposed to X-rays, each of them gives its own diffraction pattern which will then superimpose.[54]

ii. Experimental

In this thesis, powder XRD experiments were performed on air-stable samples. The samples were finely ground and placed on sample holder. For this purpose special set-up, including play dough, were used. In detail, the powdered sample was spread on the amorphous glass and stabilized by using two-side stickers. A piece of play dough was placed on the holder and sample holder glass was put onto it. Finally, the position of glass was corrected and fixed onto dough well.

X-ray powder diffraction analysis was employed on a HUBER image plate Guinier-camera (Huber G670) equipped with a germanium monochromator and $CuK_{\alpha 1}$ radiation. The data collections were made in the range of $3° \leq 2\theta \leq 100°$ with a step size of 0.005° 2θ. For the preliminary analysis, Stoe WinXPOW Software[55] was used to compare experimental XRD patterns with Inorganic Crystal Structure Database (ICSD).[56]

2.3.2. Inductively Coupled Plasma - Optical Emission Spectroscopy

i. Theory

ICP-OES is commonly used instrument in modern laboratories for the analysis of metals in various fields. Sample introduced into the ICP as liquid form as shown in Figure 2.3.3. The first process called nebulization where sample is converted to a mist of finely divided droplet called aerosol. In the spray chamber, separation of aerosol occurred where the large droplets go to drain the fine droplet carried to the plasma. The Plasma is a highly energized 'cloud' of gaseous ions and their electrons. The resulting ions, and their associated electrons, then interact with the fluctuating magnetic field produced by the induction coil. This interaction causes the ions and electrons within the coil to flow in the closed annular paths depicted ohmic heating is consequence of the resistance of the ions and electrons to this movements. Adding mechanical energy to the electrons/ions by the use of the induced field within the heart of the plasma in this manner is called "Inductively Coupling". Where the argon ions inside the magnetic field are accelerated base on the right hand rule.

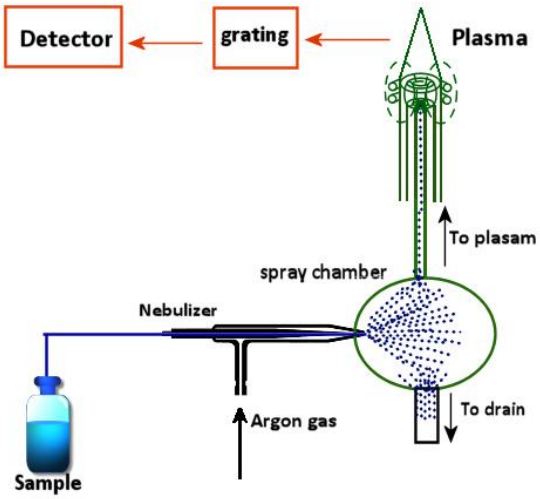

Figure 2.3.3 Diagram of Sample introduction to ICP-OES

Quantitative analysis of rhenium and boron was performed by using Inductively Coupled Plasma – Optical Emission Spectroscopy (ICP – OES). Spectro Genesis ICP – OES device is illustrated in Figure 2.3.4. ICP – OES system basically measures the optical emission spectrum of the analyte solution and converts it to a quantitative result (in ppm, ppb or mg/L), by using a regression curve of known standards. The linearity of this curve, given by the R value, determines the accuracy of the measurement and must be ≥ 0.9999 for a reliable result. A method should be created for the element(s) of choice with measurements of calibration curve taken at least from three different concentrations.

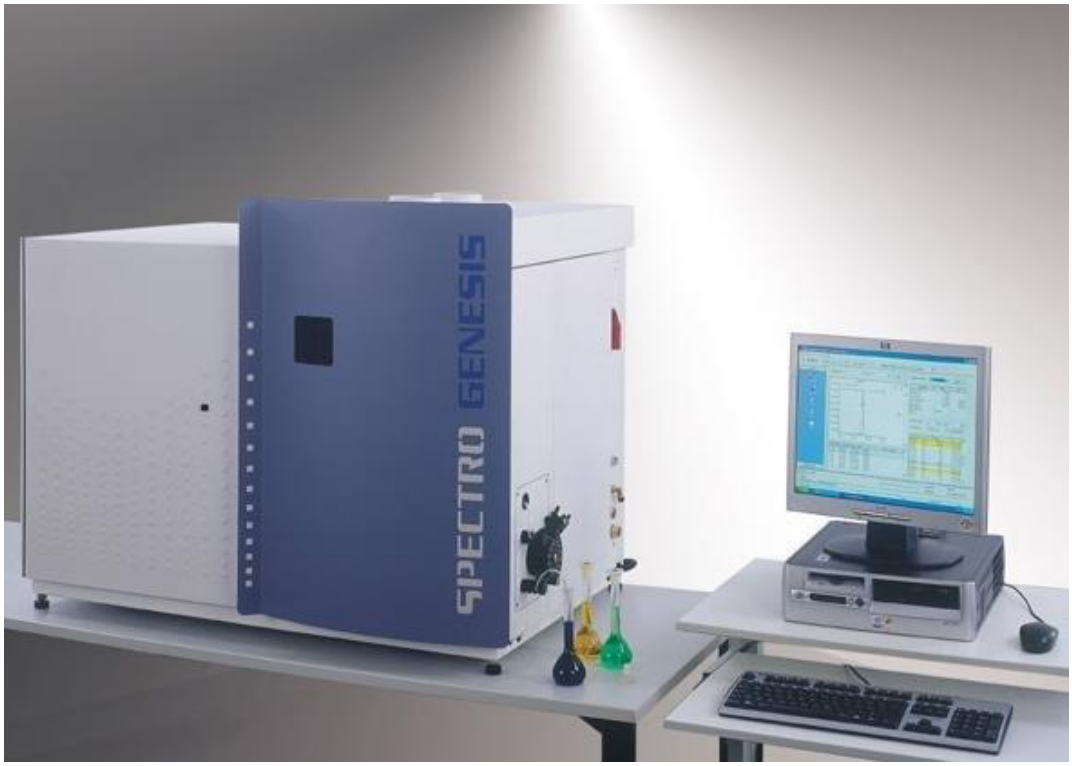

Figure 2.3.4 Spectro Genesis ICP – OES

ii. Experimental

Since ICP-OES system is a very sensitive system, each equipment used in the measurement is cleaned properly. A standard method was formed for the quantification of the analyses. Therefore, ICP-OES standards for rhenium and boron were purchased and different concentrations of those solutions were prepared. For the characterization of ReB_2 and Re_7B_3 compounds, samples were dissolved in HNO_3 and then diluted to 50 ml. Results obtained from analyses was sensitive in ppm level.

2.3.3. Field Emission Scanning Electron Microscopy

The Field Emission Scanning Electron Microscopy (FESEM) measurements were carried out in a Zeiss Evo Ultra Plus 40 SEM furnished with a LaB_6 electron source.

Figure 2.3.5 Zeiss Evo Ultra Plus FE-SEM

2.3.4. Magnetic Susceptibility Measurements

i. Theory

Magnetic susceptibility measurements were performed to determine the ratio magnetization of the samples in an applied magnetic field. The magnetic susceptibility of the samples was extracted by taking the linear slope of the inverse magnetic susceptibility with respect to temperature by applying Curie - Weiss law.

The measurements of magnetic susceptibilities of samples were carried out with a Quantum Design's Magnetic Property Measurement System (MPMS XL – 7, Quantum Design). The principle components of this measurement system comprise temperature controller system, magnet control system, superconducting SQUID (superconducting

quantum interference device) amplifier system, sample handling system and computer operating system.

ii. Experimental

To do the measurements, the samples were sealed inside a pre-calibrated thin walled quartz tube (wall thickness 1 mm) under a He-pressure of 400 mbar. The magnetic susceptibilities were measured in the temperature range of 1.8-300 K with a fixed magnetic field from 20 Oe to 70 kOe (1Oe=79.6 A/m).

2.3.5. Specific Heat Capacity Measurements

i. Theory

The amount of heat which must be supplied to raise the temperature of unit mass by one degree is called as the specific heat. Heat capacity or the specific heat is determined mainly by the lattice structure. The vibration of a crystal lattice is related to the heat content of the system and so to the thermodynamic temperature.

ii. Experimental

Low-temperature specific heat, C_p, was measured in the temperature range 1.8-320 K using a thermal-relaxation type micro-calorimeter in a ^{3}He cryostat. A big piece of specimen (≈30mg) was thermally anchored with small amount of an Apiezon N grease (≈0.06mg) to a sapphire holder on which thin films of ruthenium oxide and nickel-chromium alloy were deposited to serve as a temperature sensor and joule-heating

element, respectively. The holder then was thermally linked by four Au-Cu alloy wires to a temperature regulated copper block. The heat capacity of the sample holder and grease were measured separately for addenda correction.

2.3.6. Hardness Measurements

i. Theory

Hardness is indicated in various ways. It can be basically defined as resistance of materials to deformation, usually by indentation. The term may also refer deformation from scratching, abrasion, cutting or bending. The deformation is considered as plastic deformation of the surface in the hardness tests for metals, ceramics and most polymers. On the other hands, elastic deformation of the surface takes places for elastomers and some polymers. Hardness is usually explained as the combination of yield strength, work hardening, true tensile strength, modulus and other factors because there is no single definition of hardness.

Hardness measurements are the most widely used mechanical test of examining the properties of metals and other materials. They determine the suitability of a material for an application. They are simple, easy and nondestructive.

For metals and alloys, indentation hardness tests are mostly employed. The indentation hardness is the resistance of a material to indentation. This is the usual type of hardness tests. In this type of tests, a ball, cone, or pyramid is pressed into a surface under a substantially static load. The relationship of load to the area or depth of indentation is the measure of hardness. Rockwell, Vickers, Brinnel and Knoop are the most common types of this category. The hardness may be defined by measuring the depth of indentation in Rockwell technique while the measuring the indentation area is valid for Vickers, Brinnel and Knoop.

Recently, the hardness tests are divided into two groups: macrohardness and microhardness depending on the applied forces and obtained displacements. If the applied load on the indenter is more than 1 kg, it is macrohardness testing. If the applied load is 1 kg or below, it is called as microhardness testing.

The Vickers hardness test has been developed in the early 1920s. The Vickers microhardness tester is the most common technique for the indentation method in Figure 2.3.6.a. It has a diamond indenter which has a square pyramid shape with the angle of 136 degrees between the opposite faces in Figure 2.3.6.b. After a full load was applied for 10 or 15 second, there remains a plastic deformation on the surface of specimen as it is seen in Figure 2.3.6.b. The Vickers hardness is calculated from the residual indentation. The average value for the diagonals of the residual indentation was taken and applied into equation 2.2:

$$HV = \varphi \frac{P}{d^2} \qquad \text{(Eq. 2.2)}$$

where HV is the Vickers hardness (kg/mm^2), P is the applied load (kg), d is the indentation length of the diagonal (mm), and φ is the constant depending on the specific indenter geometry. φ has the value of 1.8544 for Vickers indenter. Recently, hardness values have begun to be given in gigapascals (GPa). Thus, the results obtained from the equation X.1 is converted to GPa by multiplying a factor of 0.009807.

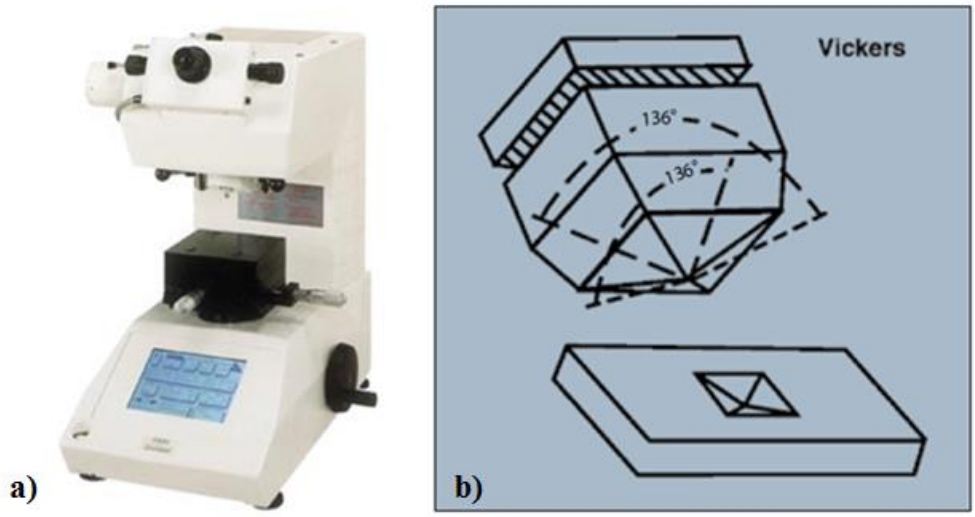

Figure 2.3.6 a) HMV-2 Series Microhardness Tester **b)** Schemetic of the Vickers indenter and the shape of an impression

ii. Experimental

For sample preparation, all samples were encased in a slow-curing epoxy resin. These ingots were polished using 120, 240, 360, 480, 600, 1200, and 2400 mesh silicon carbide sand papers to get fine measurement surfaces. Finally, they were shined with diamond polishing grease on velvet sand paper under water flow to prevent surface burning. The microhardness tests were performed on HMV Shimadzu conventional microhardness tester. In Figure 2.3.7, the indenter of hardness terster is illustrated. There are several applied load options, they all are tabulated Table 2.3.3. Five to ten indents were made with diamond tip at each load, from 490.9 mN to 9.807 N. The average value for the diagonals of the residual indentation for each load was taken separately using an attached camera.

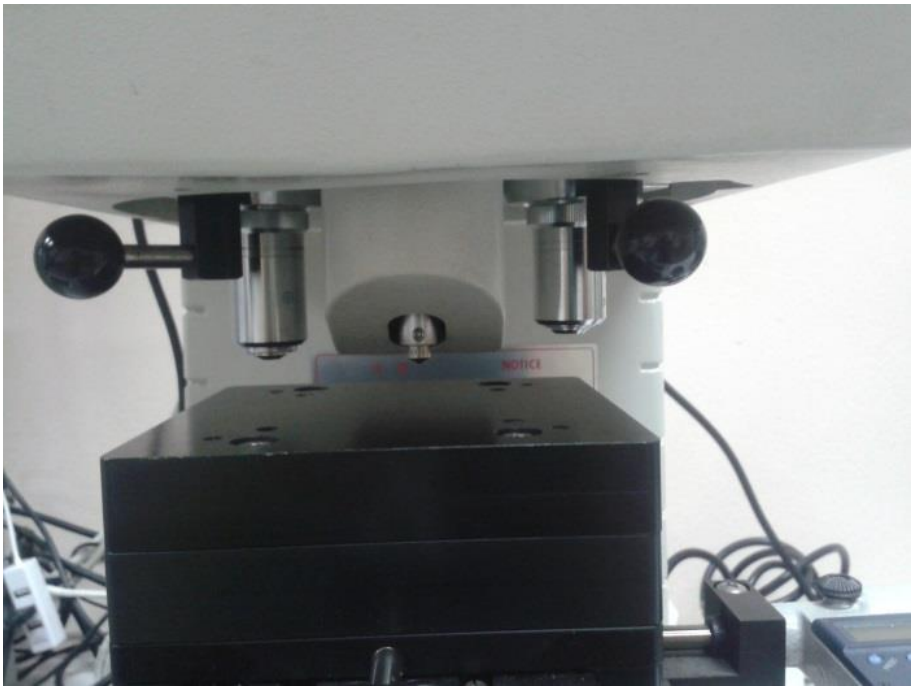

Figure 2.3.7 The Vickers indenter of HMV Shimadzu microhardness tester

In Table 2.3.3, possible loads of HMV Shimadzu microhardness tester are listed.

Table 2.3.3 Options of applied loads in N and HV

Load options	HV
98.07 mN	0.01
245.2 mN	0.025
490.3 mN	0.05
980.7 mN	0.1
1.961 N	0.2
2.952 N	0.3
4.903 N	0.5
9.807 N	1
19.614 N	2

2.3.7. Wear Test

i. Experimental

A micro-scale abrasion test has recently been developed that allows measurement of the wear resistance of the surface regions of a material. The typical penetration depth is less than 30 μm. The test uses a simple mechanical and optical system and involves rotating a hard steel sphere against a specimen in the presence of small abrasive particles. The method has been used to investigate the wear resistance of thin PVD coatings (1 to 5 μm), metallic glass ribbons, and paint films in addition to bulk samples of metals, ceramics, and glasses.

ii. Experimental

Wear tests applied to specimens which embedded into epoxy resin were conducted by Tribotester device with reciprocating movements. The used WC ball rubbed on the polished surfaces of the samples under the conditions of the temperature range of 20-30^{o}C and the humidity rate between 30-40%. The testing time is approximately 5 h 30 min. The length of the wear track is 6 mm and the sliding speed of the WC ball is 4,00 mm/s. During wear tests, the frictional force data was recorded constantly. The load of the dry sliding wear test was 6 N. Results of the wear test were analysed by the 2D profiles of the wear tracks. The horizantal and vertical distances of the wear tracks were measured by the profilometer (Veeco Dectac 6M) under the load of the stylus of 1 mg and the measured distance of 1000 μm.

Chapter 3

Rhenium Diboride (ReB_2)

3.1. Experimental Procedure

For the synthesis of ReB_2, excess amount of boron has been applied by the most of the techniques because of the evaporation loss of boron during the high temperature reactions, especially in arc melting technique. Eventually, this makes higher the risks to produce the final product with unreacted boron. The samples with the starting molar ratios of Re:B from 1:4 to 1:7 clearly form ReB_2 by our group, probably in coexistence with excess boron. Unfortunately, the excess amorphous boron is not detectable by X-ray diffraction. As a result of excess boron, the amorphous boron would affect the hardness of ReB_2.

To investigate the effect of excess boron in the final product, a set of ReB_2 was designed with different boron contents. The flow diagram of the experimental progress is given in Figure 3.1.1. In the present study, the arc melting synthesis conditions of ReB_2 with the range of excess boron and the purification methods have been researched. To reduce remained amorphous boron from the system, different methods have been investigated: dissolving final product in diluted HNO_3, and cracking final product and re-melting ReB_2. Additionally, crystal boron was used as a reactant instead of amorphous boron to investigate the effect of boron quality on the ReB_2 synthesis.

Consequently, chemical, physical, and mechanical properties of the final products were measured with XRD, ICP-OES, EDSX, SEM, micro indentation Vickers hardness test and wear test, as a function of boron content.

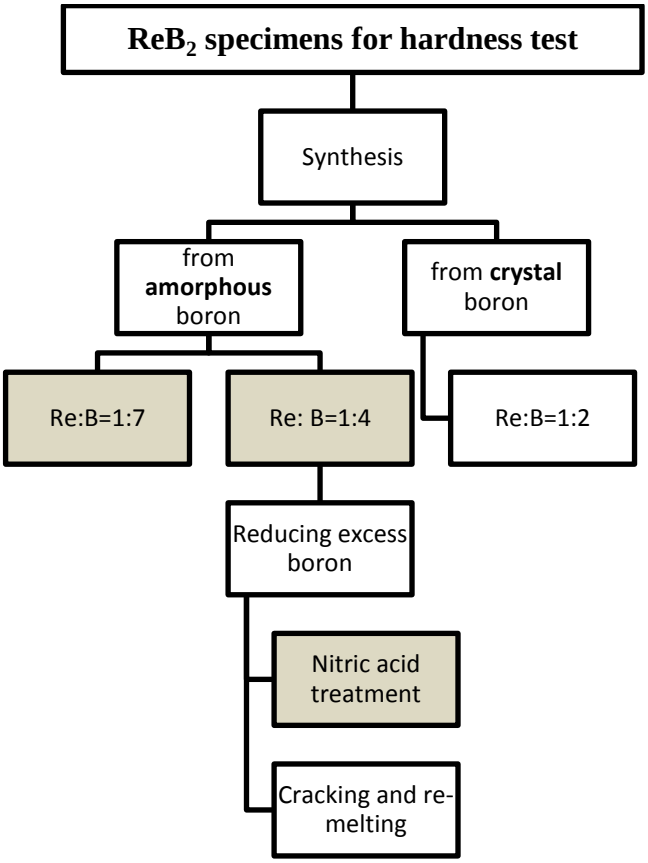

Figure 3.1.1 Flow diagram of selecting proper ReB_2 specimen for mechanical tests

3.1.1. Synthesis

Rhenium diboride was synthesized by arc melting the elements under argon atmosphere. Starting composition of Re:B was defined as 1:4 and 1:7 according to previous study of our group. As explained before, excess amount of boron was used to compensate the evaporation loss of boron during the high temperature synthesis because the vapor pressure of boron is much higher than rhenium. The Re- B mixture was pressed into a pellet with diameter of 13 mm. After the pellet was positioned on the water cooled copper hearth, the reaction chamber was evacuated and refilled several times with argon to minimize air contamination. The pellet was melted 2-3 times after repositioning the pellet upside-down to ensure chemical homogeneity.

3.1.2. Removing excess boron

Removing excess boron from ReB_2 has not been studied previously. It is the first time ever investigation reducing excess boron from the ReB_2 system. For the arc melting synthesis of ReB_2, two different starting boron ratio were defined as Re:B=1:4 and 1:7 according to our previous study. Since there is no information how to reduce boron from the system, we have started with the two different ideas.

First, ReB_2 specimen with the ratio of Re:B=1:4 was again made fine powder and washed with diluted nitric acid (HNO_3) to reduce excess boron from the final product. Boron normally does not react with acids but in powder form, boron is oxidized by nitric acid to boric acid (H_3BO_3). The chemical equation is shown below:

$$3\ HNO_3 + B \rightarrow H_3BO_3 + 3\ NO_2$$

Since nitrogen dioxide (NO_2) is toxic acid, the washing ReB_2 was handled under hood because of safety issues. During the reaction the red brownish color of NO_2 was observed. Boric acid is soluble in boiling water. So, it was removed from the system by washing with hot water. During the experiments, we observed that nitric acid reacts even with ReB_2 depending on the concentration of nitric acid. Therefore, we need to optimize the concentration of nitric acid enough to react with amorphous boron but not ReB_2.

In order to optimize concentration of nitric acid, amorphous boron powder was put into 20 test tubes. Different concentration of nitric acid, varying from 7 M to 1 M, was added into test tubes. As a control group, water was added into test tube instead of nitric acid. Then, the observations were recorded as a function of time. As a result of macroscopic observations, suitable concentration of nitric acid was roughly determined as 2-3 M.

Secondly, we took the ReB_2 specimen with the starting composition of Re.B=1:4 and grinded it until to get a fine powder using tungsten carbide mortar. Then, the ReB_2 powders were pressed into pellet. Finally, the arc melting reaction was repeated with the same conditions.

Additionally, the difference of the synthesis of ReB_2 from amorphous boron and crystal boron was also investigated to get pure phase of ReB_2.

3.1.3. Preparation for mechanical tests

Before mechanical tests, all samples were encased in a slow-curing epoxy resin. The Figure 3.1.2 b illustrates the final product in epoxy resin. To get fine measurement surfaces, these ingots were polished with 120, 240, 360, 480, 600, 1200, and 2400 mesh silicon carbide (SiC) sand papers. During the polishing, isopropyl alcohol or distilled water was used to avoid surface burning. Finally, they were shined with diamond polishing grease on velvet sand paper. After polishing, all samples were cleaned with water and dried. Finished forms of the ingots are shown in detailed in Figure 3.1.2 and Figure 3.1.3.

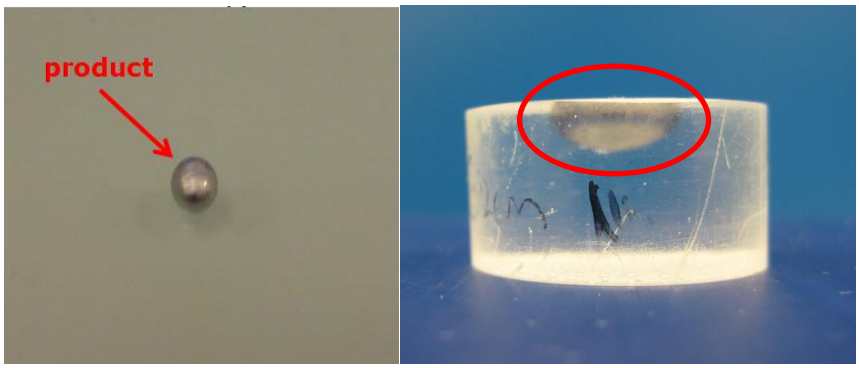

Figure 3.1.2 a) Arc melted product **b)** The same product encased into slow curing epoxy resin

Figure 3.1.3 Polished sample with the radius of 6.58 mm

3.2. Results and Discussion

There is a controversial Vickers hardness range of ReB_2, as stated in introduction section. This large range, reported as 20 GPa to 48 GPa, causes an argument on whether ReB_2 is a superhard material or not. In order to clear this point and understand the actual hardness, we have examined how hardness of ReB_2 changes depending on the excess boron in the compound.

As mentioned in experimental section, arc melting synthesis of ReB_2 is only possible when excess amount of boron was employed. Until now, there is no clear information how much excess boron should be applied at the beginning of the experiment. Uslu *et. al.* showed that ReB_2 was successfully synthesized with the starting ratio of elements from Re:B= 1:4 to 1:7 by arc melting technique. Attempts –lower than Re:B=1:4 and higher than Re:B=1:7- ended up with the side product of Re_3B or Re_7B_3. Therefore, the ratios of Re:B= 1:4 and 1:7 were chosen as starting ratio to synthesize ReB_2 and examine their effect on mechanical properties of ReB_2.

In this thesis, synthesis of ReB_2 with different boron amounts, investigating of the effect of excess boron in ReB_2 system on its mechanical properties and finally removal techniques of excess boron from the ReB_2 system were studied.

3.2.1. Effect of excess boron in ReB_2 system on mechanical properties

i. Crystal structure analysis of ReB_2

Since there is no previous study on effect of excess boron on hardness of ReB_2, we have determined two starting boron ratio to synthesize ReB_2. One is **Re:B=1:7** which is the highest boron ratio to synthesize ReB_2 and the other is **Re:B=1:4** which is the

lowest boron ratio. The two ReB_2 products with different starting boron contents were analyzed by X-ray diffraction (XRD) technique. The syntheses of the desired ReB_2 are monitored by powder XRD in Figure 3.2.1.

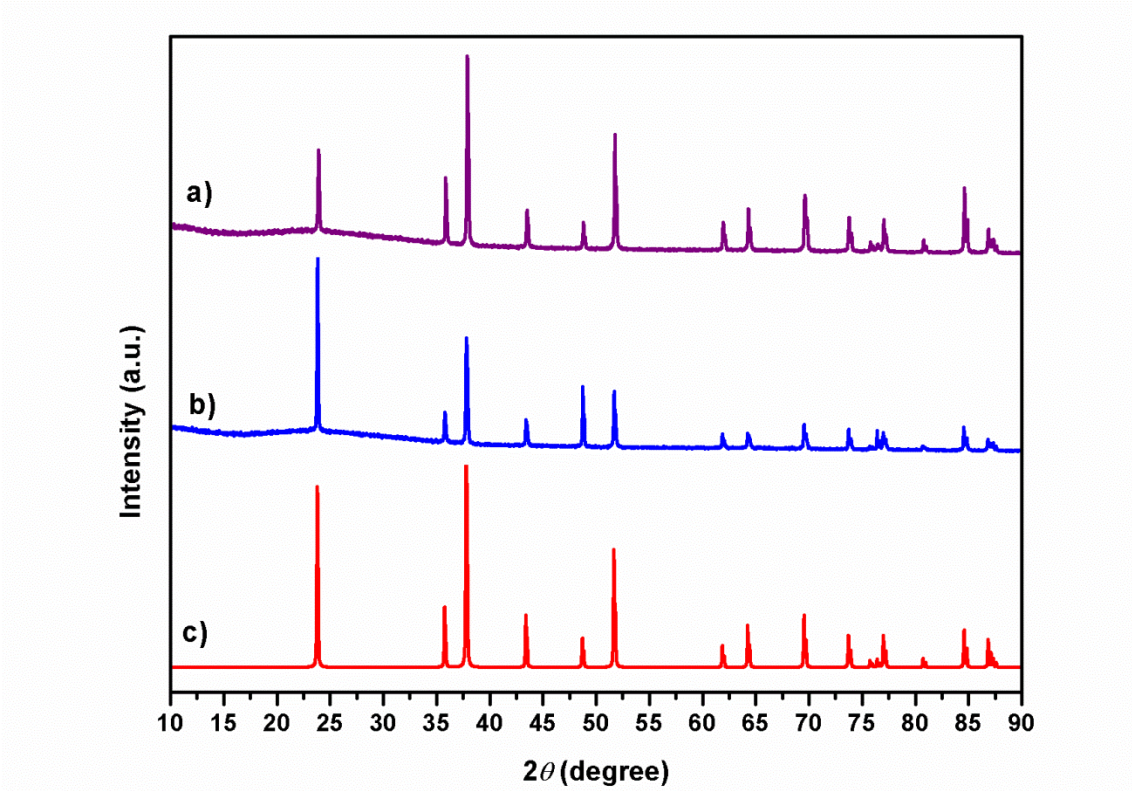

Figure 3.2.1 X-ray diagram of (a) ReB_2 with the starting molar ratio Re:B = 1:4 and (b) ReB_2 with the starting molar ratio Re:B = 1:7 in comparison with (c) the theoretical ReB_2 (ICSD, card number 11-581)

Figure 3.2.1 shows the XRD patterns of (a) ReB_2 with the starting ratio Re:B= 1:4, (b) ReB_2 with the starting ratio Re:B=1:7 in comparison with (c) the theoretical XRD pattern of ReB_2. According to the XRD results, it is clearly seen that peak positions of both samples are exactly the same with the calculated peak positions of ReB_2. For the calculation of peak positions, hexagonal type unit cell was used. Although they have different initial boron ratios, XRD patterns are indicated that they both ended up with the ReB_2, probably in coexistence with excess unreacted amorphous boron.

ii. Compositional analyses of ReB_2

To investigate the exact chemical compositions of ReB_2 products, chemical analyses were performed by Inductively Coupled Plasma Optical Emission Spectroscopy (ICP-OES). Based on the chemical analysis results, there is excess amount of boron in the final products. According to the results of ICP-OES measurements of ReB_2 samples, the sample compositions correspond to $ReB_{3.5}$ and $ReB_{5.5}$ for the samples with starting molar ratios of Re:B = 1:4 and Re:B = 1:7, respectively. Hence; starting from molar ratios of Re:B = 1:4 and 1:7 ended up with the surplus of unreacted boron. The excess boron amount in the final product increased with the increase of the starting boron ratios, dramatically. For further investigation, Energy Dispersive X-ray Spectroscopy (EDXS) measurements were performed to check other impurities. Figure 3.2.2 and Figure 3.2.3 show the EDXS results of ReB_2 samples.

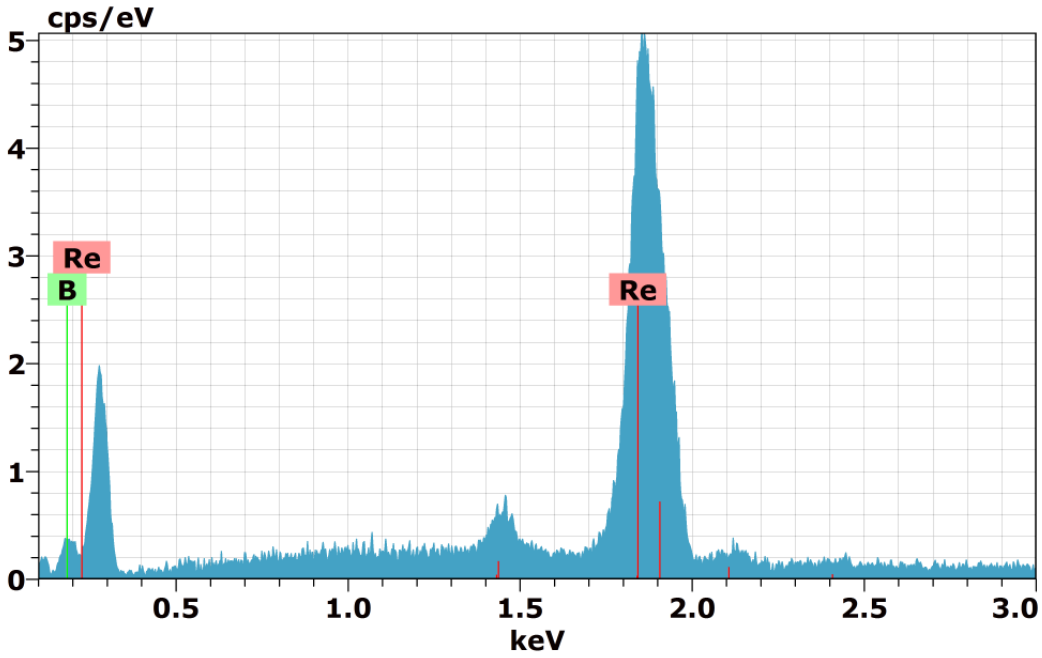

Figure 3.2.2 EDXS analysis of ReB_2 specimen with the starting boron composition Re:B=1:4

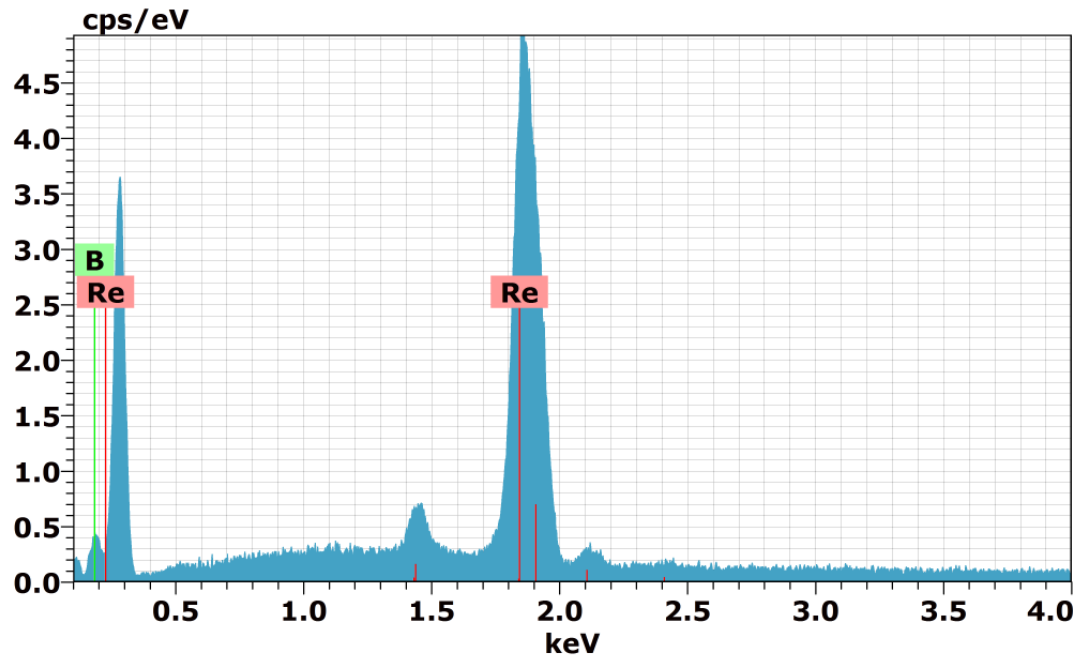

Figure 3.2.3 EDXS analysis of ReB_2 specimen with the starting boron composition Re:B=1:7

EDXS analyses of both ReB_2 specimens indicated the existence of rhenium and boron. Results clearly confirmed that no oxygen or any other impurity was incorporated into the target compound ReB_2. Hence; ReB_2 specimens were successfully produced with the different boron amount without other impurity phases.

iii. Mechanical properties of ReB_2

To investigate the actual hardness and the effect of excess boron on the mechanical properties of ReB_2, Vickers hardness test and wear test were performed.

Vickers hardness test

Vickers micro-hardness indentation technique was employed to evaluate the hardness of the arc-melted ReB_2 samples. A square pyramidal-shaped diamond indenter tip was inserted into a polished ingot within the range of 1 to 5 Newton force. After 10 seconds, tip was removed and it caused a plastic deformation on the surface. A sample of an indentation mark was shown in Figure 3.2.4. To determine the Vickers hardness, five indentations were made under applied loads for each sample.

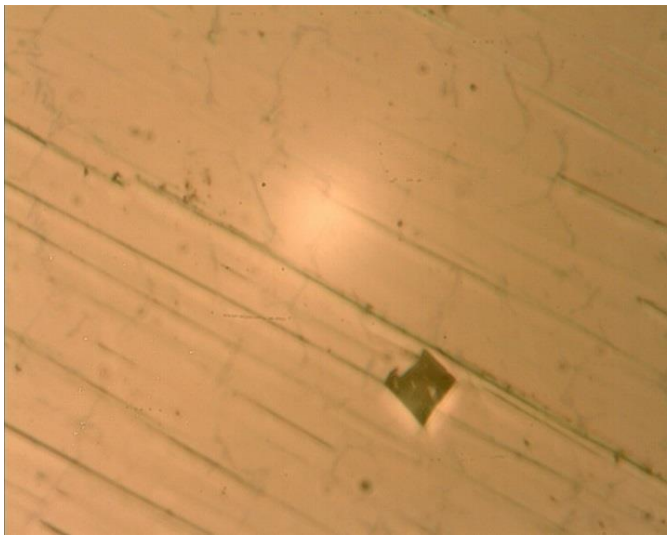

Figure 3.2.4 A representational indentation mark on a specimen surface

First hardness measurement was performed on ReB_2 sample with the starting molar ratio of Re:B=1:4. Figure 3.2.5 shows the Vickers micro-hardness results of arc melted $ReB_{3.5}$ as a function of the indentation load of 1N and 2N.

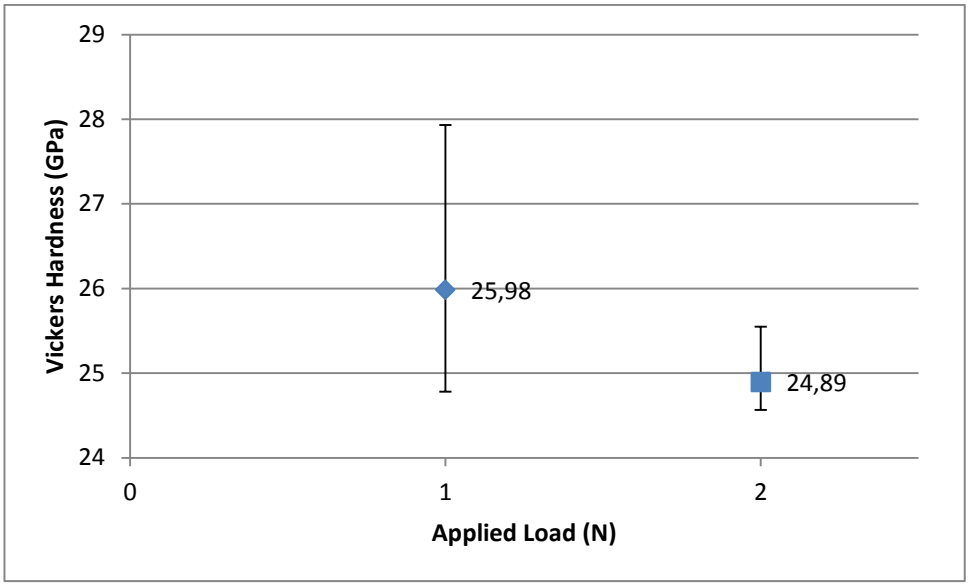

Figure 3.2.5 Vickers micro-hardness results of arc-melted ReB_2 sample with the starting molar ratio of reactant Re:B=1:4 as a function of the indentation load of 1 and 2N

In Figure 3.2.5, the X axis shows applied force to the surface with the unit of Newton and y axis represents the Vickers micro-hardness with the unit of GPa. The average hardness values are shown with the error bar. Under 0.5 N, the indentation deformation was not detectable. At forces greater than 2N, crack formation from the edges of the indentation mark was observed, likely due to the brittleness of the material. Therefore, measurements were performed under applied load of 1N and 2N, properly. The maximum hardness was observed as 25.98 ±1.2 GPa under applied load of 1N. The hardness of the sample decreased to 24.89 ±0.66 GPa as shown in Figure 3.2.5. This value steadily decreased with increasing load due to the well-known indentation size effect.[57] It is basically related with strain gradient plasticity under the indenter.[20] When the indentation test force increases, the indentation size becomes larger and volume about the indentation also increases. This activates multiple slip systems and causes larger plastic deformation on the material. So, this extensive multiple slip significantly decrease the hardness value at high load.

Second hardness measurement was performed on ReB_2 sample with the starting molar ratio of Re:B=1:7. The Vickers micro-hardness results of arc melted $ReB_{5.5}$ was presented in the Figure 3.2.6 as a function of the indentation load of 2N and 3N.

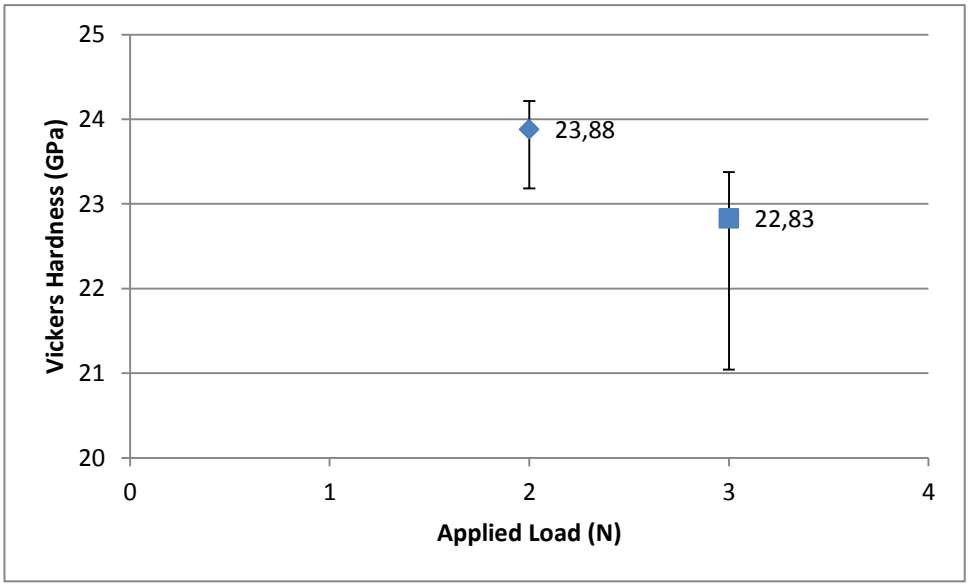

Figure 3.2.6 Vickers micro-hardness results of arc-melted ReB_2 sample with the starting molar ratio of reactant Re:B=1:7 as a function of the indentation load of 2N and 3N

At forces lower than 2 N, the indentation marks were too small to detect due to the quality of the surface of the sample. At forces greater than 3N, the indentation tented to collapse. Therefore, measurements were performed with the applied load of 2 N and 3 N. Figure 3.2.6 exhibits that the hardness of the arc-melted ReB_2 ingot was 23.88 ±0.34 GPa and 22.83 ±1.2 GPa, under a load of 2 and 3 N, respectively.

In order to compare the different boron content on the hardness value clearly, micro-indentation data of $ReB_{3.5}$ and $ReB_{5.5}$ were reported in the same graph. Since 2 N was the common applied load value, the graph for Vickers hardness of $ReB_{3.5}$ and $ReB_{5.5}$ was drawn according to applied load of 2 N. In Figure 3.2.7, Vickers micro-hardness test results for ReB_2 were shown depending on the boron content of ReB_2 compound.

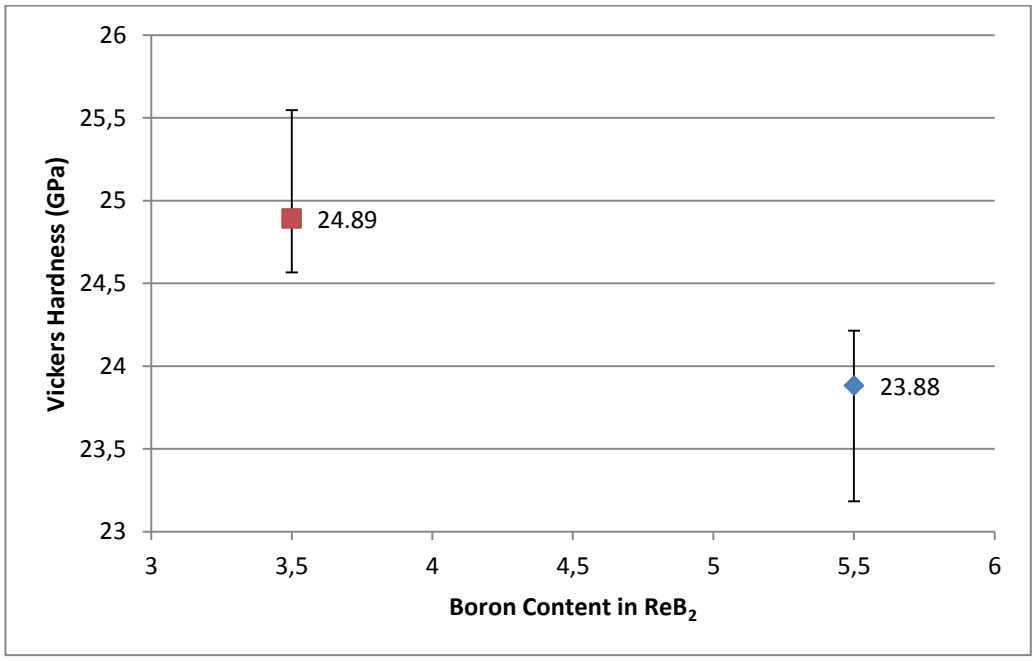

Figure 3.2.7 Vickers micro-hardness test results for ReB_2 depending on the boron content in the compound under 1.961 N for 10 seconds.

According to Figure 3.2.7, as the free boron content increased from $ReB_{3.5}$ to $ReB_{5.5}$, the average hardness decreased from 24.89 ±0.66 GPa to 23.88 ±0.34 GPa. It is the first graph ever that compares the hardness values of ReB_2 depending on the boron excess in the ReB_2 structure. As reported by the Vickers micro-indentation graph, it clearly indicated that the hardness of ReB_2 decreases when the excess boron amount increases in the compound. Hence, the inverse relationship between excess boron amount and the hardness of ReB_2 was successfully proved by a hardness test for the first time ever.

Wear Test

For further mechanical property investigations, wear tests were applied to ReB_2 for the first time ever by TriboTechnic Reciprocating Tribotester at Istanbul Technical University. Even the maximum parameter is applied for the test, the wear test result shows that the product is resistant to abrasion. The test parameters are not enough to form micro abrasions to measure.

iv. Morphological Analyses of ReB_2

For the further understanding on how boron degrades the mechanical properties of ReB_2, morphological analyses were performed using Field Emission Scanning Electron Microscope (Zeiss Evo Ultra Plus 40 FESEM). For this purpose, FESEM images were collected from ReB_2 samples according to their boron contents. Chemical nature of the observed samples was carried out by EDXS analyses. For the further vision, mapping technique was applied to see easily boron and rhenium distributions on the compound. First FESEM image was presented in Figure 3.2.8.

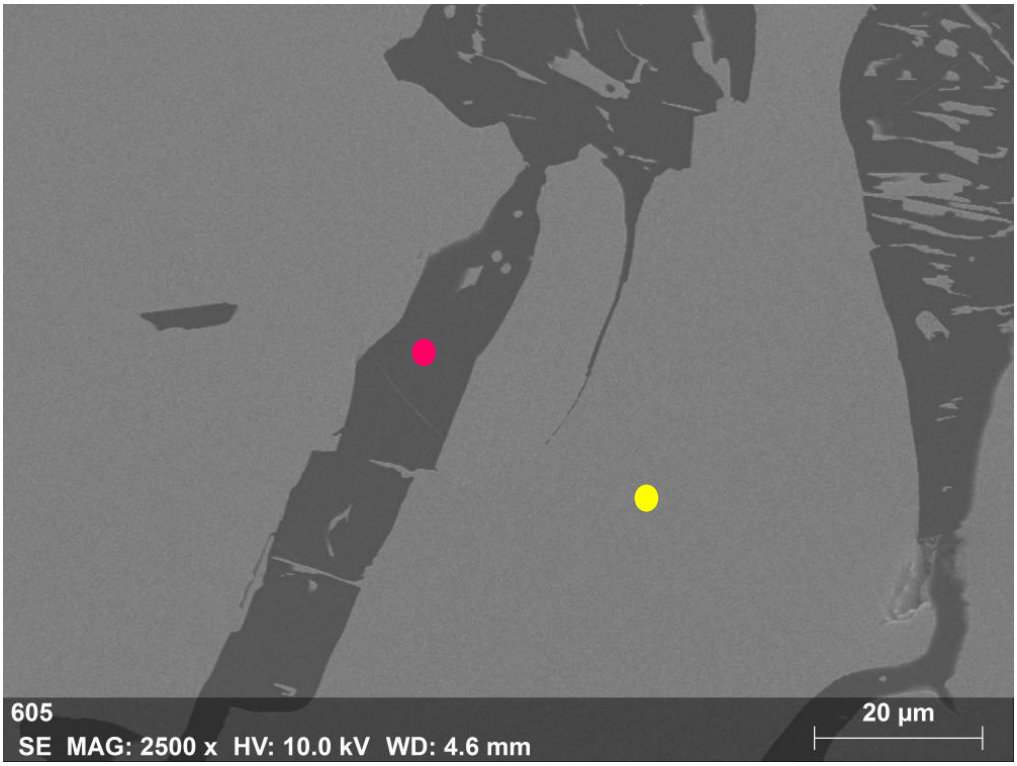

Figure 3.2.8 Scanning electron micrograph of $ReB_{3.5}$

Figure 3.2.8 presents the SEM micrograph of $ReB_{3.5}$. The morphology and the grain size of $ReB_{3.5}$ have been seen with 20 µm scale magnification. The image has bright and dark phases. To confirm the results of the atomic number contrast, we have carried out the EDXS analyses of the chemical nature of the dark and bright phases. So, the bright region which labeled yellow dot and dark region which labeled pink were analyzed. Figure 3.2.9 and Figure 3.2.10 show EDXS analyses of bright and dark regions.

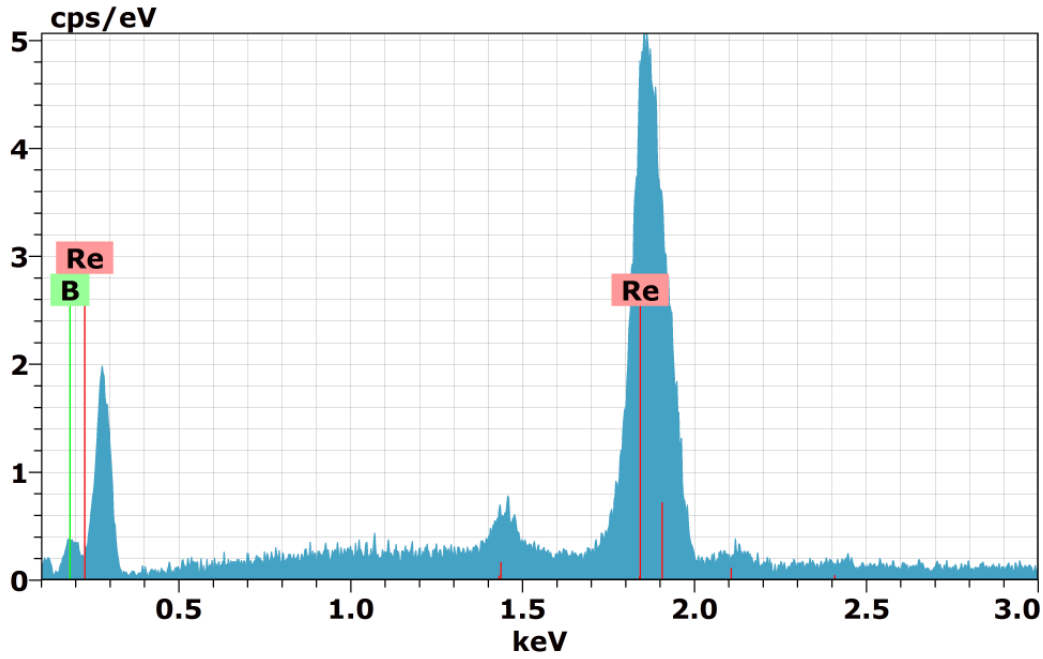

Figure 3.2.9 EDXS analysis of $ReB_{3.5}$ from the bright region which labeled with yellow dot

EDXS results showed that the bright region consists of rhenium and boron in Figure 3.2.9. According to the atomic percentage ratio of elements were detected as 30% for Re and 70% for B. In agreement with the atomic percentage calculation, ReB_2 is located on the bright region as $ReB_{2.33}$ with the little trace of B.

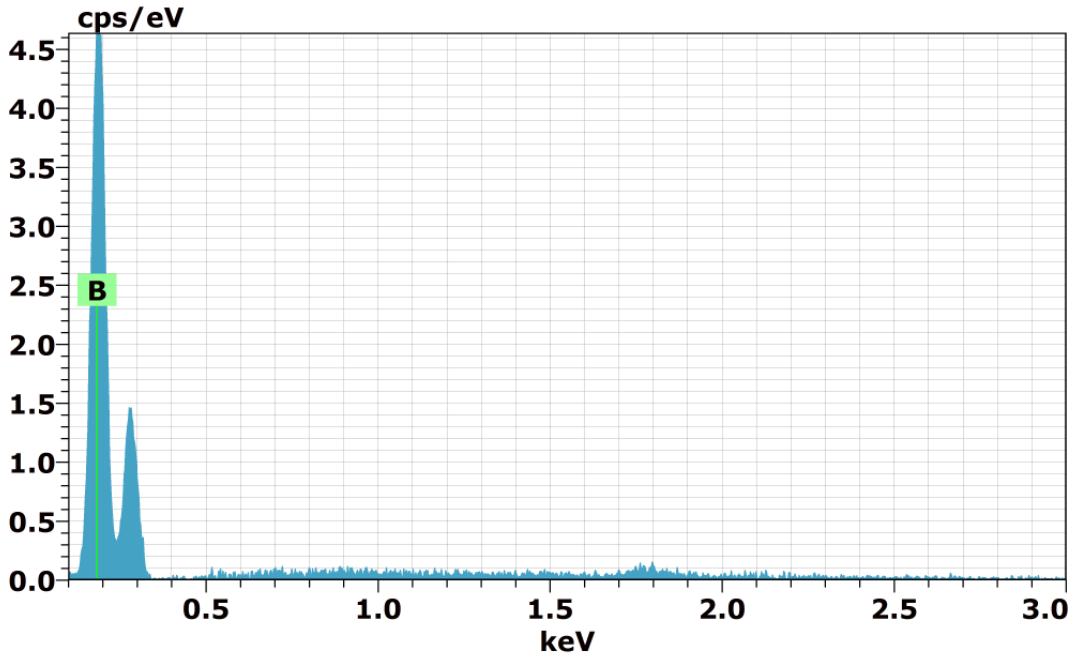

Figure 3.2.10 EDXS analysis of $ReB_{3.5}$ from the dark region which labeled with pink dot

Figure 3.2.10 display that the dark phase consists of only boron, not rhenium. FESEM and EDXS study of $ReB_{3.5}$ showed that there is some of excess boron in the ReB_2 crystal structure which is bright region. After all, the major excess boron is located in between of ReB_2 grain boundaries. For the comparison of boron effect on morphology -thereby on hardness- of the $ReB_{5.5}$, FESEM image was taken with the same magnification. Figure 3.2.11 shows the scanning electron microscopy micrograph of $ReB_{5.5}$.

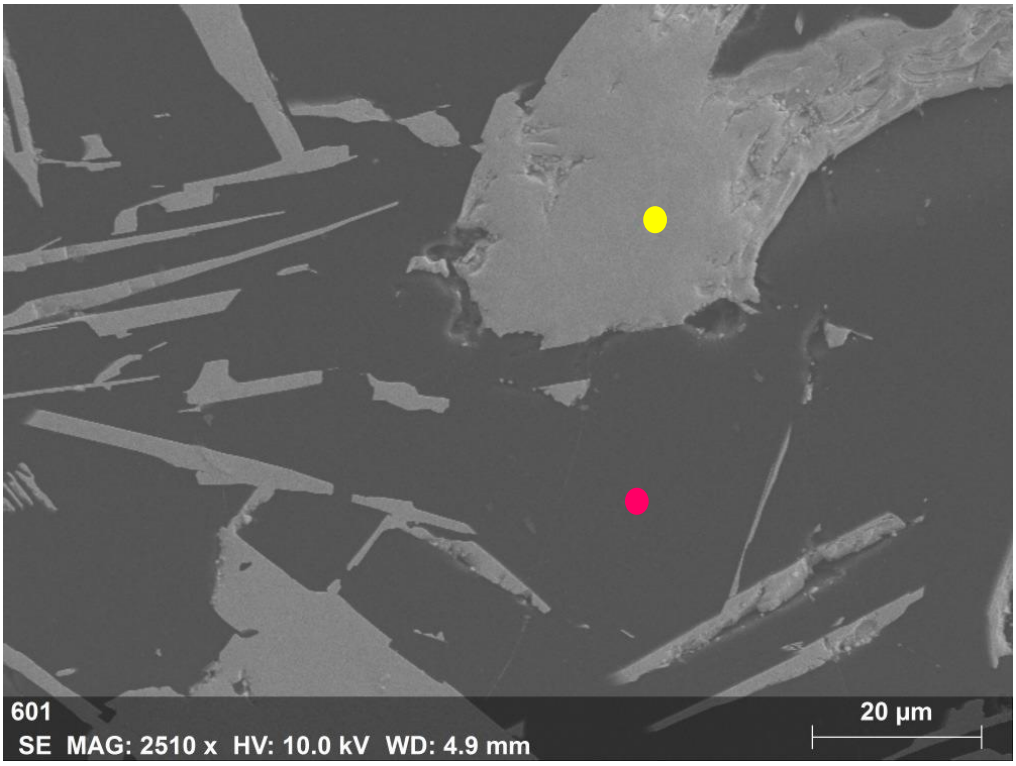

Figure 3.2.11 Scanning electron microscopy image of $ReB_{5.5}$ with 20 µm scale magnification

Figure 3.2.11 presents SEM micrograph of $ReB_{5.5}$ with 20 µm scale magnification. There are dark and bright phases in this image, as like the image of $ReB_{3.5}$. Grains are smaller than $ReB_{3.5}$ and dark regions become domain phase.

To investigate the contribution of rhenium and boron, EDXS measurements were performed. Figure 3.2.12 and Figure 3.2.13 displays the EDXS measurements of the regions labeled with yellow and pink dots.

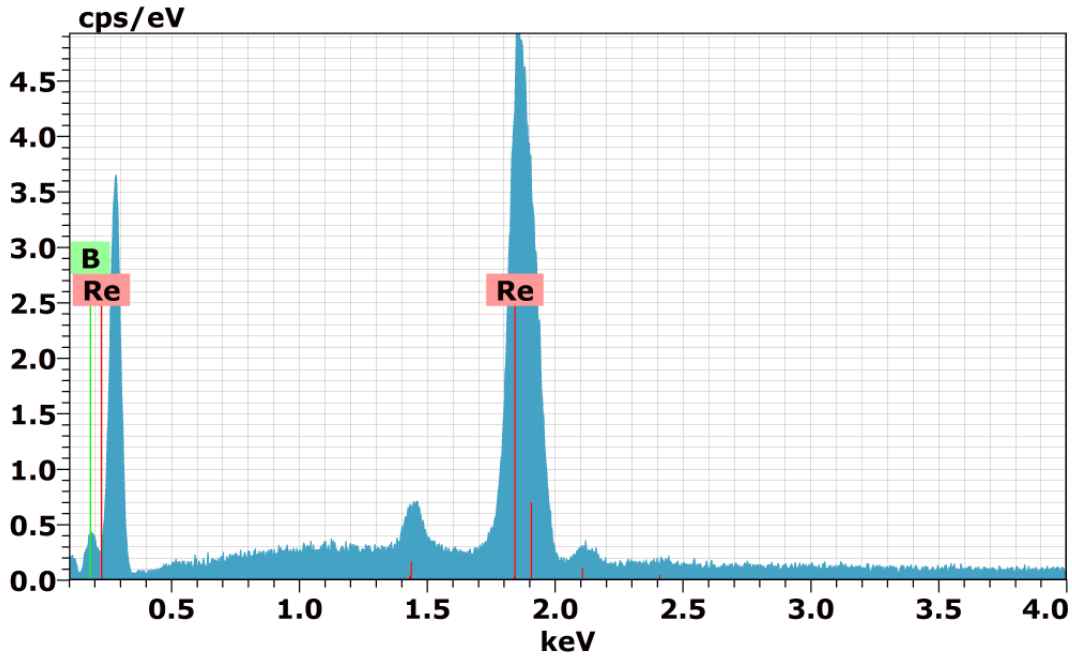

Figure 3.2.12 EDXS analysis of $ReB_{5.5}$ from the bright region which labeled with yellow dot

EDXS analysis, taken from the yellow dot, confirmed that rhenium and boron are located in the bright phase in Figure 3.2.12. Atomic percentage was determined as 32 % for Re and 68% for B. So, ReB_2 is again located in bright phase with the exact chemical composition of $ReB_{2.1}$.

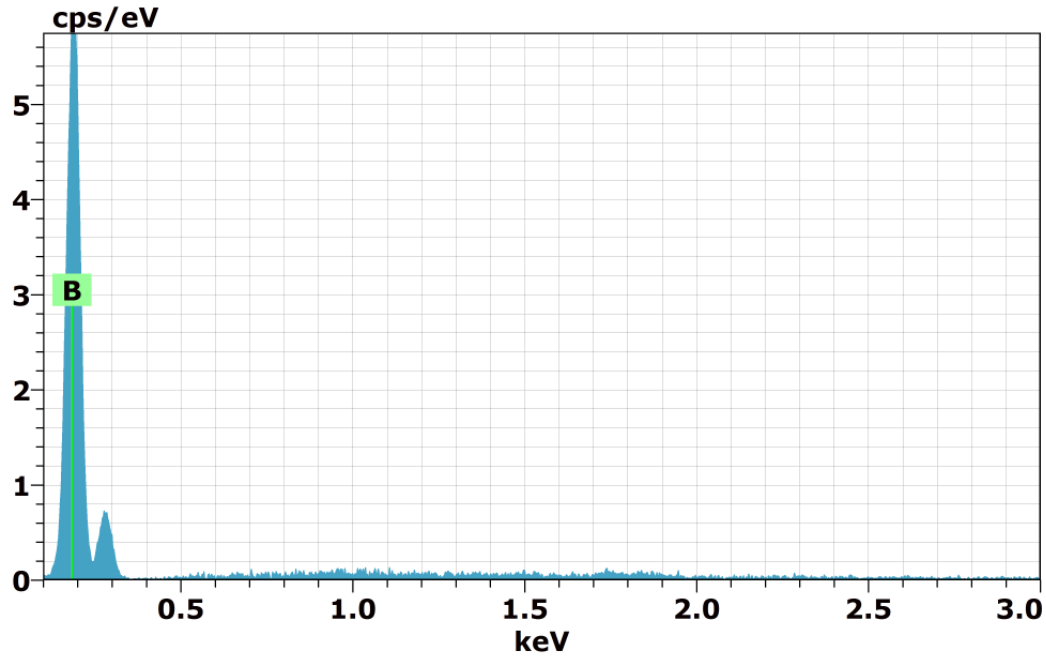

Figure 3.2.13 EDXS analysis of $ReB_{5.5}$ from the bright region which labeled with pink dot

EDXS analysis, taken from the pink dot, indicates the dark region is completely boron in Figure 3.2.13. For further understanding, the bigger picture was shown in the Figure 3.2.14 by using elemental mapping technique.

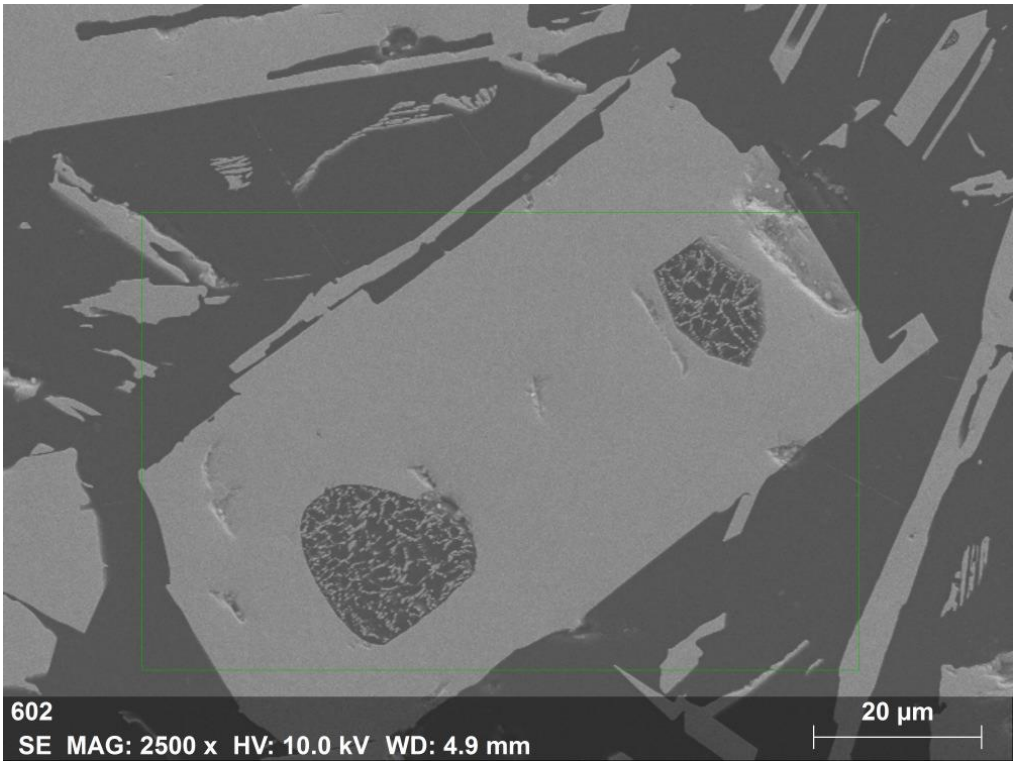

Figure 3.2.14 Another scanning electron microscopy image of $ReB_{5.5}$

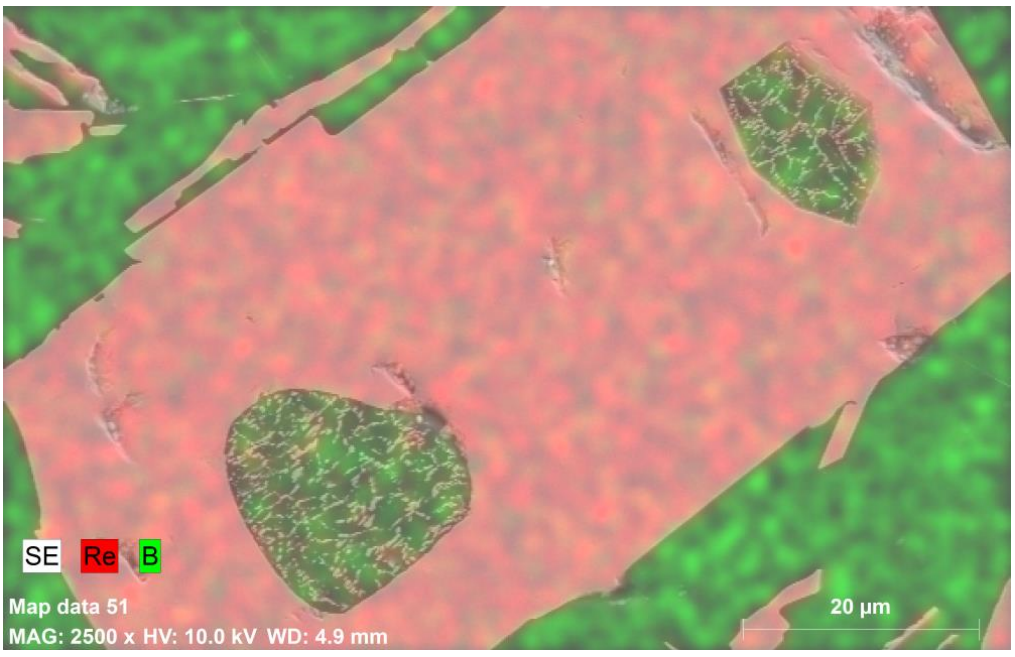

Figure 3.2.15 Rhenium and boron distribution of $ReB_{5.5}$

Figure 3.2.14 turned to Figure 3.2.15 by the mapping technique. The mapping of the rhenium and boron shows that the distribution of Re is not homogeneous as much as B and a high concentration of boron can be seen in the location in between ReB_2 grains.

In order to compare scanning electron microscopy images of $ReB_{3.5}$ and $ReB_{5.5}$, 500 times focused images were taken. Figure 3.2.16 belongs to $ReB_{3.5}$ analysis and Figure 3.2.17 belongs to $ReB_{5.5}$ analysis.

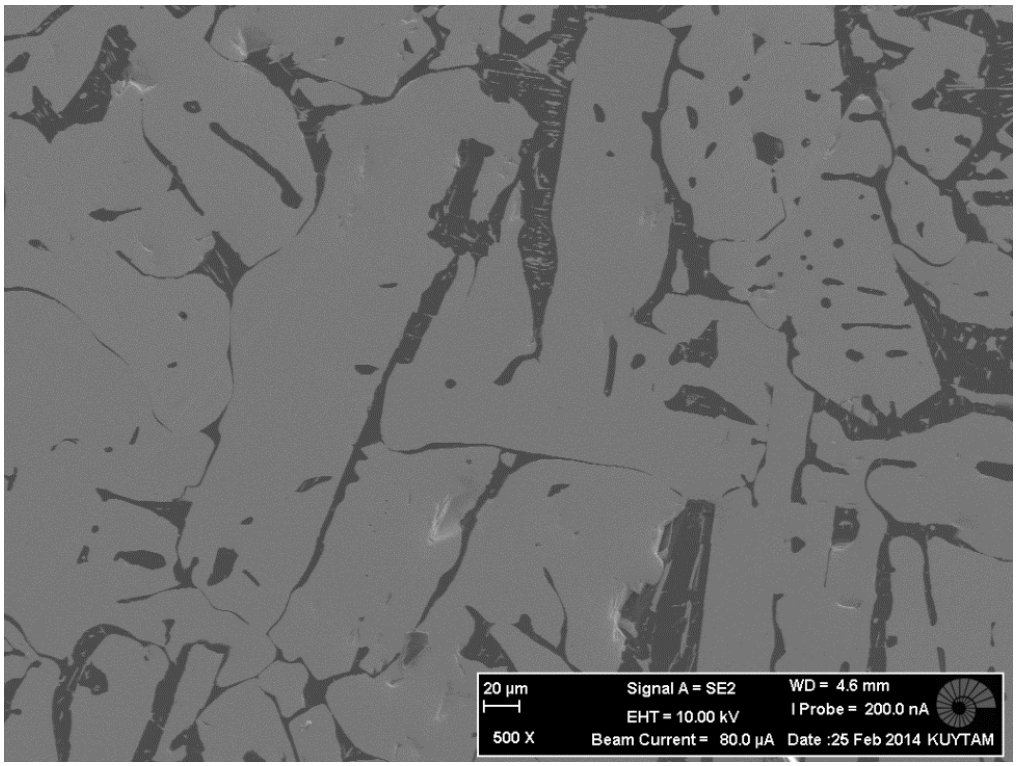

Figure 3.2.16 Scanning electron micrograph of $ReB_{3.5}$ with 500 time magnification

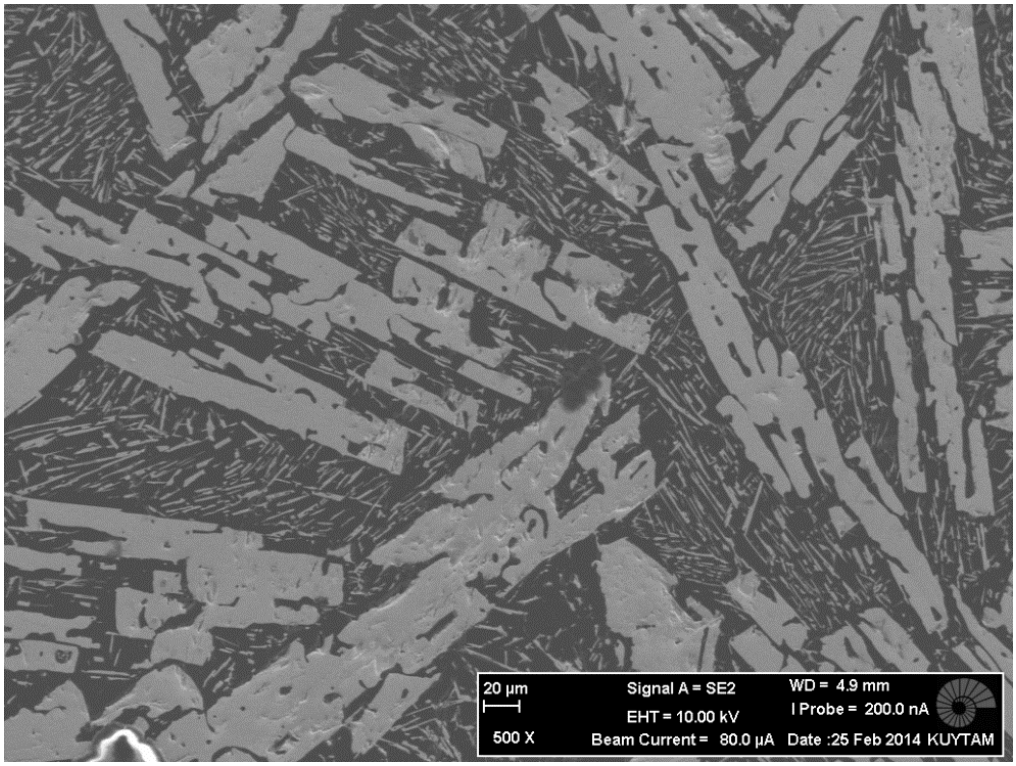

Figure 3.2.17 Scanning electron micrograph of $ReB_{5.5}$ with 500 time magnification

Figure 3.2.17 presents the SEM image of $ReB_{3.5}$. The bright phases – ReB_2- domain higher area in the image. In Figure 3.2.17, by the increase on excess boron in the compound, dark phases become distinguish. These comparison from two images clearly showed that when the boron content increased, ReB_2 integrity gets smaller. As stated before, excess boron is located in the grain boundaries of ReB_2. This excess boron destroys the integrity of the ReB_2 formation. As a result of increase in the excess boron amount, ReB_2 get smaller. Therefore, reducing grain size of ReB_2 explains the decrease on Vickers hardness value of $ReB_{5.5}$.

3.2.2. Further purification

Since the limitation of excess boron on mechanical properties was proved by Vickers micro-indentation hardness test, we focused on how to remove excess boron

from the system. To reduce remained amorphous boron from the system, arc-melted ReB_2 product was dissolved in diluted HNO_3. Then, the samples were investigated by XRD, EDXS, ICP-OES, SEM and Vickers micro-indentation hardness test. Addition to HNO_3 treatment, cracking and re-melting method was studied to reduce boron excess from the ReB_2 system. Both studies successfully decreased the boron excess as aimed.

i. Nitric acid treatment

It is the first time ever investigation of reducing excess boron from the ReB_2 system. As stated in experimental section, boron normally does not react with acids but in powder form. It is oxidized by nitric acid to boric acid (H_3BO_3) as in the following equation.

$$3\ HNO_3 + B \rightarrow H_3BO_3 + 3\ NO_2$$

By washing with hot water, boric acid was removed from the system so that excess boron was removed. Since ReB_2 is thermodynamically stable than elemental boron, nitric acid reacted with available boron in the system rather than ReB_2. However, during the experiments, we observed that concentrated nitric acid reacts even with ReB_2. Therefore, we optimized the concentration of nitric acid enough to react with amorphous boron but not ReB_2. As a result, suitable concentration of nitric acid was determined as 2-3 M.

In order to dissolve the boron excess in 3 M of nitric acid, the pair of the arc melted $ReB_{3.5}$ was grinded with tungsten carbide mortar until a fine powder was obtained. At room temperature, the grinded product was washed several times with 3M of HNO_3 to remove excess boron. After nitric acid treatment, the formation of boric acid was removed from the system. To do that, the powder was washed with hot distilled water. When pH of the powder-water mixture switched from acid to neutral region, washing procedure was completed. The X-ray powder diagram of the washed ReB_2 is shown in Figure 3.2.18.

Crystal structure analysis of $ReB_{3.5}$ after nitric acid treatment

Treated $ReB_{3.5}$ sample with HNO_3 sample was analyzed by X-ray Powder Diffraction (XRD). Figure 3.2.18 shows the XRD data of the HNO_3 treated $ReB_{3.5}$.

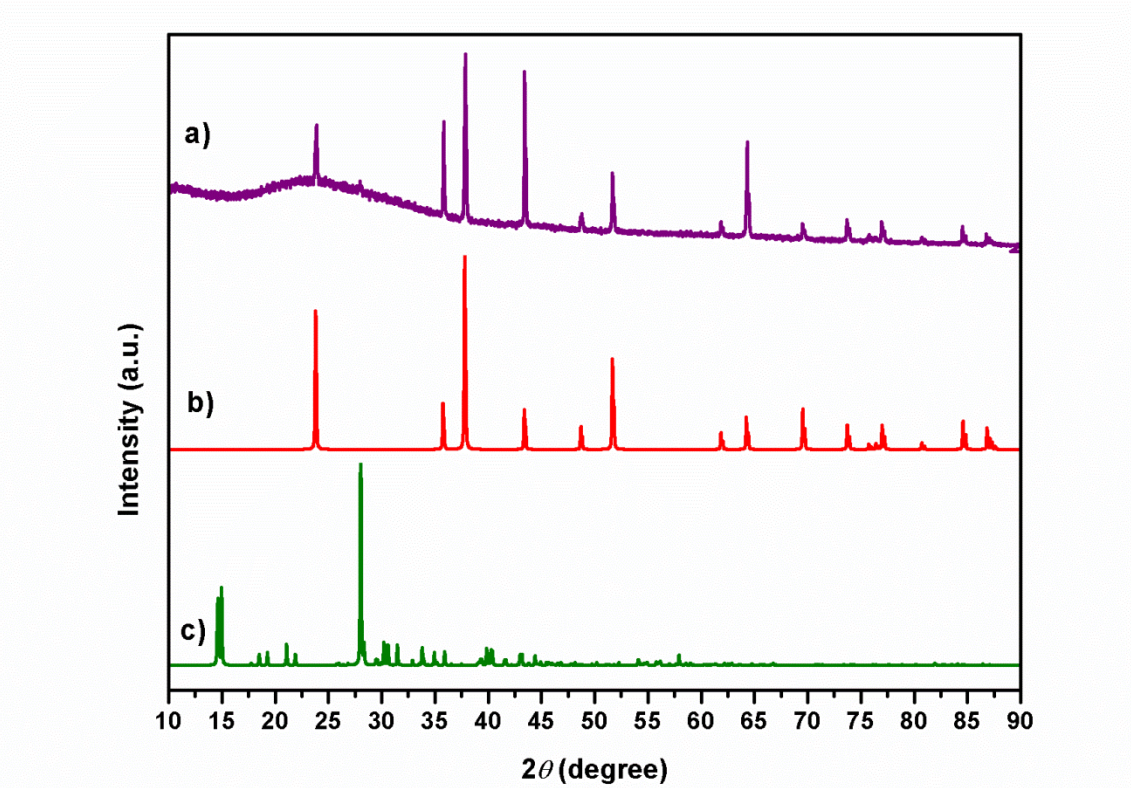

Figure 3.2.18 X-ray diagram of (a) $ReB_{3.5}$ after 3M of HNO_3 treatment in comparison with (b) the theoretical ReB_2 (ICSD, card number 11-581) and (c) theoretical H_3BO_3 (ICSD, card number 73-2158)

Figure 3.2.18 shows the X-ray diffraction patterns of (a) treated $ReB_{3.5}$ with 3 M of nitric acid in comparison with (b) theoretical XRD pattern of ReB_2 and (c) theoretical H_3BO_3. Although the theoretical pattern matches completely with the XRD pattern of sample, there is one unmatched peak remains at 2θ values of 28.006º. This unmatched peak comes from the most intense peak of boric acid (H_3BO_3). Since the amount of the impurity is less, the other peaks of boric acid are not visible on the XRD pattern of the sample.

Compositional analyses of $ReB_{3.5}$ after nitric acid treatment

Elemental analysis of $ReB_{3.5}$ after nitric acid treatment was accomplished by EDXS measurement. Figure 3.2.19 shows the EDXS results of the specimen.

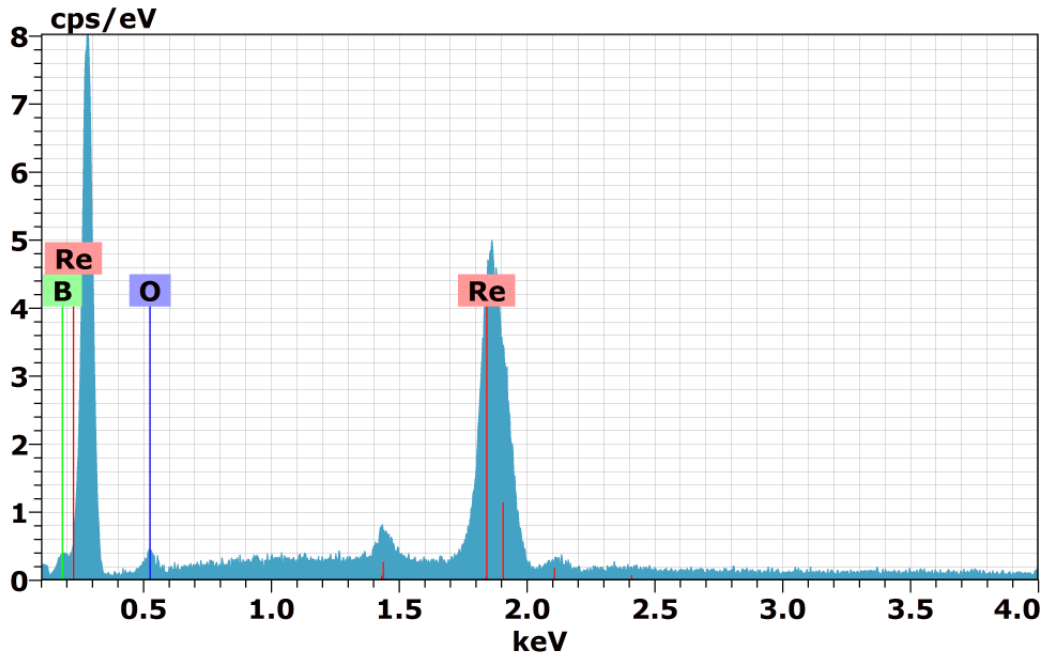

Figure 3.2.19 EDXS analysis of $ReB_{3.3}$ specimen which was treated with HNO_3

Analysis of the final product shows the existence of rhenium, boron and oxygen in the final product. So, elemental analysis confirms that final product is oxidized during the acid treatment. ICP-OES measurements were performed for double check of elemental analysis. According to the results, the sample composition corresponds to $ReB_{3.3}$ with the trace of oxygen which might come from H_3BO_3.

Mechanical property of $ReB_{3.3}$

To investigate the hardness of $ReB_{3.3}$ and compare the hardness value of $ReB_{3.3}$ with $ReB_{3.5}$ and $ReB_{5.5}$ Vickers hardness test was performed. Vickers micro-indentation technique was employed to evaluate the hardness of the $ReB_{3.3}$. Figure 3.2.20 shows the Vickers micro-hardness results of $ReB_{3.3}$ as a function of the indentation load of 2N, 3N and 5N.

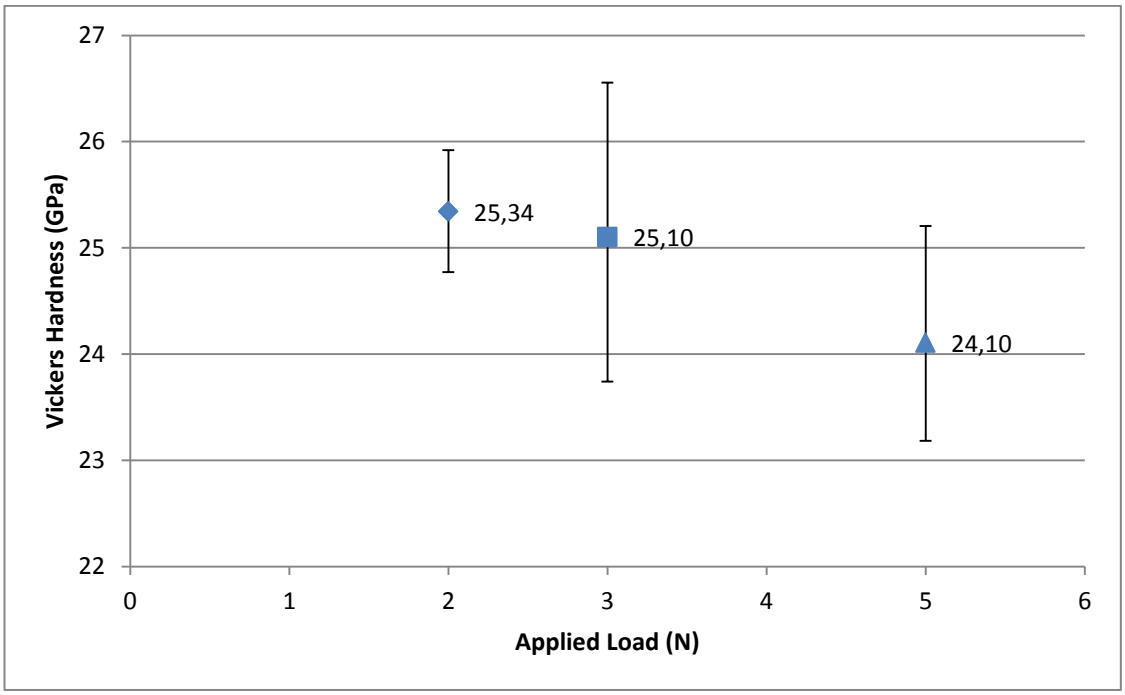

Figure 3.2.20 Vickers micro-hardness results of arc-melted ReB_2 sample washed with 3 M HNO_3 as a function of the indentation load of 2, 3, and 5N

Figure 3.2.20 shows experimental average micro-hardness test results performed on the $ReB_{3.3}$ sample with 5 loads ranging from 2 N to 5 N. Under 2 N, the specimen exhibits a maximum hardness value of 25.34 ±0.56 GPa. The observed inverse relationship of applied load to hardness is due to the well-known indentation size effect.

In order to compare Vickers hardness of $ReB_{3.3}$ with $ReB_{3.5}$ and $ReB_{5.5}$ specimens according to boron content on the hardness value, micro-indentation data of ReB_2

specimens were reported in the same graph. In Figure 3.2.21, Vickers micro-hardness test results for ReB_2 were shown depending on the boron content of ReB_2 compound.

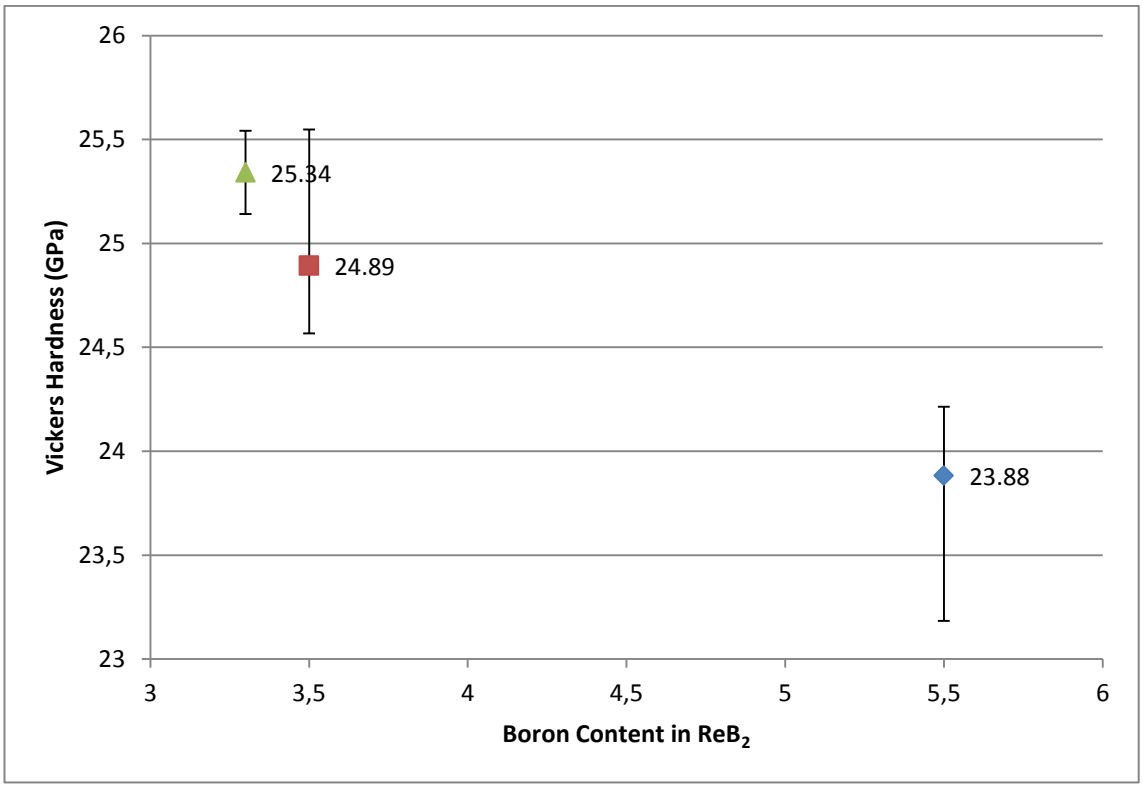

Figure 3.2.21 Vickers micro-hardness test results for ReB_2 depending on the boron content in the compound under 1.961 N for 10 seconds.

Micro-indentation data are reported in Figure 3.2.21 for ReB_2 samples which have different boron amount in the structure. Force of 2 N was applied for 10 seconds for each sample. As the free boron content increased from Re:B=1:3.3 to 5.5, the average hardness decreased from 25.34 ±0.56 GPa to 23.88 ±0.34 GPa. The obtained micro-hardness values are lower than the corresponding values of 35 GPa under load of 2 N reported by Chung et. al. [1] This may be due to the fact that the limitation effect of excess amorphous boron in the structure.

Even though nitric acid treated $ReB_{3.3}$ was oxidized and had boric acid phase, surprisingly it is still harder than $ReB_{3.5}$. It might be explained by boric acid might have higher hardness value than amorphous boron. As a result of hardness comparison

depending on excess boron content on ReB_2, highest Vickers hardness was observed on $ReB_{3.3}$ which has the lowest boron excess in the structure.

ii. Cracking and re-melting

Since there is a formation of impurity phase in the nitric acid treated sample, removing excess boron in the ReB_2 system was investigated by a novel trial. In this attempt, the arc melted product with the starting ratio Re:B=1:4 was cracked and grinded finely. Then, it was pressed into pellet and re-melted under the same condition. X-ray powder diffraction results of one time melted ReB_2 and cracked and re-melted ReB_2 are given in the Figure 3.2.22.

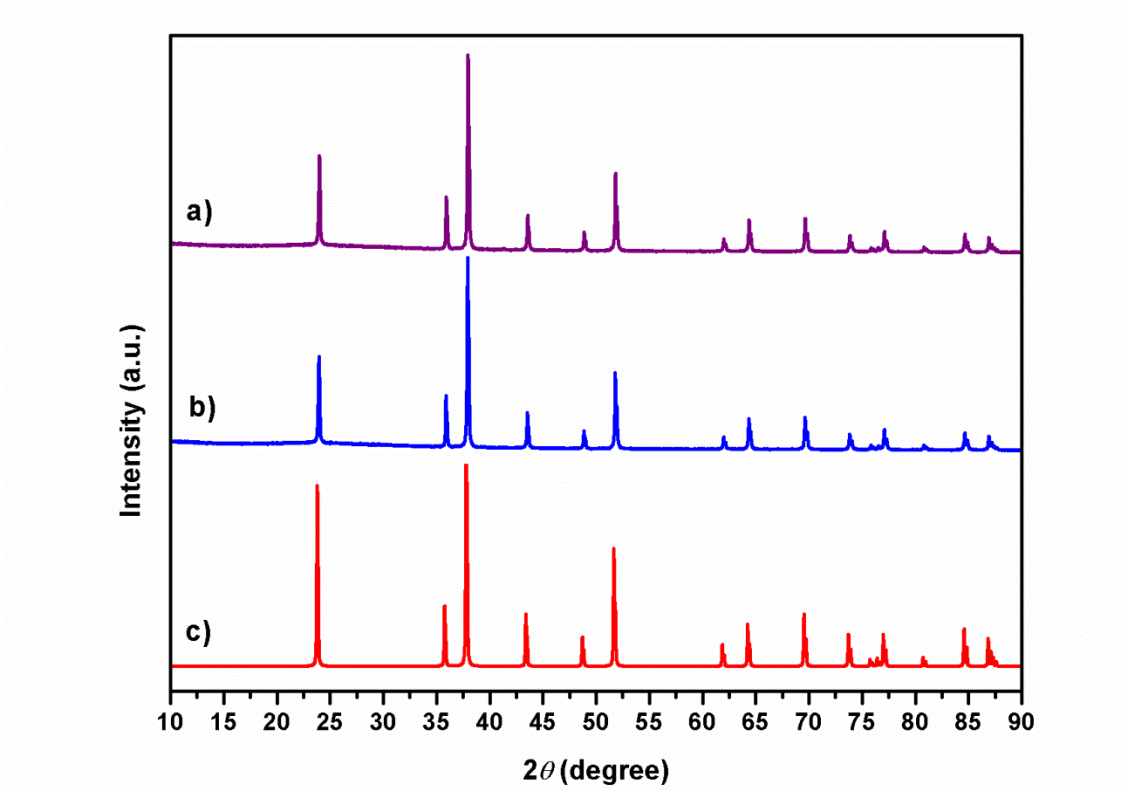

Figure 3.2.22 X-ray diagram of (a) one time arc melted ReB_2 and (b) two time arc melted ReB_2 in comparison with (c) the theoretical ReB_2 (ICSD, card number 11-581)

In Figure 3.2.22, the one-time arc melted ReB_2 sample and re-melted ReB_2 clearly indicate the pure product of ReB_2. Cracking and re-melting of initial ReB_2 has been collected with no significant difference on X-ray powder diagram. However, it is hard to comment on the existence of excess amorphous boron on the two X-ray diagrams by x-ray diffraction technique.

Elemental analyses were performed by ICP-OES. According to the results of ICP-OES measurements, while the sample compositions correspond to $ReB_{3.6}$ for one-time ReB_2, excess boron of re-melted ReB_2 decreased significantly to $ReB_{2.9}$. This attempt has been done with no other impurity formation. Hence, a new method to remove excess boron was successfully developed. As reported by ICP-OES results, $ReB_{3.5}$ decreased to $ReB_{3.3}$ by nitric acid treatment, while $ReB_{3.6}$ decreased to $ReB_{2.9}$ by cracking and re-melting method. Consequently, this method is more favorable than nitric acid treatment. As a future work, arc melting for third time might be investigated and Vickers hardness test investigations might be performed.

3.2.3. Difference of amorphous boron and crystalline boron

In this part of the study, we have changed our perspective of removing excess boron from the system. As stated before, starting with surplus of amorphous boron is a must to synthesize ReB_2 in arc melting technique. Without changing the method, the starting material quality could be changed. Therefore, we have studied with crystalline boron to see the difference with amorphous boron. Two ReB_2 was synthesized from amorphous and crystalline boron without surplus of boron, with the ratio of elements Re:B=1:2. The X-ray powder diagrams of the products were shown in the Figure 3.2.23.

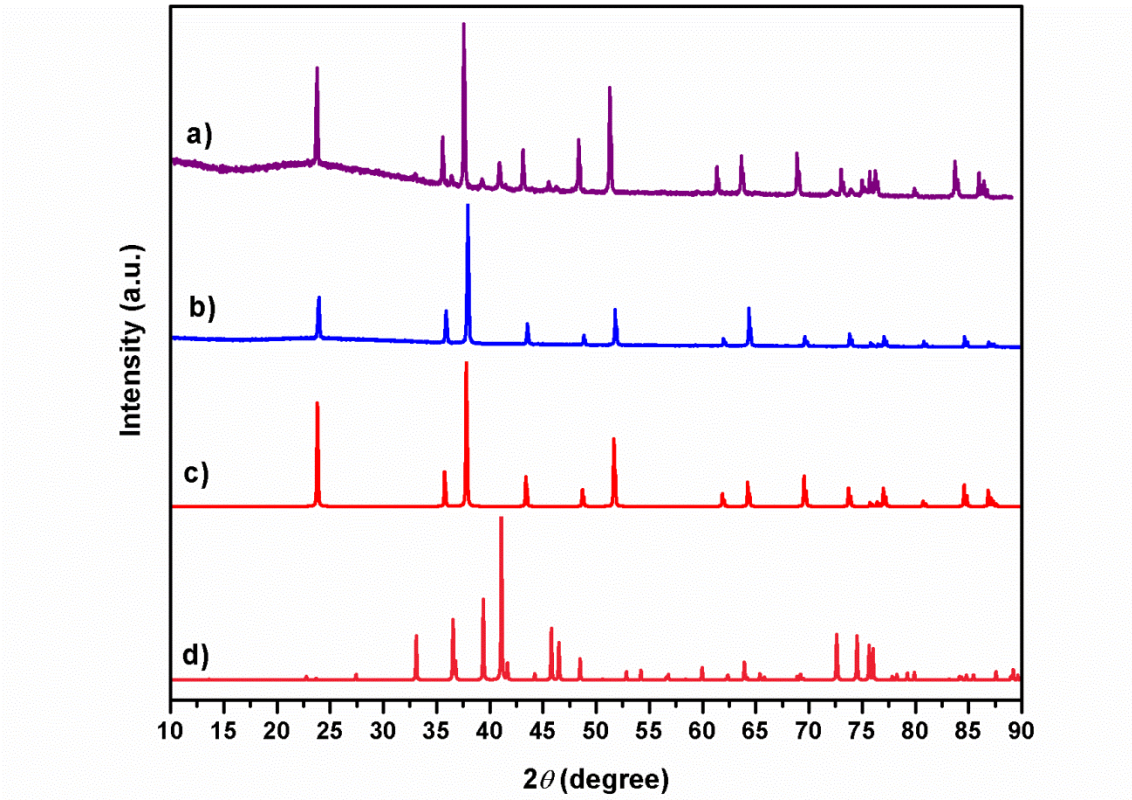

Figure 3.2.23 X-ray diagram of (a) ReB_2 synthesized from amorphous boron and (b) ReB_2 synthesized from crystalline boron in comparison with (c) the theoretical ReB_2 (ICSD, card number 11-581) and (d) the theoretical Re_7B_3 (ICSD, card number 13-362)

Figure 3.2.23 shows that the XRD pattern of (a) the sample synthesized from amorphous boron without surplus of boron Re:B=1:2 and (b) the sample synthesized from crystalline boron with the starting molar ratio Re:B = 1:2. From X-ray diffraction patterns, one can easily see that the mixture of amorphous boron and rhenium with stoichiometric ratio did not yield ReB_2. The unmatched peaks of the sample with amorphous boron might be due to the formation of Re_7B_3. So, as mentioned before, there should be employed surplus of boron. However, how much boron surplus should be employed to synthesize ReB_2 without boron impurity is not clearly reported.

In contrast, XRD pattern of the sample, synthesized from crystalline boron with the ratio of Re:B=1:2 successfully yield ReB_2 with no trace of Re-B formation. So, crystalline boron is more stable than amorphous boron. Unlike amorphous boron, it does not evaporate easily at high reaction condition of arc melting.

As a future work, chemical composition of ReB_2 synthesized from crystalline boron should be examined by ICP-OES. According to the result, Vickers hardness indentation test might be performed.

3.3. Conclusion and Outlook

- ✓ Starting from molar ratios of Re:B = 1:4 and 1:7 ended up with the surplus of unreacted boron. ICP-OES measurements of ReB_2 samples showed that the sample compositions correspond to $ReB_{3.5}$ and $ReB_{5.5}$ for the samples with starting molar ratios of Re:B = 1:4 and Re:B = 1:7, respectively.

- ✓ According to the Vickers micro-indentation measurements, hardness of ReB_2 decreases when the excess boron amount increases in the compound. Hence, the inverse relationship between excess boron amount and the hardness of ReB_2 was successfully proved by a hardness test for the first time ever.

- ✓ The wear test was applied to ReB_2 for the first time ever by TriboTechnic Reciprocating Tribotester. The wear test result shows that ReB_2 is resistant to abrasion.

- ✓ FESEM and EDXS maping results proved that excess boron is located in the grain boundaries of ReB_2.

- ✓ This excess boron destroys the integrity of the ReB_2 formation. So, reducing grain size of ReB_2 explains the decrease on Vickers hardness value.

- ✓ Average hardness of ReB_2 was measured around 24 GPa. The obtained micro-hardness values are lower than the corresponding average values of 35 GPa reported by Chung *et. al.* [1] This may be due to the fact that the limitation effect of excess amorphous boron in the structure.

- ✓ To remove excess boron, two new methods were successfully developed. As reported by ICP-OES results, $ReB_{3.5}$ decreased to $ReB_{3.3}$ by nitric acid treatment, while $ReB_{3.6}$ decreased to $ReB_{2.9}$ by cracking and re-melting method.

Consequently, cracking and re-melting method is more favorable than nitric acid treatment.

- ✓ There is no need to employ surplus of boron for the synthesis from the crystal boron.

Chapter 4

Rhenium Boride (Re_7B_3)

4.1. Experimental Procedure

The synthesis conditions for Re_7B_3 were investigated by using the three different methods: direct combination of the elements at high temperature, metal flux and arc melting methods. The earlier preparation techniques used the reaction at high temperatures followed by annealing for long hours. In the 1950s, rhenium base alloys were prepared by sintering a mixture of rhenium with boron at 1900 ºC.[58] However, this method consumes a lot of energy and time. Instead, the flux synthesis is a very useful method for performing high temperature syntheses at low temperatures. In preference to the flux method, the arc melting synthesis technique saves energy and also time. In the present study, these three different methods were performed. Figure 4.1.1 illustrates the flow diagram of synthesis methods for Re_7B_3.

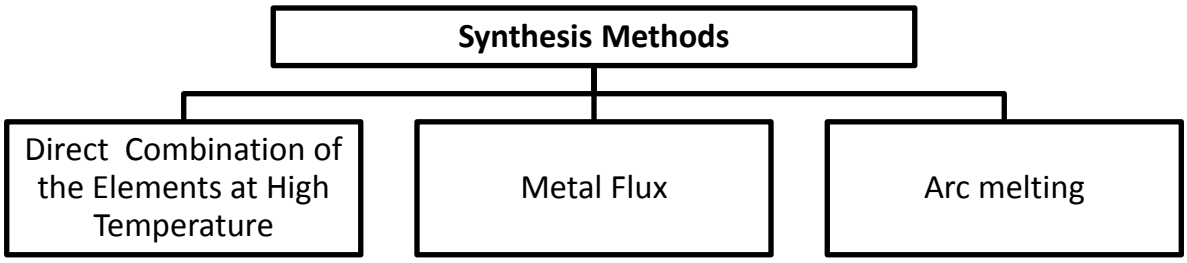

Figure 4.1.1 Flow diagram of synthesis methods for Re_7B_3

4.1.1. Direct Combination of the Elements at High Temperature

To synthesize Re_7B_3, stoichiometric amount of rhenium and amorphous boron were finely powdered via using an agate mortar, and then pressed to an 8 mm diameter pellet. The pellet was placed and sealed inside a tantalum ampoule which has a diameter of 11 mm. Arc melting furnace was used for sealing of the Ta ampoule as well as for the synthesis of Re_7B_3 in the section 4.1.3. A sealed Ta ampoule is shown in Figure 4.1.2.a.

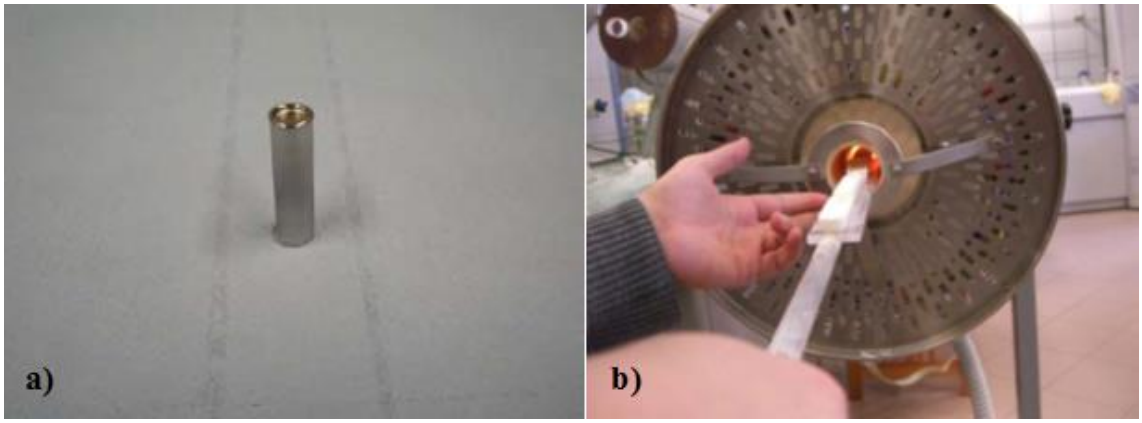

Figure 4.1.2 a) A Ta ampoule which has the pellet of Re-B mixture **b)** Tube furnace

Afterwards, Ta ampoule was placed in the tube furnace (Protherm ®) which can be programmed within the temperature range 20-1500 °C. The tube furnace is presented in Figure 4.1.2.b. The synthesis route followed in this study was based on a single annealing of the reactants at 1100 °C for 65 hours under argon flow.

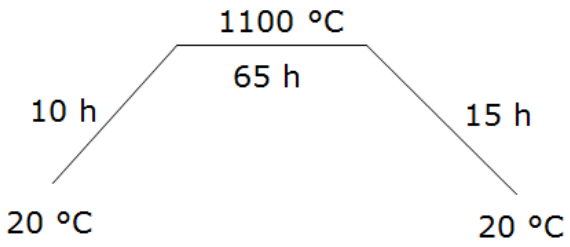

Figure 4.1.3 Thermal history diagram of the tube furnace reaction

4.1.2. Metal Flux Method

The lead flux method was applied for the first time ever for the synthesis of Re_7B_3. The preparation of Re_7B_3 by the metal flux process consists of three steps: pre-reaction, reaction, and post-reaction. In the reaction part, two different furnaces were used separately.

i. The tube furnace with argon flow

For the pre-reaction part, stoichiometric amount of rhenium was mixed with amorphous boron. The mixture was ground with an agate mortar to fine powder. The selected metal flux, lead, pieces were weighted depending on the final molar ratio of the components. The molar ratios of the reactants were kept constant but the flux ratio was increased from Re:B:Pb=7:3:**10** to Re:B:Pb=7:3:**100**. Alumina was chosen as the most appropriate container material because other crucible materials, such as tantalum, niobium, steal might incorporate into the final products and contaminate them. The mixture was then transferred into the alumina crucible and lead on the top.

In the second part, the alumina crucible was placed into the tube furnace. The reaction temperature in this novel synthesis method was determined depending on the melting and boiling point range of lead. The reaction temperature should be higher than the melting point and less than the boiling point. Lead melts at 328 ºC and boils at 1749 ºC. So, starting reaction temperature was chosen as 800 ºC. To minimize the interaction with air, the reaction was performed under argon flow. The sample was heated to 800 ºC within 8 hours, held at that temperature for 10 hours, and cooled down to room temperature within 16 hours in Figure 4.1.4.

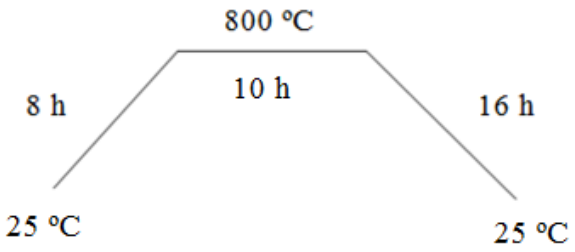

Figure 4.1.4 Thermal history diagram of the lead flux reaction in the tube furnace

There may be contaminations of the flux metal in the final compound which may alter its chemical and physical properties such as hardness, resistance to corrosion and conductivity. The third and the last part of the flux method removes the flux metal from the system. The product was boiled in hydrochloric acid (37%) to form lead (II) chloride, $PbCl_2$. A bubble formation because of H_2 releasing is a key step to observe the point where the reaction completed. Furthermore, lead salts dissolved completely in hot HCl. After acid and dissolved salt decayed, the remaining was washed several times with hot distilled water to remove all lead salt. The reaction taking place is the following:

$$Pb\ (s) + 2HCl\ (aq) \rightarrow PbCl_2\ (s) + H_2\ (g)$$

After removing all flux, the product was filtered and dried. The final product is stable in air and moisture.

ii. Vacuum furnace

As an alternative to argon flow furnace system, the vacuum furnace has been used to minimize argon consumption. In this production, all the pre-reaction part was the same. However, there was an additional preparation to evacuate the atmospheric gas in the reaction tube. For this purpose, a Schlenk line was used. Detailed information about the line is given under the section Experimental Methods and Theoretical Concepts.

For the pre-reaction part, a simple silica reaction vessel was designed for the vacuum line and the furnace. Figure 4.1.6 shows that alumina crucible was already placed in the silica vessel. The reaction mixture and the flux were poured into alumina crucible. A Schlenk line was used for the sealing of the vessel in Figure 4.1.5. After the evacuation of the vacuum line, the vessel was connected to the line through one of the valves. The pressure was decreased to 8 x 10^{-3} mbar.

Figure 4.1.5 The silica reaction vessel connected to the vacuum line

Propane gas torch was used for sealing of the vessel. The sealed reaction vessel is shown in Figure 4.1.6.

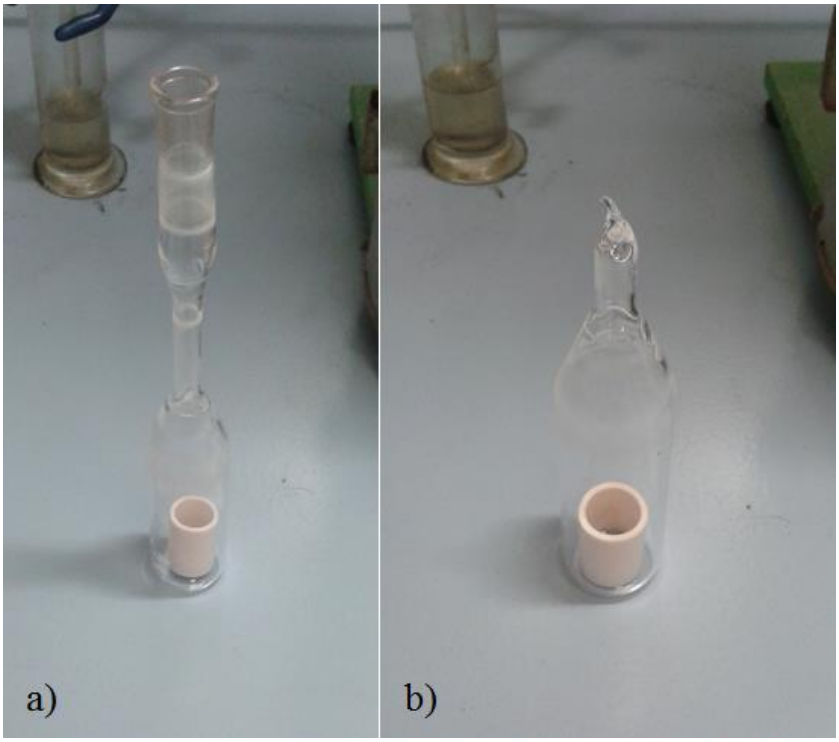

Figure 4.1.6 a) Alumina crucible placed in a silica reaction vessel **b)** The reaction vessel after sealing

In the reaction part, the sealed reaction vessel was placed into the vacuum furnace. The sample was heated to 800 ºC within 4 hours, held at that temperature for 6 hours, and allowed to cool down to room temperature.

The post reaction part is the exactly the same as previous section.

The aluminum flux was also investigated in our work but the experiments ended without mentionable success. X-ray powder diagrams of products depending on the synthesis were presented and discussed in the Results and Discussion Section.

4.1.3. Arc Melting

Re_7B_3 was synthesized by an arc melting device in a water cooled-copper sample holder under argon atmosphere. Appropriate amounts of rhenium and amorphous boron were weighed and placed in an agate mortar. The mixture was ground until a fine powder was obtained. The Re-B mixture was transferred and pressed into a 13 mm diameter pellet. 10 kN pressure was applied to a total of 0.5 gram of sample. Pressing powder to a pellet is a crucial step to enhance the mutual diffusion of the atoms located at boundary grains. Therefore the solid state reaction can start and proceed fast. Then, the pellet was placed onto the copper holder. After placement of the sample into an arc melting device, the reaction chamber was evacuated down to $2\text{-}3.10^{-3}$ mbar. Afterwards, it was refilled with high pure argon gas. These last two steps -evacuation and refilling- were repeated several times to minimize the contamination of air and moisture. The welding tip, made of tungsten, was adjusted to 31 ampere. During the synthesis, the system was cooled down with circulating water. The reaction took less than a minute to complete. To avoid oxidization, the product was not taken out until it was cooled down to room temperature. During the melting process, weight losses of boron were significant. Therefore, various molar ratios of Re versus B and temperature conditions were tried to be optimized. Finally, we synthesized the best Re_7B_3 compacts under 27 ampere starting from a powder mixture of Re and B with a molar ratio of 6.3:3.55.

The metallic grey product was cracked apart mechanically and ground using tungsten carbide mortar. The crystal structure of the product was examined by X-ray powder diffraction. The presence of the elements (i.e; rhenium, boron and oxygen) and their ratios were characterized by inductively coupled plasma-optical emission spectroscopy (ICP-OES). Scanning electron microscopy images were taken to see rhenium- boron distributions. Magnetic susceptibility and heat capacity measurements were analyzed. Additionally, the Vickers micro-hardness test was performed on a bulk sample which encased into epoxy resin in Figure 3.1.2 b.

4.2. Results and Discussion

Although Re_7B_3 is a known compound, synthesis of pure Re_7B_3 has not been reported previously. In this thesis, synthesis conditions for Re_7B_3 have been investigated. Three different methods – direct combination of elements at high temperature, metal flux and arc melting methods – were studied. Finally, Re_7B_3 was successfully obtained as a main phase by arc melting technique. Correspondingly, detailed optimization of synthesis conditions and comprehensive characterizations of Re_7B_3 were reported for the first time.

4.2.1. Direct combination of the elements at high temperature

The former production technique of rhenium boride requires high temperature and long hours. Even though rhenium base alloys were synthesized in 1950s, the final product was not pure Re_7B_3. Moreover, the detailed reaction condition was not reported. Without clear information, we have started with the reaction at 1100 ºC. The total reaction time was 90 hours: 10 hour heating, 65 hours annealing, 15 hours cooling. Figure 4.2.1 shows the X-ray powder diagram of the product.

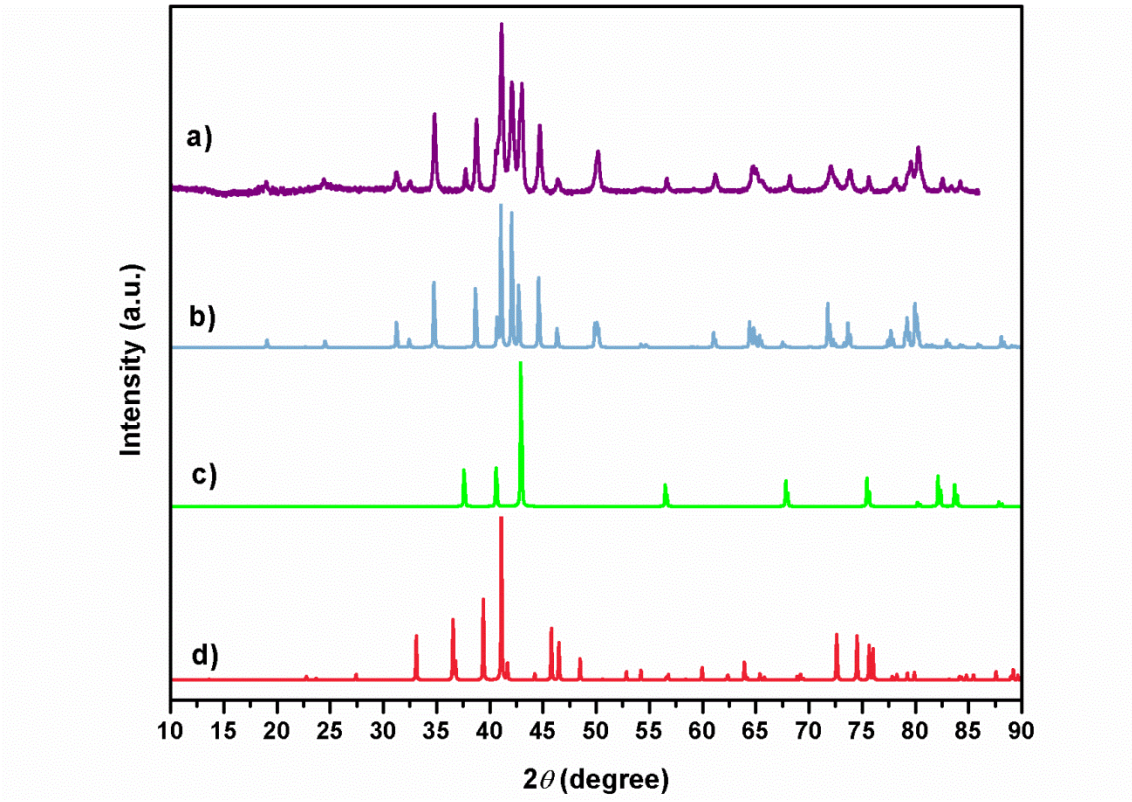

Figure 4.2.1 X-ray diagram of (a) the product from direct annealing under 1100°C for 65 hours in argon atmosphere in comparison with (b) the theoretical Re_3B (ICSD, card number 48-1739), (c) the theoretical Re (ICSD, card number 5-702) and (d) the theoretical Re_7B_3 (ICSD, card number 13-362)

As shown in Figure 4.2.1, the diffraction pattern of the product matches with the Re_3B formation and remained elemental rhenium. There is no formation of target compound Re_7B_3. Even though high reaction temperature was employed for long time, Re_7B_3 was not synthesized by straight forward. There should be more effort to optimization of synthesize conditions such as reactant ratio, reaction temperature and time. Therefore, this approach has not been carried further because of time and energy consuming.

4.2.2. Metal flux

As a second approach, the novel synthesis method of Re_7B_3 has been investigated. Metal flux method was used to decrease the high reaction temperature. Flux creates an alternative route for performing high temperature reactions at more moderate temperatures. So, this method enhances the diffusion process in solid-state synthesis, by using molten salts or metals as solvent. Details of the flux method are given under *The Flux Method in Solid State Chemistry* section.

According to the study of Uslu *et. al.*, ReB_2 was successfully synthesized by lead flux at 800º C. Attempts with tin (Sn) and aluminum (Al) failed. So, for the synthesis of Re_7B_3, lead was chosen as the flux. To optimize reaction conditions to synthesize target compound, we have done great efforts. Details of the study can be found in Appendix section. Finally, reactants were mixed with the molar ratios of Re:B:Pb =6:3.5:10. The mixture was heated up to 800 ºC within 4 hours, held at that temperature for 6 hours, and cooled down to room temperature within 4 hours. Figure 4.2.2 shows the X-ray powder diagrams of the product.

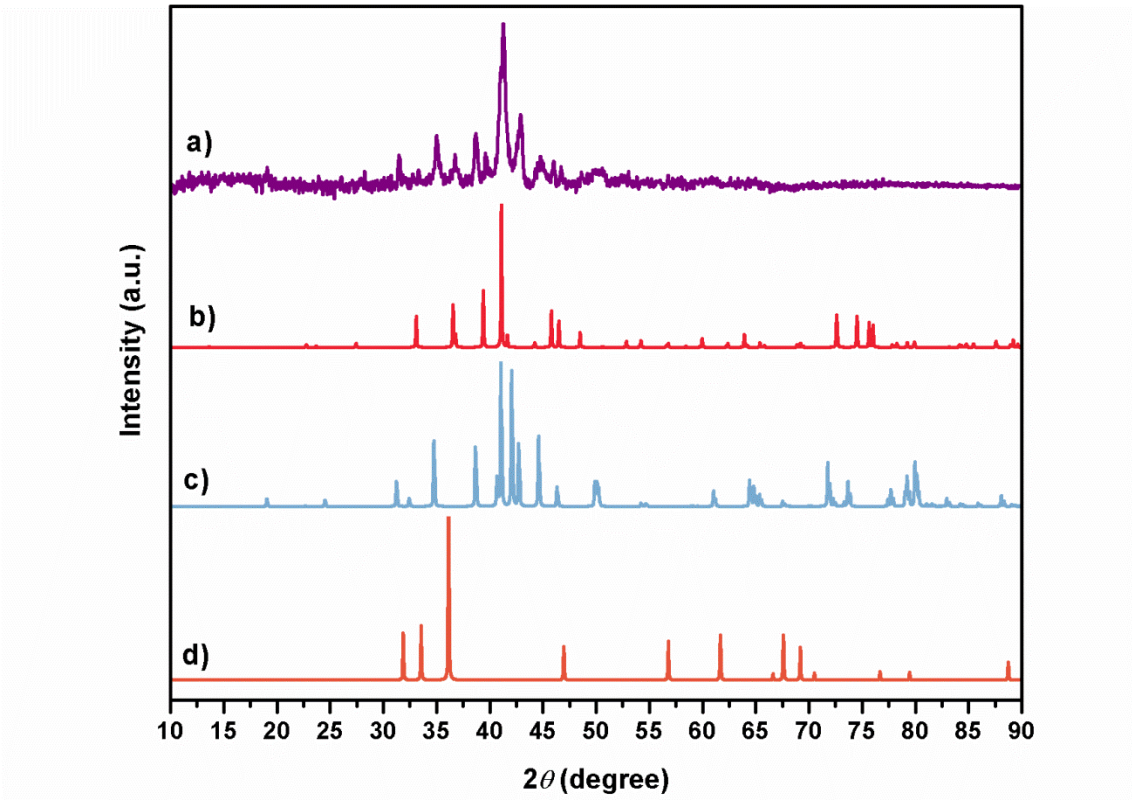

Figure 4.2.2 X-ray diagram of (a) the product from lead flux reaction at 800 ºC for 14 hour in Ar filled steal reaction tube in comparison with (b) the theoretical Re_7B_3 (ICSD, card number 13-362), (c) the theoretical Re_3B (ICSD, card number 48-1739), and (d) the theoretical Pb (ICSD, card number 23-345)

Figure 4.2.2 shows the X-ray diffraction patterns of (a) the final product in comparison with theoretical XRD pattern of (b) Re_7B_3 and (c) Re_3B, and (d) Pb. Finally, Re_7B_3 was synthesized by flux method but with the trace of Re_3B. The product is lead free. It is the first time ever Re_7B_3 was synthesized by lead flux method. As a future study, the synthesized condition of single phase of Re_7B_3 should be optimized.

4.2.3. Arc melting

i. Optimization the arc melting reaction conditions

As stated before, the compound Re_7B_3 has never been synthesized as a pure phase so far. Usually, Re_3B and ReB_2 are seen in the product as an impurity phase due to the narrow region of Re_7B_3 in the phase diagram. Furthermore, boron lost during the arc melting synthesize prevents to synthesize Re_7B_3 from stoichiometric ratio. Therefore, to synthesize Re_7B_3 as a single phase, the starting composition was tuned as it is seen in the Figure 4.2.3.

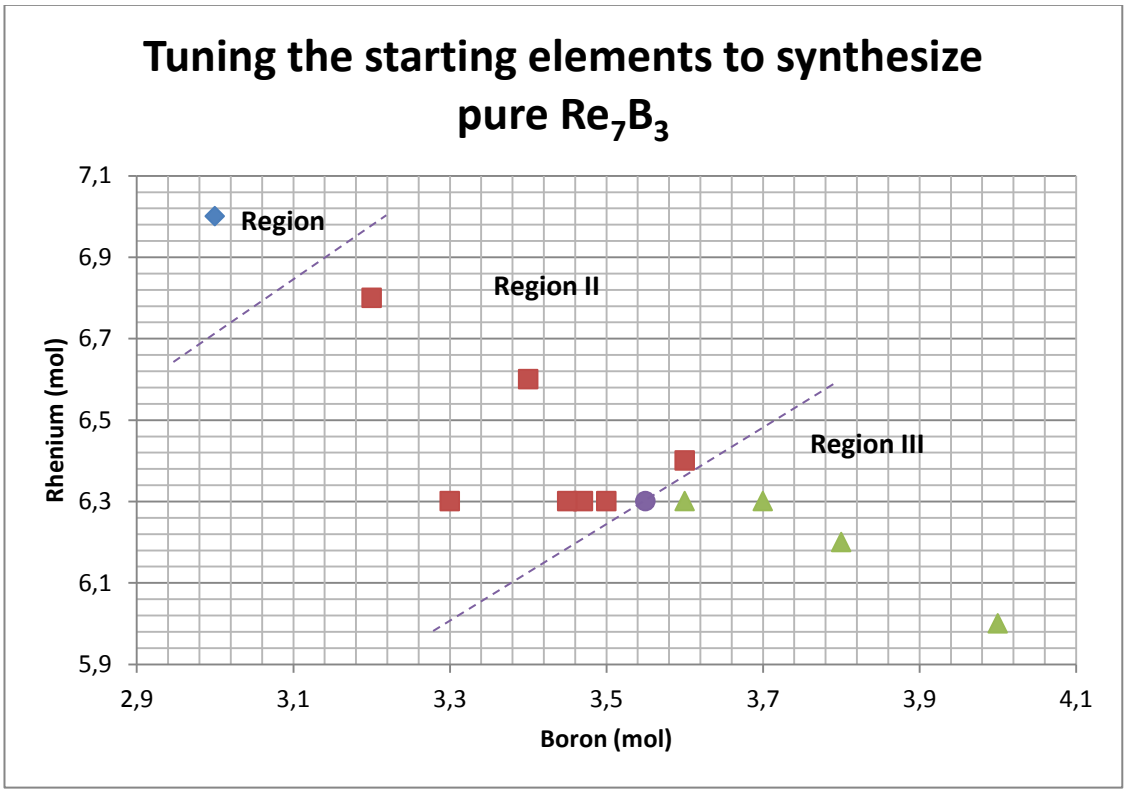

Figure 4.2.3 Optimization of synthesizing phase-pure Re_7B_3 via arc melting using different Re:B atomic ratios. Blue diamond stands for pure phase Re_3B, red squares stand for Re_7B_3 with the minor impurity phase of Re_3B, green triangles stand for Re_7B_3 with the minor impurity phase of ReB_2, purple circle stands for single phase of Re_7B_3

In Figure 4.2.3, x axis shows boron atomic ratio and y axis shows the rhenium atomic ratio in the beginning of arc synthesis. Results are represented as blue diamond for pure phase of Re_3B, red squares for Re_7B_3 with the trace of Re_3B, and green triangles for Re_7B_3 with the trace of ReB_2. The synthesis attempt of Re_7B_3 with the stoichiometric ratio of elements ended up with the production of Re_3B as shown in Figure 4.2.3. Therefore, rhenium amount decreased, while boron ratio increased until to get single phase of Re_7B_3.

In the graph, there are three regions. On the Region I, product was observed as Re_3B. Around this region, the reaction favors to Re_3B instead of Re_7B_3. On the Region II, Re_7B_3 was synthesized with the different amount of Re_3B. That means at that region rhenium boron ratio is still high to synthesize target compound pure. It includes rhenium rich impurity. On Region III, Re_7B_3 was observed with the trace of ReB_2. So, there is excess boron which favors to form ReB_2. There is an imaginary trend line which divides rhenium rich phase (Region II) from boron rich phase (Region III). Finally, on the imaginary trend line, Re_7B_3 was successfully obtained as a main phase with the starting atomic ratio of Re:B=6.3:3.5.

ii. Structure analysis of Re_7B_3

By tuning the starting composition, Re_7B_3 was obtained as the main phase (ca. 95 wt.%). Crystal analysis was performed on Max Planck Institute, Germany. Figure 4.2.4 shows the observed and theoretical powder patterns of the target compound.

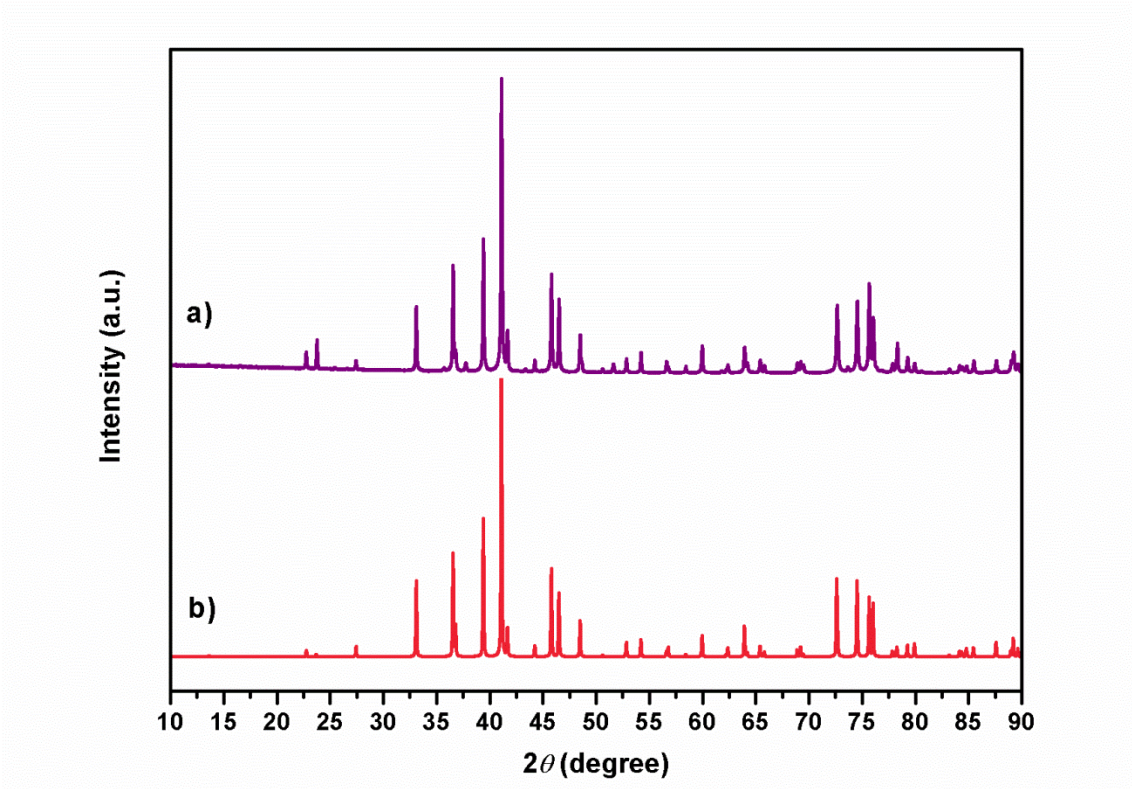

Figure 4.2.4 X-ray diagram of (a) arc-melted Re_7B_3 with the starting molar ratio of Re:B=6.3:3.5 in comparison with (b) the theoretical Re_7B_3 (ICSD, card number 13-362)

Figure 4.2.4 shows (a) the XRD patterns of Re_7B_3 with the starting ratio Re:B= 6.3:3.55 in comparison with (b) the theoretical XRD pattern of Re_7B_3. The XRD diagrams confirm the successful synthesis of Re_7B_3 as the main phase.

iii. Chemical Analysis of Re_7B_3

To investigate the exact chemical composition, chemical analyses were performed for reactants and oxygen. According to the results of ICP-OES measurements, the sample compositions correspond to $Re_{7.01}B_{3.23}$ and the product is oxygen-free.

iv. Morphological Analysis of Re_7B_3

To investigate morphology, scanning electron images of powder form of the final product were taken with the 1X, 5X, 10X, and 50 X magnifications in Figure 4.2.5.

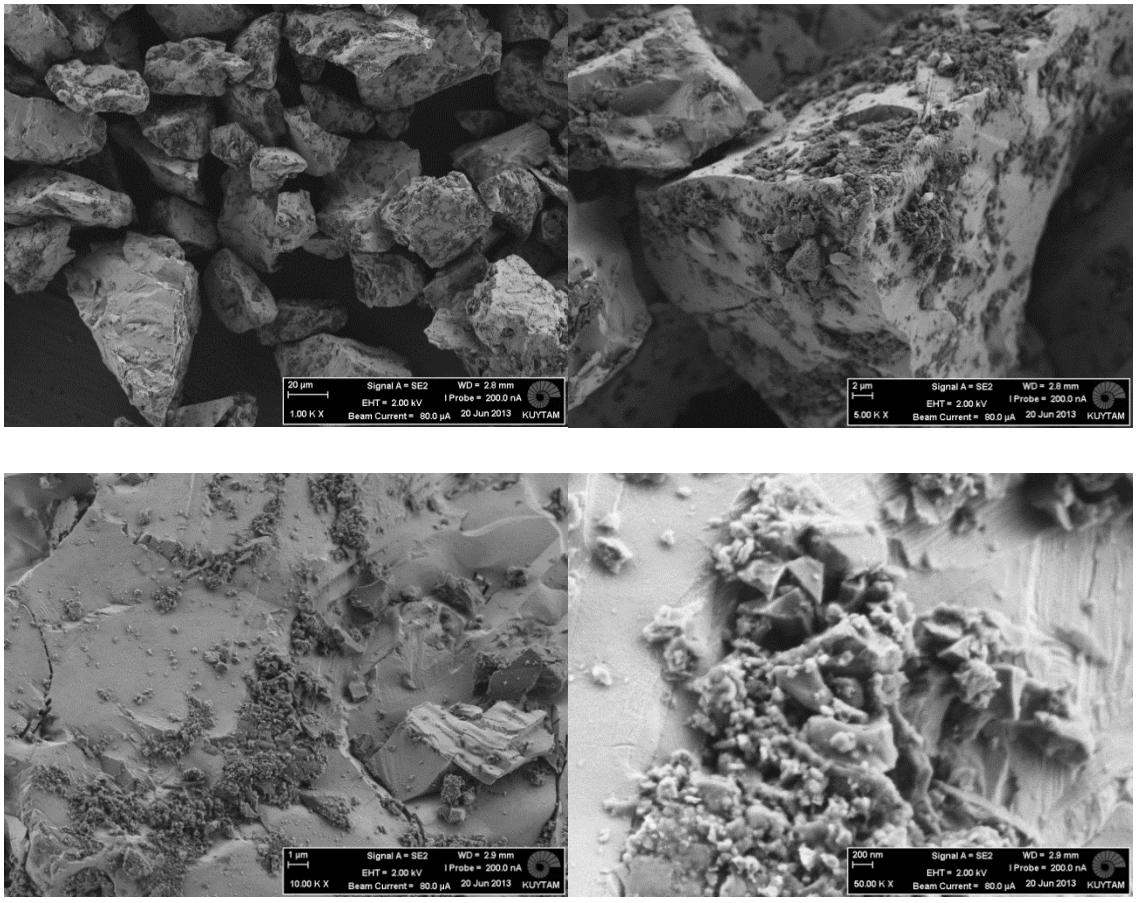

Figure 4.2.5 Scanning electron microscopy images of powder form of Re_7B_3 with different magnifications

From the SEM observations, it could be concluded that the samples exhibit a fine and dense microstructure.

Scanning electron microscopy technique working in secondary electron mode was used to observe the polished surface of bulk form of Re_7B_3. The SEM apparatus was coupled with a system for microanalysis energy dispersive X-ray spectroscopy (EDXS).

Thereby, qualitative analysis of the elements was performed. The following Figure 4.2.6 shows the SEM image of Re_7B_3.

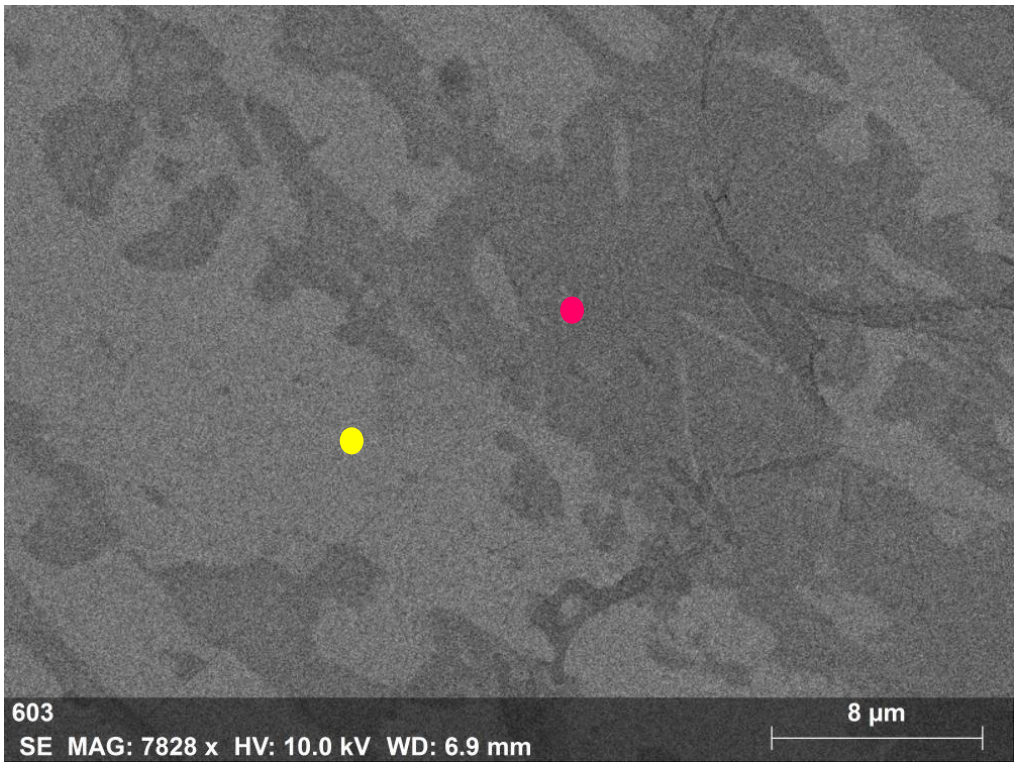

Figure 4.2.6 Scanning electron micrograph of Re_7B_3

Figure 4.2.6 presents the SEM micrograph of Re_7B_3. The morphology was seen with scale bar of 8 µm. The image has brighter and darker phases. These phases could be better investigated by EDXS measurement. So, the brighter region which labeled yellow dot and darker region which labeled pink were analyzed. The following figures show EDXS analyses of these two regions.

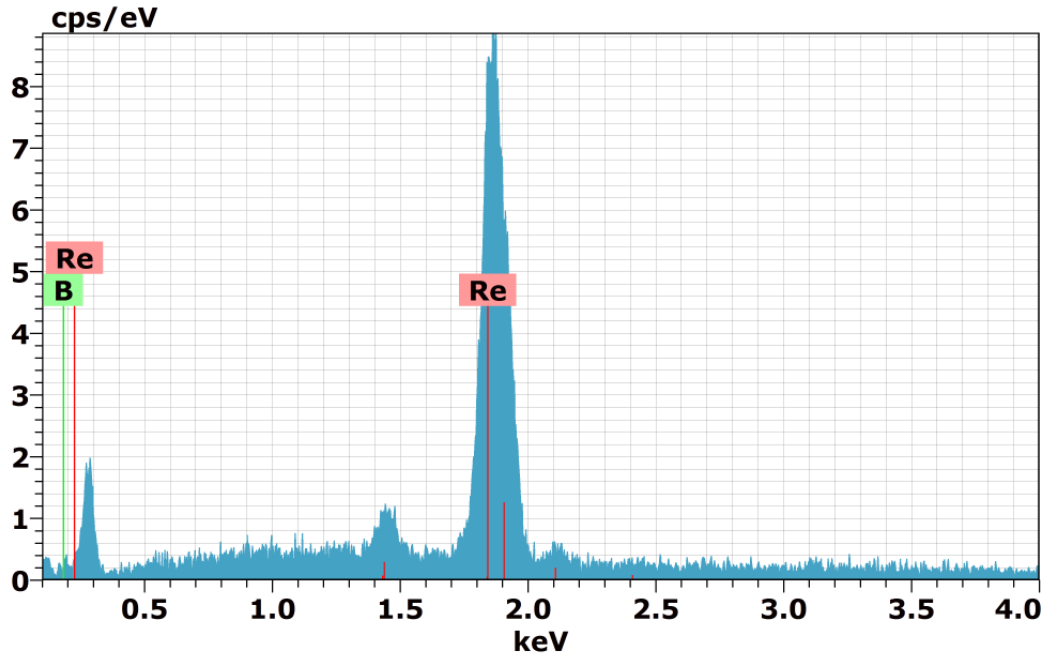

Figure 4.2.7 EDXS analysis of Re_7B_3 from the brighter region which labeled with yellow dot

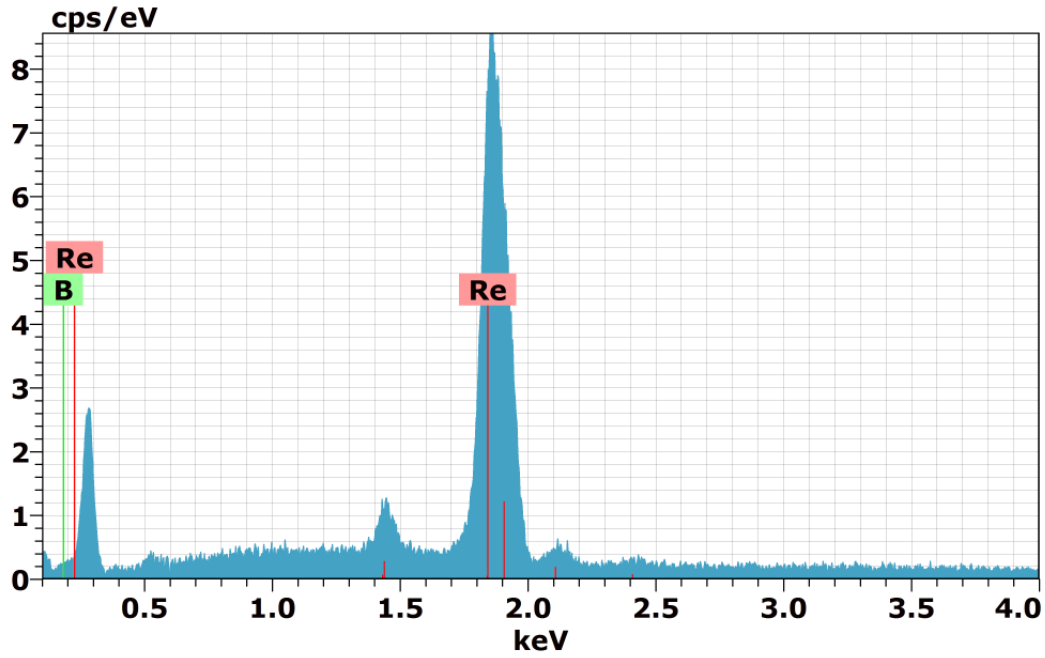

Figure 4.2.8 EDXS analysis of Re_7B_3 from the darker region which labeled with pink dot

The comparison of EDXS results showed that there is no distinct difference in between these two regions. They both have rhenium and boron without any oxygen or other traces.

v. Mechanical Properties of Re_7B_3

Hardness calculations in comparison with experimental results

Theoretical calculations of Re_7B_3 have been investigated by Örmeci *et. al.* By using the formula of Simunek *et.al.* Theoretical hardness of Re_7B_3 was calculated as 15.3 GPa without the B-B interaction and 20.0 GPa with B-B interaction. To clear the confusion between two different hardness values, the actual hardness of Re_7B_3 was measured with Vickers micro-indentation test at Istanbul Technical University. In Figure 4.2.9, the experimental results are given as a function of indentation loads of 2N, 3N, 5N and 10N.

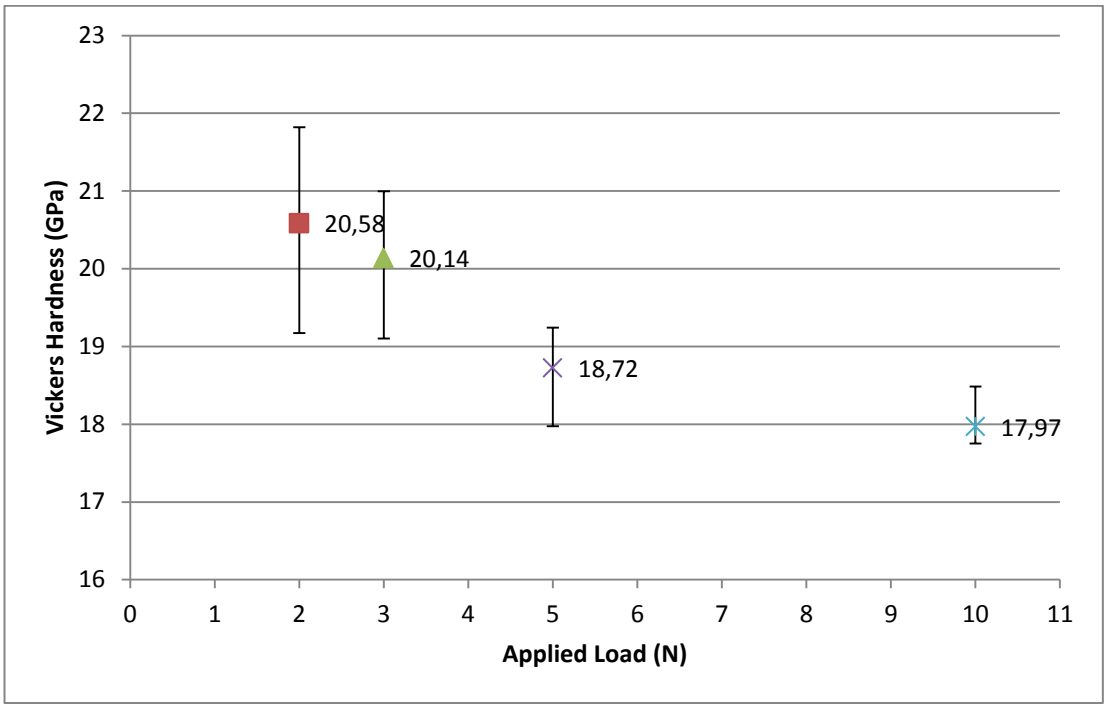

Figure 4.2.9 Vickers micro-hardness results of arc-melted Re_7B_3 sample as a function of the indentation load of 2N, 3N, 5N and 10 N

In Figure 4.2.9, applied load with the unit of Newton is shown in the x axis and the Vickers micro-hardness with the unit of GPa is represented in the y axis. The average hardness values are shown within the error bars. Indentation measurements were performed under applied load of 2N, 3N, 5N and 10N, properly. The maximum hardness was observed as 20.58 ±1.2 GPa under applied load of 2N. The hardness of the sample decreased to 17.97 ±0.51 GPa under applied load of 10 N as shown in Figure 4.2.9. This value steadily decreased with increasing load due to the indentation size effect. Consequently, experimental hardness results at 2N and 3N confirms that the calculated hardness value of 20.0 GPa. So, the B-B interaction should be considered in the hardness calculations.

Bulk modulus calculation

Additionally, bulk modulus (B) of Re_7B_3 has been calculated by Örmeci *et.al.* by quantum chemical calculations. According to calculation results, the bulk modulus of Re_7B_3 is 400 GPa. Therefore, Re_7B_3 is expected to be harder than ReB_2 which has bulk modulus of 360 GPa. In Figure 4.2.10, hardness comparison of ReB_2 and Re_7B_3 are shown under different loads.

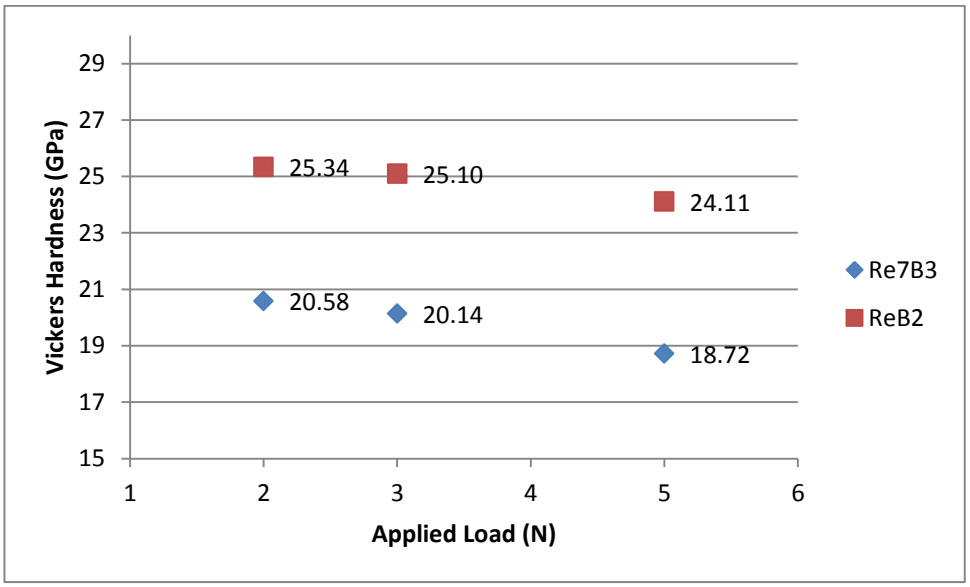

Figure 4.2.10 Vickers micro-hardness result comparison of ReB_2 (red square) and Re_7B_3 (blue diamond) as a function of the indentation load of 2N, 3N, and 5N

According to the Vickers hardness results at 2N, 3N and 5N, the hardness comparisons clearly show that Re_7B_3 is not harder than ReB_2 as expected. This can be explained by the fact that bulk modulus has little direct connection with hardness. It is not good predictor of hardness.[16] Although it is true that a hard material must have a high bulk modulus, it is a common misconception to believe that the inverse is true. As a consequence, Re_7B_3 is not hard as ReB_2, although it has a higher bulk modulus (400 GPa) than ReB_2 (359 GPa).

Wear test

For further mechanical property investigations, the wear tests were applied to Re_7B_3 for the first time ever by TriboTechnic Reciprocating Tribotester at İstanbul Technical University. The test parameters are tabulated in Table 4.2.1.

Table 4.2.1 TriboTechnic Reciprocating Tribotester Test Parameters

Test Parameters	
Eccenter	2,00 mm
Sliding speed	4,00 mm/s
Normal load	6,00 N
Total sliding length	60000 mm
Total cycle	15000
Counter material	WC
Counter material diameter	6,00 mm
Temperature	25 ± 3 °C
Humidity	30 ± 5 °C

According to the wear test results, Re_7B_3 sample had been not exposed to a massive adhesive wear by the WC ball. The wear test result shows that the product is resistant to abrasion. The test parameters are not enough to form micro abrasions. Even the maximum parameter was applied for the test, the test could be repeated by different model of wear tester under higher pressure such as 50-60 N and longer time, as a future study.

vi. Magnetic susceptibility measurement

The magnetization of polycrystalline piece of Re_7B_3 was carried out with SQUID (Superconducting Quantum Interference Device) magnetometer (MPMS-XL7, Quantum Design) at MPI-CPfS in Germany by Walter Schnell. It was measured in external magnetic fields $\mu_0 H$ of 20mT up to 7 T in a SQUID magnetometer (MPMS-XL7, Quantum Design). The sample was wrapped in a polyethylene (PE) segment stuck into

a PE straw, the diamagnetic contribution of the PE segment was measured at 300 K and subtracted. Figure 4.2.11 shows the magnetic susceptibility (M=M/H, where M is magnetization and H is magnetic field) of Re_7B_3.

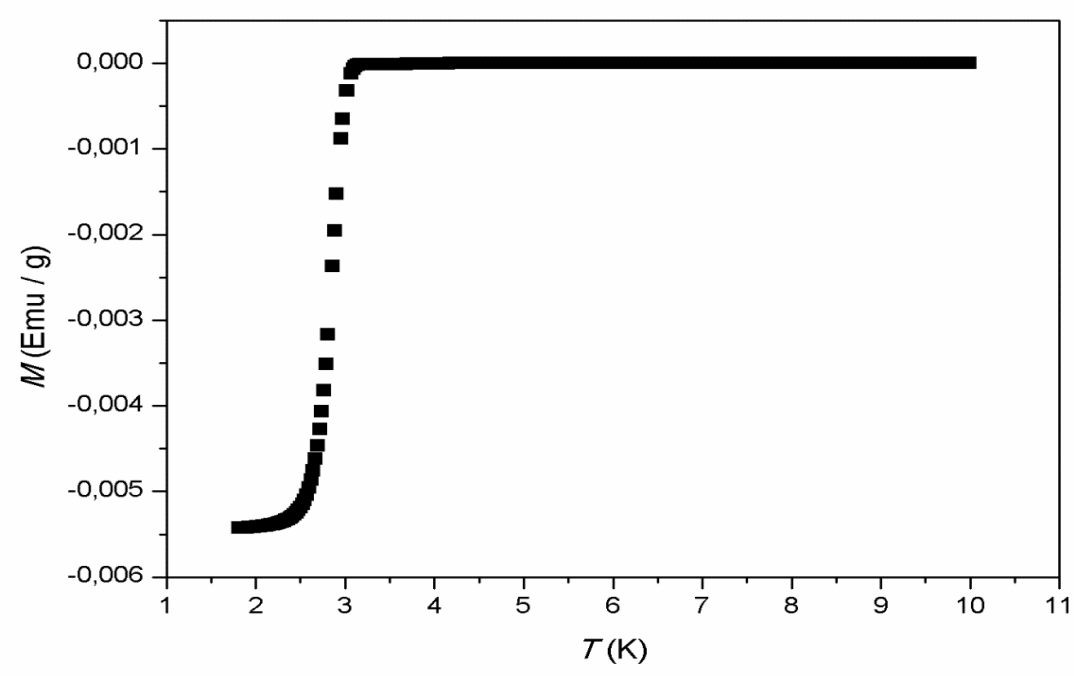

Figure 4.2.11 Temperature dependence of magnetic susceptibility of Re_7B_3 under the applied magnetic field of 2mT

The high-field magnetic susceptibility, $\chi(T) = M/H$, of Re_7B_3 is weakly temperature dependent and paramagnetic, indicating that the Pauli-paramagnetic contribution is stronger than the diamagnetism. A fit taking into account minor Curie-paramagnetic impurities (or charged defects) and a slight positive linear temperature dependence of $\chi(T)$ results in an extrapolated value $\chi_0 = +20(5) \times 10^{-6}$ emu mol^{-1} at $T = 0$. Assuming the sum of the diamagnetic core increments as $-(7 \times 12 + 3 \times 0.2) \approx -85$ in units of 10^{-6} emu mol^{-1} leads to a Pauli-paramagnetic contribution $\chi_P \approx +105 \times 10^{-6}$ emu mol^{-1}. Within the model of free electrons this corresponds to a density of states $N(E_F)$ of ≈3.2 states eV^{-1} at the Fermi level.

For low fields, superconductivity becomes visible below helium temperature. In a field $\mu_0 H = 2$ mT, in agreement with Akimitsu *et al*. [Kawano2003], a critical

temperature of 3.00(2) K is observed (value extrapolated from steepest slope of $\chi(T)$ to $\chi = 0$).

vii. Specific heat capacity measurement

The heat capacity of a smaller polycrystalline piece was determined by a relaxation method (HC option for the PPMS, Quantum Design) in Max-Planck ınstitute by Walter Schnelle. The contributions of the sample holder and of the known amount of Apiezon N grease were subtracted. The temperature dependence of the specific heat capacity of Re_7B_3 is shown in Figure 4.2.12.

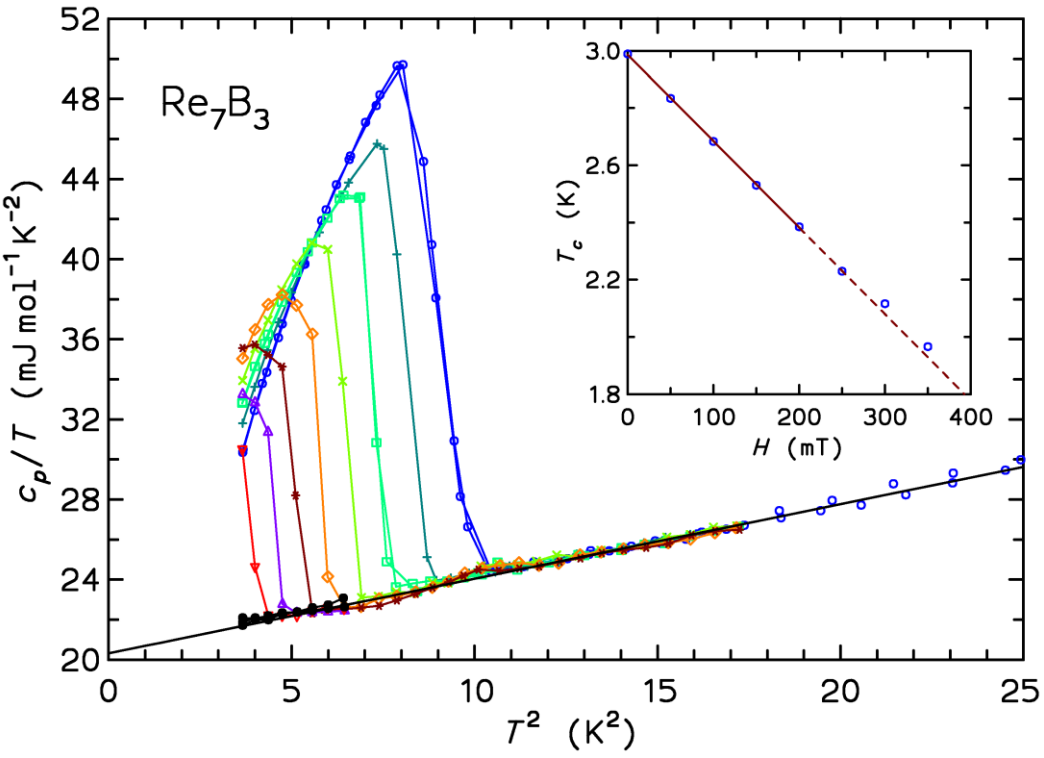

Figure 4.2.12 Specific heat of Re_7B_3 in a c_p/T *vs.* T^2 representation.

Figure 4.2.12 shows the specific heat of Re_7B_3 in a c_p/T vs T^2 representation for various magnetic fields. A sharp jump-like anomaly at T_c indicates the bulk superconductivity of a homogenous sample. The midpoint of the transition for zero field is observed at 2.99 K, the reduced jump $\delta c_p/T$c is 29.8 mJ mol^{-1} K^{-2}. With increasing field the midpoint T_c decreases as shown in the inset of Figure 4.2.12. Using the initial slope $dB_{c2}/dT = -328$ mT K^{-1} as obtained from a linear fit to $T_c(B)$ up to 200 mT and the WHH extrapolation [Werthamer] an upper critical field of $B_{c2}(0) \approx 700$ mT can be calculated. This value is in fair agreement with that of Akimitsu *et al*. [Kawano2003] (≈900 mT), which was obtained from magnetization curves.

The specific heat in the normal metallic state, $c_n(T)$, was measured in overcritical magnetic fields. Up to 5 K it is well described by $c_n(T) = \gamma T + \beta T^3$, where $\gamma = 20.3$ mJ mol^{-1} K^{-2} is the Sommerfeld coefficient of the electronic specific heat and βT^3 the lattice specific heat in the Debye approximation. The value of β corresponds to a Debye temperature of 374 K. The ratio $\delta c_p/\gamma T$c of 1.47 is very close to the ratio (1.43) from the BCS theory of superconductivity. Therefore we can conclude that electron-phonon coupling in Re_7B_3 is in the weak-coupling limit.

4.3. Conclusion and Outlook

- ✓ Synthesis from direct combination of reactant with stoichiometric ratio at high temperature is not feasible production method.

- ✓ We have synthesized Re_7B_3 with lead flux method fort the first time.

- ✓ Re_7B_3 was successfully obtained as a main phase (ca. 95 wt.%) with the starting atomic ratio of Re:B=6.3:3.5 by arc melting method. According to the results of ICP-OES measurements, the sample compositions correspond to $Re_{7.01}B_{3.23}$ and the product is oxygen-free.

- ✓ Theoretical hardness of Re_7B_3 was calculated as 15.3 GPa without the B-B interaction and 20.0 GPa with B-B interaction by Örmeci *et.al*. To clear the confusion between two different hardness values, the actual hardness of Re_7B_3 was measured. Consequently, experimental hardness results at 2N and 3N confirms that the calculated hardness value of 20.0 GPa. So, the B-B interaction should be considered in the hardness calculations.

- ✓ Bulk modulus of Re_7B_3 has been calculated by Örmeci *et.al*. by quantum chemical calculations. According to calculation results- the bulk modulus of Re_7B_3 is 400 GPa- Re_7B_3 is expected to be harder than ReB_2 which has bulk modulus of 359 GPa. Vickers hardness results clearly show that Re_7B_3 is not harder than ReB_2 as expected.

- ✓ The wear tests were applied to Re_7B_3 for the first time ever. According to the wear test results, Re_7B_3 sample had been not exposed to a massive adhesive wear by the WC ball. It is resistant to abrasion.

- ✓ Re_7B_3 is a superconductor with weak electron-phonon coupling. Albeit that its Sommerfeld coefficient divided by the number of metal atoms (*viz*. the

electronic density of stated) is higher than for Re_3B, its T_c is lower (Re_3B: T_c = 4.8 K [Kawano2003]), which is due to the moderately enhanced electron-phonon coupling in Re_3B.

Chapter 5

Appendix

5.1. Metal flux

As a second approach, the novel synthesis method of Re_7B_3 has been studied. According to the study of Uslu *et. al.*, ReB_2 was successfully synthesized by lead flux at 800º C. Attempts with tin (Sn) and aluminum (Al) failed. So, for the synthesis of Re_7B_3, lead was chosen as the flux. In the lead flux study, two different furnaces – tube and vacuum furnaces– were used. Results have showed differences with the furnace types.

5.1.1. Tube Furnace with Argon Flow

For the lead flux synthesis of Re_7B_3, the sample was heated up to 800 ºC within 8 hours, held at that temperature for 10 hours, and cooled down to room temperature within 16 hours under argon flow. Figure 5.1.1 shows the X-ray powder diagrams of the product.

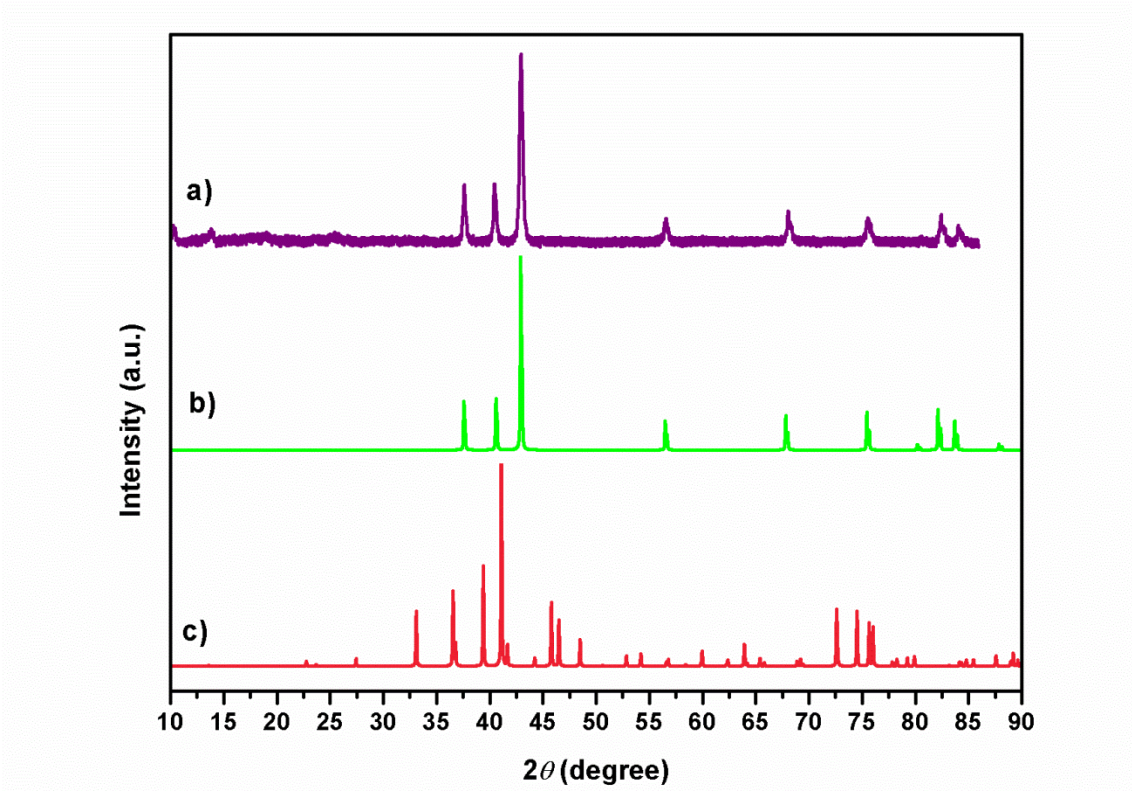

Figure 5.1.1 X-ray diagram of (a) the product from lead flux reaction at 800 ºC for 10 hours in Ar filled steal reaction tube in comparison with (b) the theoretical Re (ICSD, card number 5-702) and (c) the theoretical Re_7B_3 (ICSD, card number 13-362)

According to the X-ray powder diagram, the elemental rhenium remained as it was. There is no formation of Re_7B_3. Attempt at 800 ºC failed, very likely due to the lower reaction temperature or dwell time. Therefore, reaction temperature was increased to 900 ºC. Figure 5.1.2 shows the XRD results of the product which was synthesized at 900 ºC under argon atmosphere in tube furnace.

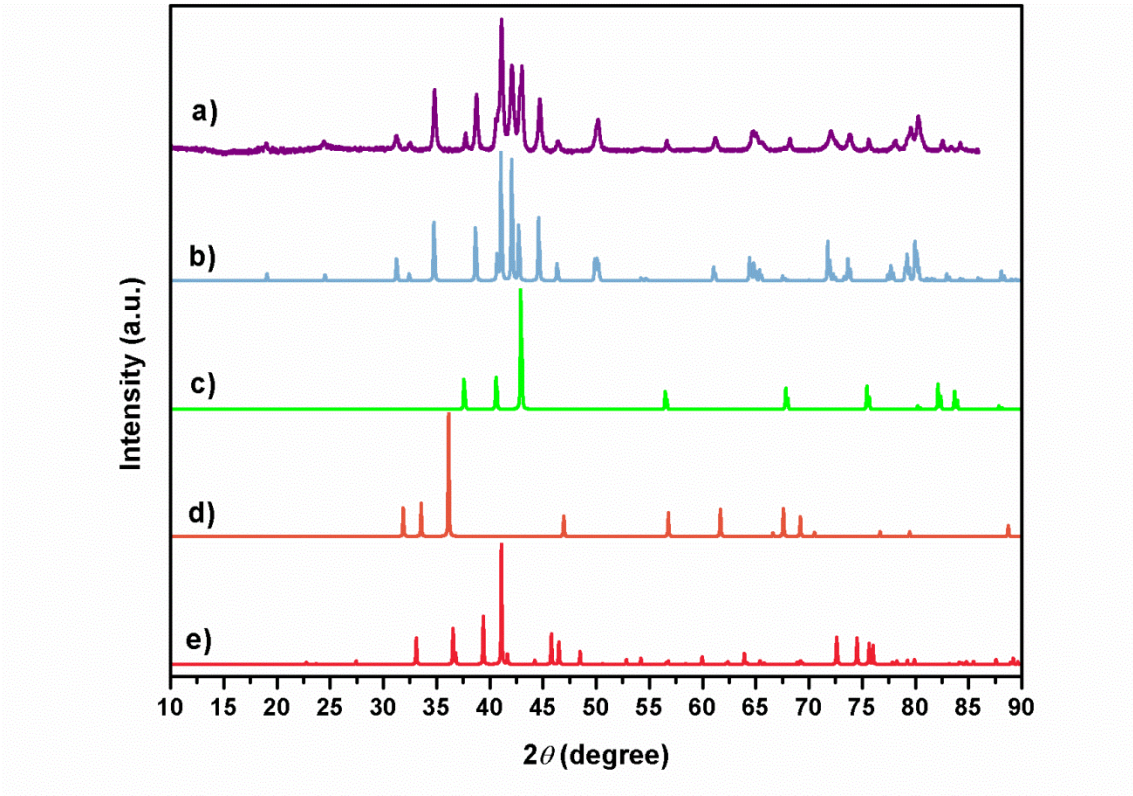

Figure 5.1.2 X-ray diagram of (a) the product from lead flux reaction at 900 ºC for 10 hour in Ar filled steal reaction tube in comparison with (b) the theoretical Re_3B (ICSD, card number 48-1739), (c) the theoretical Re (ICSD, card number 5-702), (d) the theoretical Pb (ICSD, card number 23-345) and (e) the theoretical Re_7B_3 (ICSD, card number 13-362)

Figure 5.1.2 shows the X-ray diffraction diagram of the lead flux product. Attempt at 900 ºC, Re_3B formation was detected with remained unreacted elemental rhenium. It shows that increase on reaction temperature makes easy to occur the reaction. However, a minor amount of flux dirt is detected while there is no trace of target compound of Re_7B_3. A new reaction condition was fixed to 1100 ºC for 65 h and checked what changes. Figure 5.1.3 shows the XRD results of the product.

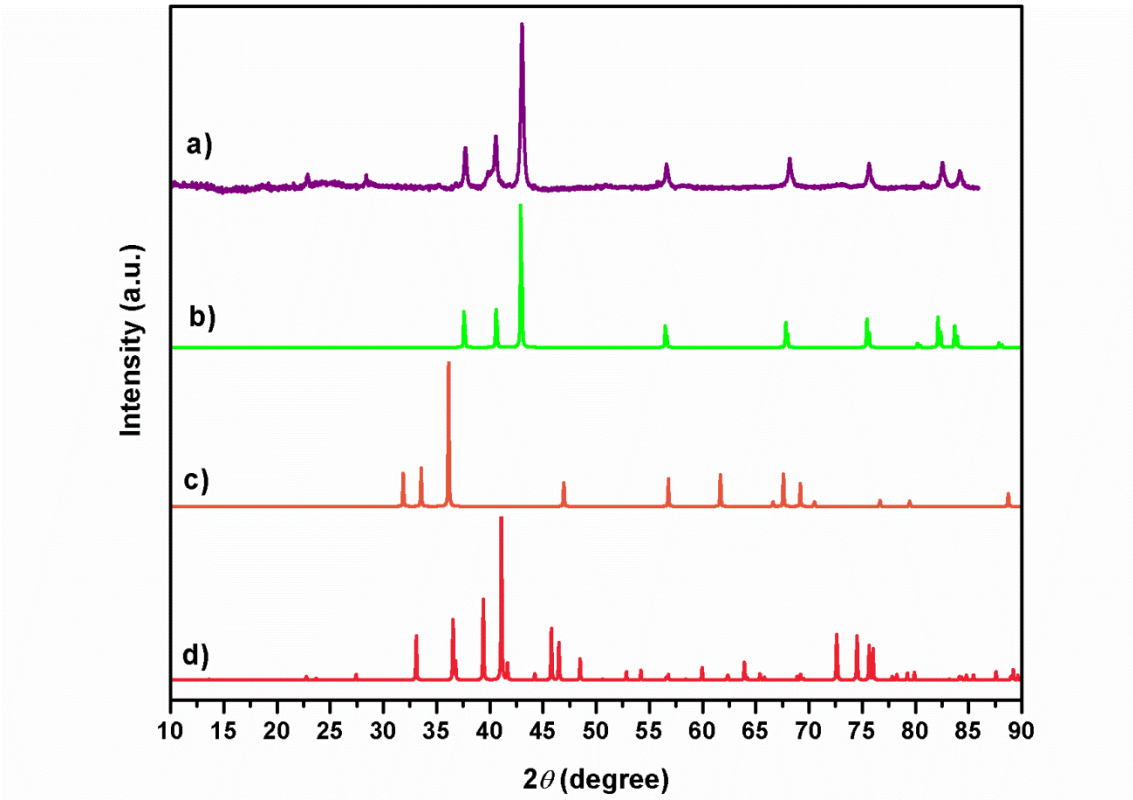

Figure 5.1.3 X-ray diagram of (a) the product from lead flux reaction at 1100 ºC for 65 hours in Ar filled steal reaction tube in comparison with (b) the theoretical Re (ICSD, card number 5-702), (c) the theoretical Pb (ICSD, card number 23-345) and (d) the theoretical Re_7B_3 (ICSD, card number 13-362)

According to the Figure 5.1.3, the product was stayed as elemental rhenium with new peak formations at 2θ values of 22.933º and 28.375º. There is no Pd dirt. Still, there is no formation of Re_7B_3. Depending on the experimental tries; new reaction temperature was fixed to 900 ºC and dwell time increased to get completed reaction. Following X- Ray pattern demonstrates the product which synthesized at 900 ºC for 216 hours.

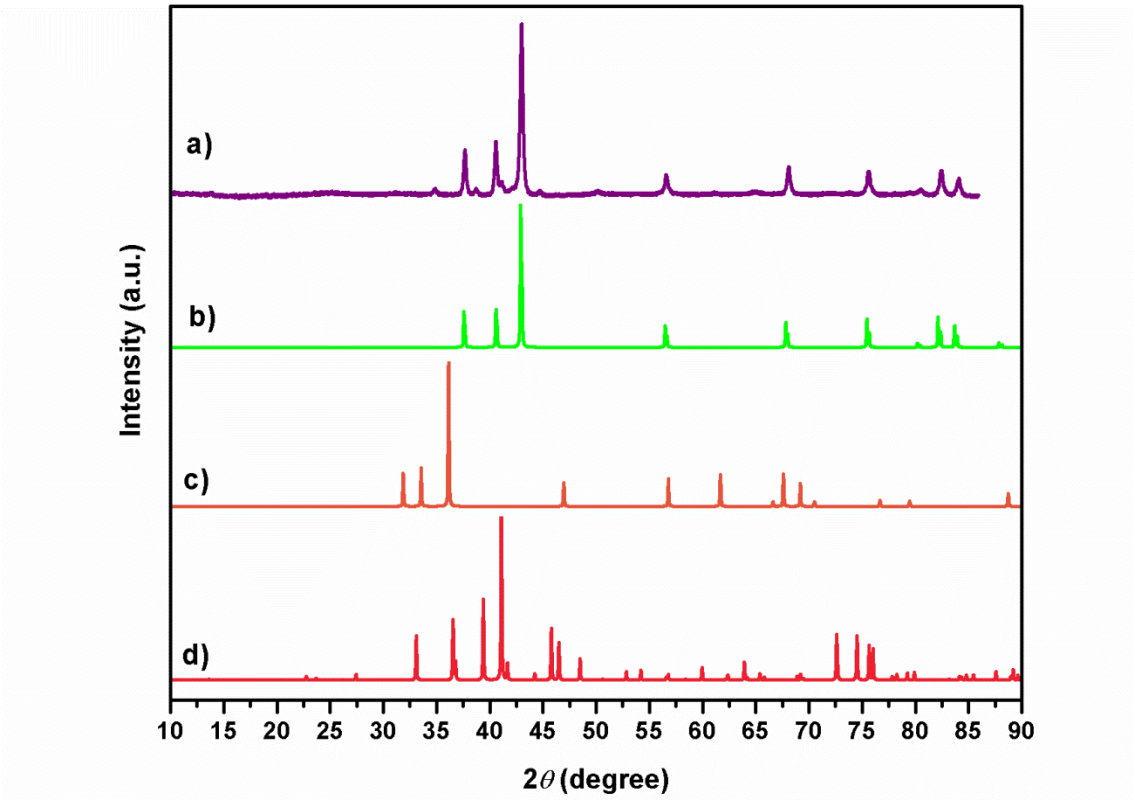

Figure 5.1.4 X-ray diagram of (a) the product from lead flux reaction at 900 ºC for 216 hours in Ar filled steal reaction tube in comparison with (b) the theoretical Re (ICSD, card number 5-702), (c) the theoretical Pb (ICSD, card number 23-345) and (d) the theoretical Re_7B_3 (ICSD, card number 13-362)

Product includes elemental rhenium with little amount impurity. Lead is cleaned from the system completely. Since the dwell time increased enormously, the formation of Re_7B_3 was not observed.

5.1.2. Vacuum Furnace

To synthesize Re_7B_3 with flux method after all these failure, the reaction conditions changed completely even type of furnace. All detailed results are given under Result and discussion part of Re_7B_3 chapter under Metal flux section.

BIBLIOGRAPHY

1. Chung, H.-Y. *et al.* Synthesis of ultra-incompressible superhard rhenium diboride at ambient pressure. *Science* **316,** 436–9 (2007).

2. Kawano, A., Mizuta, Y., Takagiwa, H., Muranaka, T. & Akimitsu, J. The Superconductivity in Re–B System. *J. Phys. Soc. Japan* **72,** 1724–1728 (2003).

3. Šimůnek, A. How to estimate hardness of crystals on a pocket calculator. *Phys. Rev. B* **75,** 172108 (2007).

4. Solozhenko, V. L., Dub, S. N. & Novikov, N. V. Mechanical properties of cubic BC 2 N , a new superhard phase. *Elsevier Diam. Relat. Mater.* **10,** 2228–2231 (2001).

5. Solozhenko, V., Kurakevych, O., Andrault, D., Le Godec, Y. & Mezouar, M. Ultimate Metastable Solubility of Boron in Diamond: Synthesis of Superhard Diamondlike BC5. *Phys. Rev. Lett.* **102,** 015506 (2009).

6. Friedrich, A., Winkler, B., Juarez-Arellano, E. a. & Bayarjargal, L. Synthesis of Binary Transition Metal Nitrides, Carbides and Borides from the Elements in the Laser-Heated Diamond Anvil Cell and Their Structure-Property Relations. *Materials (Basel).* **4,** 1648–1692 (2011).

7. Chung, H.-Y., Weinberger, M. B., Yang, J.-M., Tolbert, S. H. & Kaner, R. B. Correlation between hardness and elastic moduli of the ultraincompressible transition metal diborides RuB[sub 2], OsB[sub 2], and ReB[sub 2]. *Appl. Phys. Lett.* **92,** 261904 (2008).

8. Fokwa, B. P. T. Transition-Metal-Rich Borides - Fascinating Crystal Structures and Magnetic Properties. *Eur. J. Inorg. Chem.* **2010,** 3075–3092 (2010).

9. Zhong, M., Kuang, X. & Wang, Z. Phase Stability, Physical Properties, and Hardness of Transition-Metal Diborides MB2 (M= Tc, W, Re, and Os): First-Principles Investigations. *J. Phys. Chem.* **2,** 10643–10652 (2013).

10. Ivanovskii, a. L. Mechanical and electronic properties of diborides of transition 3d–5d metals from first principles: Toward search of novel ultra-incompressible and superhard materials. *Prog. Mater. Sci.* **57,** 184–228 (2012).

11. Gu, Q., Krauss, G. & Steurer, W. Transition Metal Borides: Superhard versus Ultra-incompressible. *Adv. Mater.* **20,** 3620–3626 (2008).

12. Li, Y. *et al.* Twofold coordinated ground-state and eightfold high-pressure phases of heavy transition metal nitrides MN(2) (M = Os, Ir, Ru, and Rh). *Inorg. Chem.* **48,** 9904–9 (2009).

13. Koehler, M. R., Keppens, V., Sales, B. C., Jin, R. & Mandrus, D. Elastic moduli of superhard rhenium diboride. *J. Phys. D. Appl. Phys.* **42,** 095414 (2009).

14. Qin, J. *et al.* Is Rhenium Diboride a Superhard Material? *Adv. Mater.* **20,** 4780–4783 (2008).

15. La Placa, S. J. & Post, B. The crystal structure of rhenium diboride. *Acta Crystallogr.* **15,** 97–99 (1962).

16. Levine, J. B., Tolbert, S. H. & Kaner, R. B. Advancements in the Search for Superhard Ultra-Incompressible Metal Borides. *Adv. Funct. Mater.* **19,** 3519–3533 (2009).

17. Frotscher, M., Hölzel, M. & Albert, B. Crystal Structures of the Metal Diborides ReB2, RuB2, and OsB2 from Neutron Powder Diffraction . *Zeitschrift für Anorg. und Allg. Chemie* **636,** 1783–1786 (2010).

18. Kaner, R. B., Gilman, J. J. & Tolbert, S. H. Materials science. Designing superhard materials. *Science* **308,** 1268–9 (2005).

19. Orlovskaya, N. *et al.* Mechanochemical synthesis of ReB2 powder. *J. Mater. Res.* **26,** 2772–2779 (2011).

20. Levine, J. B. *et al.* Preparation and properties of metallic, superhard rhenium diboride crystals. *J. Am. Chem. Soc.* **130,** 16953–8 (2008).

21. Jeitschko, W., Heumannska, D. H., Schriewer-po, M. S. & Rodewald, U. C. Preparation , Crystal Structures , and Properties of Rhenates with Multiple Re + Re Bonds : Ln 2 ReO 5 (Ln ⁄ Sm , Eu , Gd), Ln 3 Re 2 O 9 (Ln ⁄ Pr , Nd , Sm), and Ln 4 Re 6 O 19 (Ln ⁄ La + Nd). *J. Solid State Chem.* **147,** 218–228 (1999).

22. Locci, A. M., Licheri, R., Orrù, R. & Cao, G. Reactive Spark Plasma Sintering of rhenium diboride. *Ceram. Int.* **35,** 397–400 (2009).

23. Soto, G., Moreno-Armenta, M. G. & Reyes-Serrato, a. Study on the formation of rhenium borides by density functional calculations. *Comput. Mater. Sci.* **44,** 628–634 (2008).

24. Latini, A. *et al.* Superhard Rhenium Diboride Films: Preparation and Characterization. *Chem. Mater.* **20,** 4507–4511 (2008).

25. Misse, P. R. N. & Fokwa, B. P. T. Synthesis, Characterization, and Magnetic Properties of the New Boride Solid Solutions M0.5Ru6.5B3 (M = Cr, Mn, Co, Ni) . *Zeitschrift für Anorg. und Allg. Chemie* **636,** 1013–1017 (2010).

26. Kanatzidis, M. G., Pöttgen, R. & Jeitschko, W. The metal flux: a preparative tool for the exploration of intermetallic compounds. *Angew. Chem. Int. Ed. Engl.* **44,** 6996–7023 (2005).

27. Ivanovskii, a. L. The search for novel superhard and incompressible materials on the basis of higher borides of s, p, d metals. *J. Superhard Mater.* **33,** 73–87 (2011).

28. Vepřek, S. The search for novel, superhard materials. *J. Vac. Sci. Technol. A Vacuum, Surfaces, Film.* **17,** 2401 (1999).

29. Dubrovinskaia, N., Dubrovinsky, L. & Solozhenko, V. L. Comment on "Synthesis of ultra-incompressible superhard rhenium diboride at ambient pressure". *Science* **318,** 1550; author reply 1550 (2007).

30. Chung, H.-Y. *et al.* Response to Comment on "Synthesis of Ultra-Incompressible Superhard Rhenium Diboride at Ambient Pressure."*Science (80-.).* **318,** 1550d–1550d (2007).

31. Zhou, W., Wu, H. & Yildirim, T. Electronic, dynamical, and thermal properties of ultra-incompressible superhard rhenium diboride: A combined first-principles and neutron scattering study. *Phys. Rev. B* **76,** 184113 (2007).

32. Pellicer-Porres, J., Segura, a, Muñoz, a, Polian, a & Congeduti, a. Bond length compressibility in hard ReB2 investigated by x-ray absorption under high pressure. *J. Phys. Condens. Matter* **22,** 045701 (2010).

33. Levine, J. B., Tolbert, S. H. & Kaner, R. B. Advancements in the Search for Superhard Ultra-Incompressible Metal Borides. *Adv. Funct. Mater.* **19,** 3519–3533 (2009).

34. Żogał, O. J. *et al.* Crystal structure, electric field gradient, and electronic charge densities in ReB[sub 2]: A single crystal x-ray, [sup 11]B nuclear magnetic resonance, and first-principles study. *J. Appl. Phys.* **106,** 033514 (2009).

35. Otani, S., Korsukova, M. M. & Aizawa, T. High-temperature hardness of ReB2 single crystals. *J. Alloys Compd.* **477,** L28–L29 (2009).

36. Zhang, R. F., Veprek, S. & Argon, a. S. Mechanical and electronic properties of hard rhenium diboride of low elastic compressibility studied by first-principles calculation. *Appl. Phys. Lett.* **91,** 201914 (2007).

37. Liang, Y. & Zhang, B. Mechanical and electronic properties of superhard ReB2. *Phys. Rev. B* **76,** 132101 (2007).

38. Peng, F., Liu, Q., Fu, H. & Yang, X. Electronic and thermodynamic properties of under high pressure and temperature. *Solid State Commun.* **149,** 56–59 (2009).

39. Veprek, S., Zhang, R. F. & Argon, a. S. Mechanical properties and hardness of boron and boron-rich solids. *J. Superhard Mater.* **33,** 409–420 (2011).

40. Gou, H., Wang, Z., Zhang, J., Yan, S. & Gao, F. Structural stability and elastic and electronic properties of rhenium borides: first principle investigations. *Inorg. Chem.* **48,** 581–7 (2009).

41. Zhao, E., Wang, J., Meng, J. & Wu, Z. Phase Stability and Mechanical Properties of Rhenium Borides by First-Principles Calculations. *Wiley Intersci.* **31,** 1904–1910 (2010).

42. Mohammadi, R., Lech, A. T., Xie, M., Weaver, B. E. & Yeung, M. T. Tungsten tetraboride , an inexpensive superhard material. *PNAS* **108,** 10958–10962 (2011).

43. Search, H. *et al.* All-electron study of ultra-incompressible superhard material ReB 2 : structural and electronic properties ∗. *Chinese Phys. B* **18,** 4437–06 (2009).

44. Zhong, M.-M. *et al.* Phase stability, physical properties of rhenium diboride under high pressure and the effect of metallic bonding on its hardness. *J. Alloys Compd.* **581,** 206–212 (2013).

45. Wang, Y. *et al.* Thermal equation of state of rhenium diboride by high pressure-temperature synchrotron x-ray studies. *Phys. Rev. B* **78,** 224106 (2008).

46. Liang, Y., Zhong, Z. & Zhang, W. A thermodynamic criterion for designing superhard transition-metal borides with ultimate boron content. *Comput. Mater. Sci.* **68,** 222–228 (2013).

47. Nagamatsu, J., Nakagawa, N., Muranaka, T., Zenitani, Y. & Akimitsu, J. Superconductivity at 39 K in magnesium diboride. *Nature* **410,** 63–4 (2001).

48. Superconductivity in the Re-B system. 142432 (2013).

49. Portnoi, K. I. and R. V. M. Phase Diagram of the system rhenium-boron. *Acta Crystallogr.* 112–114 (1968).

50. Wilson, B. A. J. C. International Tables for Crystallography (2006). *Int. Tables Crystallogr.* **C,** 490 (2006).

51. Laing, M. *An Introduction to the Scope , Potential and Applications of X-ray Analysis by*. 1–36 (2001).

52. Massa, W. *Springer-Verlag Berlin Heidelberg GmbH*. 1–210 (2004).

53. Vitalij P., Z. P. *Fundamentals of Powder Diffraction and Structural Characterization of Materials*. 1–728 (2008).

54. Callister, W. D. *Materials Science and Engineering An Introduction*. 1–975 (2007).

55. Stoe WINXPOW 1.2, 2000, Stoe & Cie GmbH: Darmstadt.

56. Bergerhoff, G. Inorganic Crystal Structure Database (ICSD), 2009, FIZ Karlsruhe: Germany.

57. Aguilar-Santillan, J. Elastic and hardness anisotropy and the indentation size effect of pyrite (FeS2) single crystal. *Acta Mater.* **56,** 2476–2487 (2008).

58. Romasov, K. I. and P. V. M. Phase diagram of the system rhenium- boron. *Acta Metall.* 112–114 (1968).

VITA

Zeynep Gizem Narin was born in Kahramanmaraş, Turkey, in 1989. She graduated from Savaştepe Anadolu Öğretmen Lisesi, Balıkesir, in 2007, as the second best student. She received her B.S. degrees in Chemistry from Koç University, İstanbul, in 2012. The same year, she started her study in the Department of Materials Science and Engineering as a M.S. candidate. Her current research interests are investigation on mechanical properties of superhard materials and synthesis and characterization of transitional metal borides.